國立臺灣大學生物資源暨農學院生物環境系統工程學系

碩士論文

Graduate Institute of Bioenvironmental Systems Engineering
College of Bioresources and Agriculture
National Taiwan University

Master Thesis

山地柳杉森林之地表通量量測

Surface Flux Measurements Above a Mountainous Cryptomeria Forest

鄭詩憫

Shih-Min Cheng

指導教授：謝正義 博士

Advisor: Cheng-I Hsieh, Ph. D.

中華民國九十九年六月

June, 2010

國立臺灣大學（碩）博士學位論文
口試委員會審定書

山地柳杉森林之地表通量量測

Surface flux measurements

above a mountainous Cryptomeria forest

本論文係鄭詩惘君（R97622008）在國立臺灣大學生物環境系統工程學系、所完成之碩（博）士學位論文，於民國 99 年 06 月 11 日承下列考試委員審查通過及口試及格，特此證明

口試委員：謝正義（簽名）（指導教授）

朱佳仁　張倉榮

陳明志

系主任、所長　（簽名）

Acknowledgement

謝謝我的指導教授謝正義老師，在系上六年的時間，受老師許多的教導和照顧，也因此我才能順利完成碩士論文；也謝謝朱佳仁老師、陳明志老師以及張倉榮老師百忙中抽空幫我口試，並給了我許多寶貴的意見和往後在研究上可努力的方向。另外，還要謝謝台灣大學實驗林管理處王亞男處長、魏聰輝博士、余瑞珠小姐及管理處許多同仁在實驗上的協助。

謝謝研究室的成員們，丞瑋學長、軒梅和阿苗學姊，是你們耐心的教導我，給我許多的幫助，我才得以有一點的研究成果。還有常陪在身旁的朋友、同學和弟兄姊妹們，是你們的扶持和鼓勵，加上很多的禱告，使我這兩年的生活不只有研究，還有許多值得述說的回憶。

謝謝我最親愛的家人，總是叮嚀我也安慰我，更常聽我說，也陪我禱告，在各方面都做我的後盾；最後要謝謝最愛我的主耶穌，為我安排了這一切的人、事、物，感謝讚美主!

摘要

地表之可感熱、潛熱以及二氧化碳通量，常以渦流相關法估測於近似理想的地形，但如何在複雜地形中合適地使用，仍是一大挑戰，而檢測單一測點是否能有效代表複雜地形中的流體特性是必須的。本研究選擇的實驗地位於台灣南投的溪頭實驗林，是一 57 年生的人工柳杉山林地，海拔高度介於 800~2000 公尺高，且山地坡度為 13.6 度。研究結果顯示，雖然實驗地地形複雜，空間的變異係數幾乎都小於 15%，另外，白天之變異係數小於晚上的變異係數，可見白天有較好的均質特性，而地表通量的空間變異性比較中，潛熱會大於可感熱及二氧化碳通量，原因可能是水氣有較複雜的源或匯存在。在大氣於不穩定的狀況下，垂直與水平風速會符合 Monin-Obukhov 相似理論，但相似常數因位置不同而有不同；在純量部分，以溫度最符合 Monin-Obukhov 相似理論，二氧化碳普通，而水氣並不符合。

關鍵詞： 地表通量，空間變異，變異係數，相似理論，複雜地形

Abstract

Under ideal or near-ideal conditions, the eddy-covariance (EC) method is a widely used technique in the measurement of sensible heat, water vapor, and CO_2 fluxes. Nowadays, adapting the EC method to complex terrain measurements is a challenging topic. It is necessary to examine whether measurements from single eddy covariance system can represent the flow properties of turbulence at complex terrain. The experimental site in this study is located in a valley covered with 57-year-old Cryptomeria plantation at Sitou, Taiwan. The weather is warm and humid through the whole year. The elevation of this area is from 800 to 2000 m above sea level, and the averaged slope is 13.6 degree. The results showed that almost all the coefficient of spatial variation (CV) values for surface fluxes in this study are less than 15%. Moreover, the values of CV in the daytime are smaller than those in the nighttime. This indicates that the flow variables are more homogeneous during daytime. It is noted that the spatial variability of water vapor flux is larger than those for sensible heat and CO_2 fluxes; this may due to the complex sources/sinks distribution of water vapor in this site. Under unstable condition, vertical and horizontal wind velocities meet the Monin-Obukhov similarity theory (MOST) predictions, though the similarity constants at different locations are not the same. For scalar variances, temperature follows MOST well, CO_2 meets it fairly, but water vapor does not follow the MOST predictions for all the three locations.

Keywords: Surface fluxes, Spatial variance, Coefficient of variance, Similarity theory, Complex terrain

Contents

List of Tables

List of Figures

1 Introduction

Surface fluxes of temperature, water vapor and carbon dioxide concentration are important parameters for understanding the interactions and energy/mass transport processes between land-surface and atmosphere. The surface fluxes – the exchange of heat, mass and momentum at the surface – are controlled with turbulent exchange in the surface layer. Under nature chaotic and unpredictable variations, understanding and measuring turbulence had difficulties in handing the mathematical description and difficulties in measurement. Over the past 40 years, in the mathematical description, in brief, the conservation equation provides the basic framework for measuring and interpreting flux measurements with two most important assumptions which are horizontal homogeneity and steady-state (Gockede et al., 2004). Based on the assumptions, despite the complicity of the turbulent structure, the statistical description of turbulent is commonly assumed varying in vertical (z) direction (Wilson and Shaw, 1977; Moritz, 1989; Raupach et al., 1996; Katul et al., 1999). Moreover, in measurement, G. I. Taylor may be the earliest attempted to make quantitative measurements of atmosphere turbulence in 1917 and suggested that turbulence might be considered to be frozen as it passes a sensor in 1938 (Stull, 1988). Taylor's hypothesis, which is necessary for measurement made in time at a fixed point, be utilized when the turbulent eddies evolve with a timescale longer than the time of eddies pass a sensor (Garratt, 1992). According to these simplification, there were many methods for quantifying fluxes have been developed, including the eddy-covariance method, the dissipation method, the surface renewal method and the profile method. Among the various methods, the eddy covariance method is the most widely used technique for measuring surface fluxes in the FLUXNET network (Baldocchi et al., 2000; Hsieh et al., 2008).

In the eddy covariance method, the covariance of wind velocity and concentration of scalar of interest (e.g. temperature, water vapor, or carbon dioxide) are sampled with high frequency at one point above the surface or the plant canopy. Even though it is simple to acquire data that is necessary for the eddy covariance method, the rigorous requirements of eddy covariance are demanding even for ideal sites. In 1960s, this method was simply performed in very uniform, flat grass land or crop. However, now experimental site could be extended to complex terrain such as tall forest, valley or urban, and the measure time were lengthened form short-term campaigns to long-term monitoring. The application of the eddy-covariance method under relative complex terrain conditions, especially for continuous long-term monitoring, is still a major challenge (Baldocchi et al., 2000; Hollinger et al., 2004; Hiller et al., 2008). Because of just one point measurement, the spatial variability is an imperative issue to examine whether single-tower turbulence statistics represent the flow properties of turbulence (Katul et al., 1999; Wilson and Meyers, 2001). A recent study in a uniformly-aged pine plantation of Duke Forest settled seven eddy-covariance systems at 15.5 meters heights at seven separated towers. The mean canopy height was 14 meters. Results collected four continuous days were shown that the stable minima of the coefficient of spatial variation (CV) of variables were reached at the averaging interval of 6-7 hours during daytime and the values of the stable minima CVs were around 0.09 – 0.11 for sensible heat, latent heat and carbon dioxide flux (Oren et al., 2006). Another experiment was conducted with two towers in a conifer- dominated forest (Hollinger et al., 2004). It is noted that the footprints of the two measured systems were no overlapping. However, the comparing results made at high temporal resolution suggested that the carbon dioxide flux differed by 0.11 (11%) and the latent heat flux by 0.15 (15%). Particularly

long-term monitoring of water vapor and CO_2 fluxes under less-than-ideal conditions has yet fully explored. Hence, more studies are needed for investigating the spatial variability to confirm the representativeness of a single eddy covariance system above the canopy in measuring the flow properties of turbulence under relative complex terrain and ecosystems such as tall forest.

The object of this study is to examine whether single eddy covariance system measures represent the flow properties of turbulence above a Cryptomeria humid forest with a slope of 13.6° inclination in Sitou, Taiwan. In this study, sensible heat, latent heat and carbon dioxide flux and the turbulence statistics were collected. Specifically, the spatial variability of the turbulence statistics and flux-variance similarity relationships are analyzed. For conducting the study of the spatial variability, we used two towers (A, B) setting three eddy covariance systems (heights: A at 28 m, B at 32 m and 40 m) within a 1000-m by 800-m Japanese Ceder (Cryptomeria Japonica) plantations (averaging height = 27 m) at Sitou, the national Taiwan university experimental forest in Nantou, Taiwan. High frequency measurements of velocity, water vapor and carbon dioxide concentrations were simultaneously collected from three eddy covariance systems from July 23, 2009 to April 30, 2010.

2 Experiment

2.1 Site Description

The Sitou site is located at the National Taiwan University Experimental Forest in Nantou, Taiwan. Sitou terrain is a valley surrounded by mountains on its three sides. Ling-Tou Mountain, the highest mountain in the south, extends to the north and connects to Feng-Huang mountain range, which forms the east mountain boundary. Ling-Tou Mountain also extends to the west to Nei-Shu and turns to the north, forming the south and west mountain boundaries in this area. The area of Sitou is around 2,500 ha at an altitude ranged from 800 to 2000 m. This experimental forest can be categorized as three different main zones - the forest plantation (954 ha), the natural forest (509 ha), and the bamboo forest (728 ha). The measurement towers, A and B, were set up in 57-year-old Japanese Cedar (Cryptomeria japonica) forest plantation within the experimental forest. The area of this Japanese Cedar forest plantation is up to 80 hectares with a average slope of 13.6° as Figure 1(a) shows. The average canopy height is approximately 27 m. Figure 1(b) shows a hilltop-toward-valley view of the experiment region from Google Earth. In Figure 1(b), Tower A and B are presented as the blue and yellow marks, respectively. The location of tower A is 23°39’50.1”N, 120°47’46.4”E and 1252 m above sea level. 64 m from the tower A, the location of tower B is 23°39’51.09”N、120°47’44.57”E and 1233 m above sea level. The heights of tower A and B are 35 m and 40 m, respectively.

The climate of Sitou belongs to AB'ra' type, which is based on the Thornthwaite climate classification, means a warm and humid weather. The annual average temperature and the annual average rainfall are 16.6 ℃ and 2,635.18 mm, respectively.

Within this humid experimental region, fogs often appear in the afternoon in fall and winter and the average relative humidity is nearly 86 % or more. (The data were given by Sitou meteorological station). Table 1 shows brief site description mentioned above.

2.2 The Instruments and Data Logging

For analyzing the study of the spatial variability, there are three eddy covariance systems set up on two different towers. The following is the description of the instruments that is used to conduct the experiment.

Tower A is equipped with one open-path eddy-covariance system at 28 m above ground surface. The eddy-covariance system is consisting of a three-dimensional sonic anemometer (CSAT3, Campbell Scientific, INC., USA) pointing towards north and an open-path infrared gas analyzer (LI-7500, LI-COR, USA). There are two the same open-path eddy-covariance systems on Tower B at 40 m and 32 m. The 10 Hz analog signals are simultaneously gathered by a data logger (CR3000, Campbell Scientific, INC., USA) each tower. Not only are the 10 Hz raw data collected, also the values of mean and covariance of 10 Hz analog signals are calculated for every 30 minutes by the data logger. Then the data loggers transmit the results to computers.

Additionally, a net radiometer (NR-LITE, Campbell Scientific, INC., USA) and a rain gauge (TE525MM, Campbell Scientific, INC., USA) are installed at each tower- 27.5 m for tower A and 30 m for tower B -for measuring net radiation and precipitation. Two temperature and relative humidity probes (HMP45C, Campbell Scientific, INC., USA) and one the precision infrared temperature sensor (IRTS-P, Campbell Scientific, INC., USA) are installed at each tower. The heights of temperature and relative humidity probes at tower A are 13 m and 28 m. At tower B,

they are placed at 32 m and 40 m above the ground. The precision infrared temperature sensors aim at the canopy to collected average leaves temperature data and its height at tower A and B are 28 m and 30 m. All the sensors mentioned above are connected to a data logger each tower (CR23X, Campbell Scientific, INC., USA). The data logger captures signals each 30 seconds that afterwards are averaged for every 30 minutes. Different from the way that we average the data, total amount precipitation is recorded every 30 minutes. A brief description of the instruments is presented in Table 2. Figure 2 is shown the diagram of the installation of towers. Some photos of the experiment are presented in Figure 3.

3 Theory and Method

3.1 The Monin-Obukhov similarity theory

The Monin-Obukhov similarity theory (MOST) is a scientific theory applied to the surface layer. The surface layer is defined as the part of the boundary layer where the fluxes vary by less than 10% of the magnitude with height. The important assumptions implied in the MOST are that (1) the flow is horizontal homogeneous, (2) the flow is in steady state and (3) the turbulent fluxes of heat and momentum are independent of heights (Arya, 1998). If the flow properties of the surface layer conform to all assumptions, this surface layer is also called a constant layer. According to these assumptions, the use of MOST is limited by the validity only in the surface layer above the roughness sublayer and is limited to homogeneous surface (Foken, 2006).

This theory describes the relationship between the vertical behavior of non-dimensional mean flow and turbulence properties within the atmospheric surface layer. The similarity functions of wind velocities and scalars can be presented as a function of the thermal stability ζ :

Under stable condition ($\zeta > 0$):

for horizontal wind $$\frac{\sigma_u}{u_*} = C_1 + C_2(\zeta) \quad (1)$$

for vertical wind $$\frac{\sigma_w}{u_*} = C_1 + C_2(\zeta) \quad (2)$$

for scalar $$\frac{\sigma_x}{x_*} = C_1[1 + C_2(-\zeta)]^{-\frac{1}{3}} \quad (3)$$

Under unstable condition ($\zeta < 0$):

for horizontal wind $$\frac{\sigma_u}{u_*} = C_1 \cdot [1 + C_3(-\zeta)]^{\frac{1}{3}} \quad (4)$$

for vertical wind $$\frac{\sigma_w}{u_*} = C_1 \cdot [1 + C_3(-\zeta)]^{\frac{1}{3}} \quad (5)$$

for scalar $$\frac{\sigma_x}{x_*} = C_3(-\zeta)^{-\frac{1}{3}}, \quad C_3 = C_1 C_2^{-\frac{1}{3}} \quad (6)$$

Under neutral condition ($\zeta \sim 0$):

for horizontal wind $$\frac{\sigma_u}{u_*} = C_1 \quad (7)$$

for vertical wind $$\frac{\sigma_w}{u_*} = C_1 \quad (8)$$

for scalar $$\frac{\sigma_x}{x_*} = C_1 \quad (9)$$

where C_1, C_2 and C_3 are the similarity constants. σ_u, σ_w and σ_x are the standard deviations of horizontal, vertical wind and scalar x, u_* is the friction velocity defined as $u_* = \sqrt[4]{\overline{u'w'}^2 + \overline{v'w'}^2}$, x_* is defined as $x_* = \frac{\overline{w'x'}}{u_*}$. ζ is the thermal stability defined as $\zeta = (\frac{z-d}{L})$, in which L is the Obukov length, z is the measurement height, and d is the zero-plane displacement height (= 0.65h, h is canopy height). The Obukov length L is defined as $L = -\frac{Tu_*^3}{k \cdot g \cdot \overline{w't'}}$, where T is the air temperature (K), k (=0.4) is the von Karman constant, and g (= 9.8 m s^{-1}) is the gravitational acceleration.

The Monin-Obukhov similarity theory (MOST) was proposed as a hypothesis in

1954. In the last 60 years, empirical evidence from filed experiments conducted over flat terrain points to a surface layer where the structure of turbulence is determined by the Monin–Obukhov key parameters. The results shows that the more flat and uniform the terrain is, the nearer to 1 the value of C_x will be. In this study, the fluxes are measured by the eddy covariance method above non-ideal terrain. For checking the validity of the measured results, the MOST may suitable for test. The test focuses on examining whether single-tower turbulence statistics represent the flow properties of turbulence in the sloped tall forest.

3.2 Tools for Analysis

The coefficient of spatial variation (CV) of a variable x considering with time interval is defined as (after Katul et al., 1999, Oren et al., 2006)

$$CVx(t) = \frac{\sqrt{[x(t) - < x(t) >]^2}}{|< x(t) >|} \tag{10}$$

where t is the period of averaging time. The minimum t is 30 minutes. The overbar in the equation represents time averaging, and <.> represents spatial averaging. <x(t)> is the spatial mean of x and $\sqrt{[x(t) - < x(t) >]^2}$ is the spatial standard deviation of x. Noted that when spatial mean of x approach to 0, the value of CV can become ill with spuriously large.

To eliminate the limitation of CV, the relative variation parameter (RV) is proposed (Katul et al., 1999).

$$RVx(t) = \frac{\sqrt{[x(t) - < x(t) >]^2}}{|< x(t) >| + \sqrt{[x(t) - < x(t) >]^2}} \tag{11}$$

RV is well bounded between 0 and 1. When the spatial standard deviation of x approach 0 (<x(t)>≠0), then RV will be near zero. If the spatial mean of x approach

to 0, RV will approach 1. If a flow variable is planar homogeneous, RV will be near zero. In the limited range, it is easy to set a standard to assess the degree that a flow variable changed with space.

4 Results and discussion

To examine whether measurement of a single eddy covariance system represents the flow properties of turbulence above this sloped Cryptomeria humid forest, sensible heat, latent heat and carbon dioxide flux and the turbulence statistics were collected from three eddy covariance systems. In this section, we discuss the time series of environmental statistics and comparisons of flow statistics between three measured locations first. Then, the temporal and spatial variability of the turbulence statistics are analyzed. Also, the homogeneity of similarity relationships is examined.

4.1 The Time Series of Environmental Statistics and Comparisons of Flow Statistics

Figure 4(a), (b) and (c) shows the time series of sensible heat, latent heat and carbon dioxide flux (H, LE and Fco_2) for three days, respectively, from day 335 to 338, 2009. The changes in three fluxes are following the trend of net radiation. The diurnal patterns of fluxes are regular and typical that these three fluxes have the maximum values around noon. Sensible heat and carbon dioxide flux recorded simultaneously at three locations are similar. Difference in latent heat flux is larger than sensible heat and carbon dioxide flux. The time series of standard deviations of friction velocity u_*, horizontal and vertical wind velocity, temperature, water vapor and carbon dioxide are presented in Figure 5 and 6. It is clear that the diurnal change is less significant and less regular than of the fluxes, particularly of scalars. Especially, it seems that the variation of σ_q is time-independent as shown in Figure 6(b). It is noticed that the half-hourly values of u_* in the daytime usually larger than at night. This indicates that the atmosphere mixing at night is usually poorer than in the daytime. Moreover, the values of u_* measured at tower B at 40 m at night are

much smaller than the values measured at other two locations. We suggest that the atmosphere mixing degree at higher (at tower B 40 m) and lower (at tower A 28 m and at tower B 32 m) measured points might different in the nighttime conditions.

Next, comparisons of flow statistics between three measured locations are discussed. We assumed that the coefficient of determination from linear regression analysis as R^2 over 0.7 (in linear regression, R^2 is the square of r, Pearson's correlation coefficient) is considered as highly correlated linearly existed between variable from two measured points. During daytime, the highly linearly relationship are found in all compared variables recorded at the tower B at 32m and 40m. The linear analysis results are shown in Figures 7(a) – 15(a). Half-hourly data are nearly identical as indicated by the slopes close to 1 with high R^2 values (> 0.8). The comparisons of the flow statistics also show high linearly relationship between measured at the tower B at 32m and at the tower A at 28m in Figures 7(b) – 15(b). It should be noticed that the linear regressions of the variables which are related to water vapor and carbon dioxide are almost with lower R^2 values. The phenomenon of the scatters spread out can be found in Figure 8 of LE, Figure 9 of Fco_2 and Figure 15 of σ_c. The linear analysis results are listed in Table 3.

At night, the comparisons of sensible heat, latent heat and carbon dioxide fluxes as shown in Figures 16-18, the scatter is obvious. The coefficients of determination for these fluxes at night are lower than that in the daytime. This effect may due to the poorer atmosphere mixing at night. Because of the poor atmosphere mixing, the relationship of latent heat and carbon dioxide flux at three locations is not significant. However, the deviation for u_* in the slope of the relationship between tower A at 28 m and tower B at 32 m made in the day or at night were similar (0.82 v.s. 0.79) with similar R^2 values (0.8 v.s. 0.78). It indicates that the measured locations of tower A

at 28 m and tower B at 32 m are in the same atmosphere condition all day. For the measured locations of tower B at 40 m, the atmosphere condition as of tower A at 28 m and tower B at 32 m is just the same in the daytime and differ at night. The different also display in the standard deviations. The linearly relationship of the standard deviations (the slopes and the values of R^2) between measured points at tower A at 28 m and at tower B at 32 m is no significant under daytime and nighttime conditions. But the linearly relationship between measured points at tower B at 40 m and at tower B at 32 m at night is poorer than the relationship in the daytime. All the comparisons under nighttime are shown in Figures 16-24 and the results are summarized in Table 4.

4.2 Temporal Variability of Flow Statistics

Katul et al. (1999) discussed the spatial variability of the turbulent flow statistics with half-hour averaging interval and demonstrated that it varied in time. Wilson and Meyers (2000) also asserted that the coefficients of variance (CV) of turbulent fluxes ($\overline{w'x'}$) and standard deviation of turbulent fluctuations (σ_x) are strong time-dependent parameters in the eddy covariance method used below the canopy. Variability between systems decreased as the averaging period is increased. When the mean sampling period lengthen to 48 hours, CV values were performed as the minima and almost no further reduced with longer mean period (Figure 7 in Wilson and Meyers, 2000). Oren et al. (2006) suggested that there was a stable minimum of the spatial CV that was independent of further lengthening the averaging time. The stable minima CVs were reached at the averaging interval of 6-7 hours during daytime. Compared with the analysis of Katul et al.(1999), in which the spatial CVs were stated at high temporal resolution (half-hourly), the stable minimum CV might exclude micrometeorological sampling errors and is just dependent on the variability

of ecosystem structural properties (Oren et al., 2006).

In this study, we used five days data to investigate the difference of the spatial variability of statistics between the different averaging intervals. Data are separated to daytime (6 hours) and nighttime (8 hours) without transition periods, because data represent the biological sources and sinks much more reliably during daytime than nighttime (Staebler and Fitzjarrald, 2004). As Figures 25 (a) and (b) shown, in the daytime (am 9:00 – pm 3:00), the CV values of the fluxes and standard deviations of wind velocities and scalars (e.g. for temperature, σ_T) are decreasing and reach to stable asymptotic values after about 6 hours. When at the six–hours time scale, the values of CVs did not exceed 0.1, except LE (0.22) and σ_w (0.13). It is similar to Oren et al.(2006) that the stable minima CVs reached at the averaging period of 7 hours during daytime. There were no statistical different in the averages of the turbulence variables when averaged over 6-7 hours. However, for normalized standard deviations, we only find the decline trend presents in vertical and horizontal wind velocities. The patterns of normalized standard deviations of scalars shown in Figure 25(c) are not stabilizing throughout 30 hours. During nighttime (pm 9:00 – am 5:00), CV reduction also works well on standard deviations of wind velocity and scalars though the integral average time need more than 20 hours (Fig. 26(b)). It should be noted that if the average of flow variable approach to 0, the value of CV can become ill with spuriously large (Katul et al., 1999). This irregular phenomena are found in Figures 26 (a) and (c) for variables of water vapor and carbon dioxide (i.e. LE, Fco_2, σ_q/q_* and σ_c/c_*). The results of CV values are shown in Tables 5 and 6 under daytime and nighttime.

To eliminate the limitation of CV, the relative variation parameter (RV) is proposed (Katul et al., 1999). Based on the trend in Figure 27(a) and (b), during

daytime, the trend of RV with fluxes and standard deviation of variables is similar to that of CV in Figure 25 but with smaller values. It is surprising that the trend of the normalized standard deviation of scalars is still irregular whether in the daytime or at nighttime (Figure 27(c) and 28(c)). Moreover, in our study, RV of LE and Fco_2 does not vary to stable asymptotic over 30 hours during night time. This is contrary to the finding of Oren et al. (2006) which the CV of Fco_2 stabilized after 14 hours and of LE stabilized after 18 hours. This condition may due to the fact that the average time for CV or RV reaching stabilized is place-dependent. The results of RV values are given in Table 7 and 8 under daytime and nighttime.

In general, the decline of the CV and RV values associated to wind are little, even could obtain the minima values at high temporal resolution (half-hourly). This condition is also adapted in normalized standard deviation of wind. It may be a consequence of the fact that the ability of planer homogeneous in wind field exists in this sloped tall forest.

4.3 Spatial Variability of Flow Statistics

The following discussion of the spatial variability in environmental variables and fluxes includes the values of CV during daytime (am 9:00-pm 3:00) and RV during nighttime (pm 9:00-am 5:00) at high temporal resolution (30 minutes).

Due to the highly relations on all flow variables between three systems are pointed out formerly, we observe the CVs of all variables to find and assumed that it is spatial similarity when the value of CV under 0.15. Based on the CV results in Table 9 for daytime condition, it is clear that the CV value of σ_u is the smallest (CV = 0.06), consistent with Wilson and Meyers (2000), both when systems separated horizontally and vertically (Table 11). In terms of standard deviations have closely

spatial variability (~0.12). The CV value of surface fluxes, H, LE and Fco_2 are 0.12, 0.17 and 0.13. The rank of spatial variability of fluxes is LE > Fco_2 ≒ H, consisting with the rank in Oren et al. (2006) in Duke Forest (<5% slopes, six towers) and Hollinger et al. (2004) in Howland forest (two towers with no overlapping footprints). It is common consent that heat may appear more uniformly transported than water vapor and carbon dioxide. The relationship between the turbulent flux above the canopy and sources or sinks form the canopy foliage and the ground flux differences should be considered, therefore the spatial variability of mass fluxes is usually larger than heat flux (Katul et al., 1999). Moreover, all the ranking results point to the same conclusion that the local sources or sinks of water vapor and carbon dioxide are not totally the same. It may be interpreted through the variability of the different physiological mechanism of the stomata. Moreover, the spatial variability of LE is larger than that of H and Fco_2 may due to complex sources or sinks of water vapor.

In fact, the CV values of the standard deviations and fluxes are similar and smaller than normalized standard deviation of wind and scalars. Though the CV values of normalized standard deviation of wind and scalars are presented as dissimilarity of space, they will be test with the Monin-Obukhov similarity theory next part.

Under night condition, it is noted that the RV values of group variables, of the standard deviations are smaller than of the fluxes and normalized standard deviation of wind and scalars scale (Table 10). The RV values of wind are still almost the smallest (σ_u=0.10 and σ_w =0.07) in three group variables separated. This implies that the wind filed might be homogenous not only of daytime but of night. Transportation of heat could assume be similar according to the enough small RV. Compared the mass fluxes during daytime, the RV values are about three or four times

of daytime. The small space variability depends on the good atmospheric mixing (Hollinger et al., 2004). The heterogeneity of the vapor and CO_2 fluxes may attribute to not only the complex terrain and non-uniform rising temperature but also non-uniform sources or sinks.

4.4 Homogeneity of Similarity Relationships

Though the use of MOST is limited by the validity only in the surface layer above the roughness sublayer and is limited to homogeneous surface (Foken, 2006). However, above tall forests, long-term surface fluxes are commonly limited to measure within roughness sublayer (RSL). The roughness sublayer is the region at the bottom of the boundary layer where the presence of the canopy impinges directly on the character of the turbulence (Kaimal and Finnigan, 1994). The roughness sublayer typically ranges from the mean canopy height h to 3h. In the previous studies as shown in Table 13~15, within roughness sublayer, the similarity constants at different locations may not totally the same but with similarity trends. Now the MOST is widely applied to different terrains and ecosystems. This similarity theory describes the relationship between the vertical behavior of non-dimensional mean flow and turbulence properties within the atmospheric surface layer.

The simplifying assumptions implied in the MOST are mainly that the flow is horizontal homogeneous, quasi-stationary and the turbulent fluxes of heat and momentum are independent of heights (Arya, 1998). According to the Monin-Obukhov hypothesis, atmospheric parameters and statists, such as variances and covariances, when normalized by appropriate powers of the scaling velocity u_* and the scaling scalars (e.g. T_*, q_*, c_*), become universal functions of stability parameter z/L (Kaimal and Finnigan, 1994). The characteristic is presented on the Monin–Obukhov key parameters, C_1, C_2 or C_x, that should be determined empirically

from practical observations. The MOST may be a suitable test for non-ideal surface to examine the ability of homogeneity. If the ability of homogeneity is confirmed, then the validity of the measured results can assure.

For daytime (H>30 W m^{-2}) under unstable condition, the variances of horizontal and vertical wind velocity with the stability parameter ζ are shown in Figures 29 and 30, respectively. The Monin–Obukhov key parameters C_1 and C_2 of Equations (1) and (2) are obtained by regression analysis with the least squared method. In Figure 29, the horizontal wind velocity with the suggested function Equations.(1), results in (a) $C_1 = 1.40$ and $C_2 = 3.46$ with $R^2 = 0.79$ at tower B at 40 m, (b) $C_1 = 1.42$ and $C_2 = 3.19$ $R^2 = 0.79$ at tower B at 32 m, and (c) $C_1 = 1.78$ and $C_2 = 1.28$ with $R^2 = 0.86$ at tower A at 28 m, respectively. Though the performances of the normalized horizontal wind velocity have trends with the regress function, they are scatter. σ_u / u_* may not totally follow the MOST. For comparison with other study, it seems that the scatter of σ_u/u_* is a common phenomenon. In Table 13, we can see that there are the difference of the key parameters C_1 among different experiment is large. Comparison between the experiments, the magnitude of σ_u / u_* in our study is smaller than others. The summarized resulting is listed Table 12(a).

In comparison with σ_u / u_*, σ_w / u_* is more fit to the normalized regression function. Their normalized function are $0.85\ [1+3.71\ (-\zeta)]^{1/3}$, $0.91[1+3.75\ (-\zeta)]^{1/3}$ and $0.79\ [1+3.82\ (-\zeta)]^{1/3}$ for tower B at 40m and 32m, and tower A at 28m with high R^2 (~96%), respectively (Fig.30(a), (b) and (c)). For the vertical wind velocity, good results are found under unstable condition. Moreover, the spatial averaged of the estimated parameters for σ_w/u_* are C_1=0.85 (±0.04) and C_2= 3.76 (±0.04). That is, the performances of the variances of vertical wind velocity with the stability parameter ζ are no significant different in this experiment.

Different experimental values were found in the literature and shown in Table 13. Noted that the values of C_1 gather in a small range: 1.07 to 1.25, however, the values of C_2 vary form experiment to experiment. Though the magnitude of σ_w / u_* in our study is smaller than those from other experiments as of σ_u / u_*, it just represents the characteristic of this experimental site. Because of the Monin–Obukhov key parameters, C_1 and C_2 are determined empirically from practical observations. Additionally, Pattey et al. (2002) assumed that σ_w/u_* may be affected by the types of sonic anemometers, especially with one with longer path length due to loss of covariance between u and w. The key point is the trend and the scatter of the normalized variable show good fit with universal function forms according to the Monin–Obukhov similarity theory (MOST).

To character normalized standard deviation of scalars such as temperature, water vapor and CO_2, the functions of the stability parameter are developed as the -1/3 power law with each characteristic constant C_x as Equation (3). The values of C_x are estimated with records within the free convection limit ($-\zeta > 1$). Measured σ_T/T_* exhibits a strong -1/3 law dependent for all measurements with C_T = 1.21, 1.29 and 1.46 for tower B at 40 m and 32 m, and tower A at 28 m as shown in Figure 31. The spatial mean C_T is 1.32 (±0.09). From the literature, C_T has been found to vary between 0.95 and 1.36 (Ohtaki, 1985; Katul et al., 1995; Guo et al., 2009). Notice that the spatial mean C_T values is within the range but relatively high. The higher σ_T/T_* values possibly result from surface heterogeneity. This suggestion is confirmed in the comparison between different experiment terrains as shown in Table 14. It may be the reason that the values of C_T in this site are relatively large.

σ_q/q_* and σ_c/c_* under unstable condition are shown in Figures 32 and 33. Although some of data follow the -1/3 power law, the scatters spread out for three

measured points. The departure also display in the water vapor and carbon dioxide characteristic parameters, C_q and C_C. C_q are found as 1.69, 1.88 and 1.94 for tower B at 40 m and 32 m, and tower A at 28 m. C_C varies 1.96 to 2.79 for tower B at 40 m, and 32 m and tower A at 28 m, respectively. It is noted that all the suggested functions are represented with low R^2 (<0.35). Moreover, though the magnitude of C_q is smaller than of C_C, the scatter of σ_q/q_* is larger than σ_c/c_*. In the literature, the values of C_q are with a range 1-1.61. Compared particular with the similar condition experiments (the canopy height > 10 m) (Table 14), the C_q of this site are still large. Hsieh et al.(2008) demonstrated one of the reasons of whether the humidity following the similarity is the sources/sinks distribution on the site. Due to this suggestion, in this high humidity forest, the scatter of σ_q/q_* may be understanding.

While the values of C_T are relatively universal and independent on this relative complex surface condition, it seems that C_q and C_C are dependent on not only the surface condition but also the plant canopy as sources or sinks. We speculate that the rough surface might cause the temperature rising non-uniform. This phenomenon increases the turbulent of temperature and leads to the standard deviation of temperature rising. Compared with previous studies, we believe that the characteristic constants, C_T may be larger when the non-homogeneousness of the terrain enhances. From the literature, it appears that the more flat and uniform the terrain or the is, the nearer to 1 C_C or C_q will be under unstable condition. We presumed that the impact of the terrain factor on C_q and C_C are obvious. The other effect of the larger parameter of water vapor or carbon dioxide may be the plant canopy as sources or sinks. It is recalled that the biophysical mechanisms of the ligneous plants or herbaceous plantare not totally the same. According to the results, the characteristic constant for CO_2 and water vapor may be influenced not only by the

terrain situation and temperature but each other when experimented in forest. The similarity constants for heat, water vapor and CO_2 are summarized in Table 12(b).

At nighttime, the stability of atmosphere are usually stable or near neutral. In Figure 34 and 35, horizontal and vertical wind velocities fit to normalized regression functions. The normalized function of horizontal wind velocities are 3 $[1+\zeta]^{1/3}$, 2.5$[1+2\zeta]^{1/3}$ and 2 $[1+2\zeta]^{1/3}$ for tower B at 40 m and 32 m, and tower A at 28 m. For vertical wind velocity, the normalized function are 1 $[1+3\zeta]^{1/3}$, 1$[1+3\zeta]^{1/3}$ and 1$[1+2\zeta]^{1/3}$ for tower B at 40 m and 32 m, and tower A at 28 m, respectively. The similarity constants are presented in Table 15. From the literature, $C_{1(u)}$ has been found to vary between 2.39 and 2.78 (Panofsky et al., 1984; Hogstrom, 1990; Andreas et al., 1998; Moraes et al., 2005). The $C_{1(u)}$ values is almost within the range but a little relatively high. The range of $C_{1(w)}$ is around 1.2 and 1.3 in the previous studies and is higher than our $C_{1(w)}$ value (=1). The similarity constants for temperature, water vapor and CO_2 under night time are showed in Figure 36, 37, and 38. By eye fitting, the values of C_1 for temperature and CO_2 are found as -2 and -4. For water vapor, the values of C_1 are about 2.5 and 3. However, the departures are display in the temperature, water vapor and carbon dioxide.

5 Conclusions

In this study, our goal is to examine whether measurements from single eddy covariance system can represent the flow properties of turbulence above a humid Cryptomeria forest. The flow properties of turbulence were collected from three eddy covariance systems. We discuss the time series of statistics and comparisons of flow statistics, the temporal and spatial variability of the turbulence statistics. Also, the homogeneity of similarity relationships is examined. The following results were found:

1) The daytime averaged CV for H, LE, Fco_2, u_*, σ_u, σ_w, σ_T, σ_q and σ_c are 0.12, 0.17, 0.13, 0.13, 0.06, 0.13, 0.12, 0.12 and 0.11. Almost all the values of CV in this study are less than 15%.

2) The values of CV in the daytime are smaller than those in the nighttime. The results indicate that the flow variables are more homogeneous during daytime.

3) The rank of spatial variability of fluxes is LE > Fco_2 ～ H. The spatial variability of LE is larger than those for H and Fco_2; this may due to the complex sources/sinks distribution of water vapor.

4) Though, under unstable condition, vertical and horizontal wind velocities meet the MOST predictions, the similarity constants at different locations are not the same.

5) For scalar variances, temperature follows MOST well, CO_2 meets it fairly, but water vapor does not follow the MOST predictions for all the three locations.

The above results indicated that cautions should be taken when using single tower turbulent statistics to represent the properties of the whole field.

References

Andreas, E. L., R. J. Hill, J. R. Gosz, D. I. Moore, W. D. Otto, and A. D. Sarma, 1998: Statistics of surface-layer turbulence over terrain with metre-scale heterogeneity. *Boundary-Layer Meteorology*, Vol. 86, pp.379-408.

Arya, S. P., 1994: *Introduction to micrometeorology*, pp. 213

Baldocchi, D., J. Finnigan, K. Wilson, K. T. Paw U, and E. Falge, 2000: On measuring net ecosystem carbon exchange over tall vegetation on complex terrain. *Boundary-Layer Meteorology*, Vol. 96, pp. 257-291.

Cava, D., G. G. Katul, A. M. Sempreviva, U. Giostra, and A. Scrimieri, 2008: On the anomalous behavior of scalar flux-variance similarity functions within the canopy sub-layer of a dense alpine forest. *Boundary-Layer Meteorology*, Vol. 128, pp. 33-57.

Choi, T. J., J. K. Hong, J. Kim, H. C. Lee, J. Asanuma, H. Ishikawa, O. Tsukamoto, Z. Q. Gao, Y. M. Ma, K. Ueno, J. M. Wang, T. Koike, and T. Yasunari, 2004: Turbulent exchange of heat, water vapor, and momentum over a Tibetan prairie by eddy covariance and flux variance measurements. *Journal of Geophysical Research-Atmospheres*, Res., 109, D21106.

De Bruin, H. A. R., W. Kohsiek, and B. J. J. M. Vandenhurk, 1993: A Verification of Some Methods to Determine the Fluxes of Momentum, Sensible Heat, and Water-Vapor Using Standard-Deviation and Structure Parameter of Scalar Meteorological Quantities. *Boundary-Layer Meteorology*, Vol. 63, pp. 231-257.

Detto, M., G. Katul, M. Mancini, N. Montaldo, and J. D. Albertson, 2008: Surface heterogeneity and its signature in higher-order scalar similarity relationships. *Agricultural and Forest Meteorology*, Vol. 148, pp. 902-916.

Foken, T., 2006: 50 years of the Monin-Obukhov similarity theory. *Boundary-Layer Meteorology*, Vol. 119, pp. 431-447.

Garratt, J.R.1992: *The Atmospheric Boundary Layer,* pp. 11.

Gockede, M., C. Rebmann, and T. Foken, 2004: A combination of quality assessment tools for eddy covariance measurements with footprint modelling for the characterisation of complex sites. *Agricultural and Forest Meteorology*, Vol. 127, pp. 175-188.

Guo, X., H. Zhang, X. Cai, L. Kang, T. Zhu, and M. Y. Leclerc, 2009: Flux-Variance Method for Latent Heat and Carbon Dioxide Fluxes in Unstable Conditions. *Boundary-Layer Meteorology*, Vol. 131, pp. 363-384.

Hiller, R., M. J. Zeeman, and W. Eugster, 2008: Eddy-covariance flux measurements in the complex terrain of an Alpine valley in Switzerland. *Boundary-Layer Meteorology*, Vol. 127, pp. 449-467.

Hollinger, D. Y., J. Aber, B. Dail, E. A. Davidson, S. M. Goltz, H. Hughes, M. Y. Leclerc, J. T. Lee, A. D. Richardson, C. Rodrigues, N. A. Scott, D. Achuatavarier, and J. Walsh, 2004: Spatial and temporal variability in forest-atmosphere CO_2 exchange. *Global Change Biology*, Vol. 10, pp. 1689-1706.

Högström, U. and A. S. Smedman-Högström, 1974: Turbulence mechanisms at an agricultural site. *Boundary-Layer Meteorology*, Vol. 7, pp. 373-389.

Hsieh, C. I., M. C. Lai, Y. J. Hsia, and T. J. Chang, 2008: Estimation of sensible heat, water vapor, and CO2 fluxes using the flux-variance method. *International Journal of Biometeorology*, Vol. 52, pp. 521-533.

Kaimal, J. and J. Finnigan, 1994: *Atmospheric Boundary Bayer Flows: Their*

Structure and Measurement. Oxford Univ. Press, New York, pp.71, 289.

Katul, G., C. I. Hsieh, D. Bowling, K. Clark, N. Shurpali, A. Turnipseed, J. Albertson, K. Tu, D. Hollinger, B. Evans, B. Offerle, D. Anderson, D. Ellsworth, C. Vogel, and R. Oren, 1999: Spatial variability of turbulent fluxes in the roughness sublayer of an even-aged pine forest. *Boundary-Layer Meteorology*, Vol. 93, pp. 1-28.

Lamaud, E. and M. Irvine, 2006: Temperature-humidity dissimilarity and heat-to-water-vapor transport efficiency above and within a pine forest canopy: The role of the Bowen ratio. *Boundary-Layer Meteorology*, Vol. 120, pp. 87-109.

Marques, E. P., L. D. A. Sa, H. A. Karam, R. C. S. Alvala, A. Souza, and M. M. R. Pereira, 2008: Atmospheric surface layer characteristics of turbulence above the Pantanal wetland regarding the similarity theory. *Agricultural and Forest Meteorology*, Vol. 148, pp. 883-892.

Moraes, O. L. L., O. C. Acevedo, G. A. Degrazia, D. Anfossi, R. da Silva, and V. Anabor, 2005: Surface layer turbulence parameters over a complex terrain. *Atmospheric Environment*, Vol. 39, pp. 3103-3112.

Moritz, E., 1989: Heat and Momentum Transport in an Oak Forest Canopy. *Boundary-Layer Meteorology*, Vol. 49, pp. 317-329.

Ohtaki, E., 1985: On the Similarity in Atmospheric Fluctuations of Carbon-Dioxide, Water-Vapor and Temperature over Vegetated Fields. *Boundary-Layer Meteorology*, Vol. 32, pp. 25-37.

Oren, R., C. I. Hseih, P. Stoy, J. Albertson, H. R. McCarthy, P. Harrell, and G. G. Katul, 2006: Estimating the uncertainty in annual net ecosystem carbon exchange: spatial variation in turbulent fluxes and sampling errors in eddy-covariance measurements. *Global Change Biology*, Vol. 12, pp. 883-896.

Panofsky, H. A. and A. Dutton, 1984: *Atmospheric Turbulence: Models and Method for Engineering Applications.* John Wiley &Sons, New York, pp.397.

Pattey, E., I. B. Strachan, R. L. Desjardins, and J. Massheder, 2002: Measuring nighttime CO2 flux over terrestrial ecosystems using eddy covariance and nocturnal boundary layer methods. *Agricultural and Forest Meteorology*, Vol. 113, pp. 145-158.

Raupach, M. R., J. J. Finnigan, and Y. Brunet, 1996: Coherent eddies and turbulence in vegetation canopies: The mixing-layer analogy. *Boundary-Layer Meteorology*, Vol. 78, pp. 351-382.

Staebler, R. M. and D. R. Fitzjarrald, 2004: Observing subcanopy CO2 advection. Agricultural and Forest Meteorology, Vol. 122, pp. 139-156.

Stull, R. B., 1988: *An Introduction to Boundary Layer Meteorology*, pp. 666.

Wilson, K. B. and T. P. Meyers, 2001: The spatial variability of energy and carbon dioxide fluxes at the floor of a deciduous forest. *Boundary-Layer Meteorology*, Vol. 98, pp. 443-473.

Wilson, N. R. and R. H. Shaw, 1977: Higher-Order Closure Model for Canopy Flow. *Journal of Applied Meteorology*, Vol. 16, pp. 1197-1205.

Yaglom, A. M., 1979: Similarity Laws for Constant-Pressure and Pressure-Gradient Turbulent Wall Flows. *Annual Review of Fluid Mechanics*, Vol. 11, pp. 505-540.

Table 1 Brief site description

Items	Description
Country	Taiwan
Location	National Taiwan University Experimental Forest in Sitou, Taiwan.
Site latitude and longitude	23°39’50.1”N, 120°47’46.4”E
Elevation	1252 m
Slope	About 13.6 deg
Terrain Type	Steep mountain slope
Area	80 ha uniform forest stand (1000 m*800 m)
Climate	AB'ra' type, which means warm and humid weather.
Mean annual air temperature	16.6 ℃
Mean annual precipitation	2,635.18 mm
Vegetation Type	Japanese Cedar (Cryptomeria japonica) forest plantation
Canopy height	27 m
Age of trees	About 57 years

Table 2 The summary of the instrumentation: (a) tower A (b)tower B (The average canopy height is 27 m)

(a)

Description	Instrument	Type	Unit	Location
Eddy covariance system	Three Dimensional Anemometer	CSAT3	m s^{-1}	28 (m)
	CO_2/H_2O Analyzer	LI7500	mmol m^{-3}	28 (m)
Climate measurement	Net radiometer	NR-Lite	W m^{-2}	27.5(m)
	Precision Infrared Temperature Sensor	IRTS-P	℃	28 (m)
	Temperature and Relative Humidity Probe	HMP45C	T:℃ RH:%	13, 28 (m)
	Rain Gage	TE525MM	mm	27.5 (m)

(b)

Description	Instrument	Type	Unit	Location
Eddy covariance system	Three Dimensional Anemometer	CSAT3	m s^{-1}	32, 40 (m)
	CO_2/H_2O Analyzer	LI7500	mmol m^{-3}	32, 40 (m)
Climate measurement	Net radiometer	NR-Lite	W m^{-2}	30 (m)
	Precision Infrared Temperature Sensor	IRTS-P	℃	30 (m)
	Temperature and Relative Humidity Probe	HMP45C	T:℃ RH:%	32, 40 (m)
	Rain Gage	TE525MM	mm	30 (m)

Table 3 Relationships between the variables which are measured at tower B at 40 m (BT 40m), at 32 m (BT 32m) and tower A at 28 m (AT 28m) in the daytime conditions (H>30 W m^{-2}) are shown. Here setting the variable value measured at tower B at 32 m is the base to compare with. (BT 32m v.s. BT 40m: BT40m = BT32m x slope + intercept) (BT 32m v.s. AT 28m: AT28m = BT32m x slope + intercept) R^2 is the coefficient of determination of the linear regression.

Variable	Sites	Slope	Intercept	R^2
H	BT 32m v.s. BT 40m	0.97	-3.940	0.96
	BT 32m v.s. AT 28m	0.91	0.470	0.82
LE	BT 32m v.s. BT 40m	0.85	8.230	0.88
	BT 32m v.s. AT 28m	0.71	9.300	0.68
Fco_2	BT 32m v.s. BT 40m	0.93	0.088	0.82
	BT 32m v.s. AT 28m	0.9	-0.540	0.61
u_*	BT 32m v.s. BT 40m	0.85	0.001	0.81
	BT 32m v.s. AT 28m	0.82	0.015	0.80
σu	BT 32m v.s. BT 40m	0.97	0.041	0.87
	BT 32m v.s. AT 28m	0.92	0.026	0.89
σw	BT 32m v.s. BT 40m	1.07	0.023	0.94
	BT 32m v.s. AT 28m	0.80	0.014	0.92
σT	BT 32m v.s. BT 40m	0.86	0.005	0.95
	BT 32m v.s. AT 28m	1.12	0.017	0.86
σq	BT 32m v.s. BT 40m	0.82	0.036	0.94
	BT 32m v.s. AT 28m	0.83	1.717	0.91
σc	BT 32m v.s. BT 40m	0.84	0.004	0.86
	BT 32m v.s. AT 28m	0.86	-0.002	0.57

Table 4 Relationships between the variables which are measured at tower B at 40 m (BT 40m), at 32 m (BT 32m) and tower A at 28 m (AT 28m) in the night conditions (pm 8:00- am 5:00) are shown. Here setting the variable value measured at tower B at 32 m is the base to compare with. (BT 32m v.s. BT 40m: BT40m = BT32m x slope + intercept) (BT 32m v.s. AT 28m: AT28m = BT32m x slope + intercept) R^2 is the coefficient of determination of the linear regression.

Variable	Sites	Slope	Intercept	R^2
H	BT 32m v.s. BT 40m	0.58	2.042	0.64
	BT 32m v.s. AT 28m	0.56	-9.404	0.72
LE	BT 32m v.s. BT 40m	0.42	-1.412	0.35
	BT 32m v.s. AT 28m	0.43	2.473	0.57
Fco_2	BT 32m v.s. BT 40m	0.58	0.362	0.36
	BT 32m v.s. AT 28m	0.36	0.303	0.26
u_*	BT 32m v.s. BT 40m	0.39	0.044	0.28
	BT 32m v.s. AT 28m	0.79	0.057	0.78
σ_u	BT 32m v.s. BT 40m	0.83	0.097	0.45
	BT 32m v.s. AT 28m	0.78	0.072	0.78
σ_w	BT 32m v.s. BT 40m	0.78	0.039	0.84
	BT 32m v.s. AT 28m	0.80	0.047	0.92
σ_T	BT 32m v.s. BT 40m	0.84	0.076	0.71
	BT 32m v.s. AT 28m	0.82	0.010	0.84
σ_q	BT 32m v.s. BT 40m	0.97	0.503	0.77
	BT 32m v.s. AT 28m	0.82	-0.094	0.83
σ_c	BT 32m v.s. BT 40m	0.74	0.020	0.60
	BT 32m v.s. AT 28m	0.83	-0.080	0.63

Table 5 The temporal mean values of the coefficient of variance (CV) of turbulent statistics measured at tower B at 40 m, at 32 m and at tower A at 28 m for daytime (am 9:00-pm 3:00). (a) Friction velocity (u_*) and fluxes (b) Standard deviations (c) Normalized standard deviations

(a)

Averaging time	u_*	H	LE	Fco_2
0.5h	0.12	0.15	0.32	0.14
1h	0.11	0.13	0.28	0.11
1.5h	0.09	0.11	0.24	0.10
2h	0.08	0.11	0.25	0.09
3h	0.08	0.11	0.23	0.08
6h	0.07	0.11	0.24	0.07
15h	0.07	0.11	0.23	0.06
30h	0.06	0.10	0.22	0.06

(b)

Averaging time	σ_u	σ_w	σ_T	σ_q	σ_c
0.5h	0.07	0.14	0.10	0.11	0.09
1h	0.05	0.14	0.10	0.10	0.09
1.5h	0.04	0.13	0.10	0.10	0.08
2h	0.04	0.13	0.10	0.09	0.08
3h	0.03	0.13	0.10	0.08	0.08
6h	0.03	0.13	0.10	0.07	0.07
15h	0.02	0.13	0.10	0.07	0.07
30h	0.02	0.13	0.10	0.07	0.07

(c)

Averaging time	L	σ_u/u_*	σ_w/u_*	σ_T/T_*	σ_q/q_*	σ_c/c_*
0.5h	0.27	0.11	0.17	0.36	0.44	0.20
1h	0.24	0.10	0.17	0.34	0.50	0.19
1.5h	0.20	0.10	0.17	0.33	1.15	0.17
2h	0.18	0.09	0.16	0.27	1.14	0.15
3h	0.16	0.09	0.16	0.32	0.59	0.15
6h	0.11	0.08	0.17	0.20	0.60	0.12
15h	0.10	0.07	0.17	0.14	0.55	0.06
30h	0.08	0.07	0.17	0.02	0.65	0.02

Table 6 The temporal mean values of the coefficient of variance (CV) of turbulent statistics measured at tower B at 40m and 32m, and at tower A at 28m for nighttime (pm 9:00-am 5:00). (a) Friction velocity (u_*) and fluxes (b) Standard deviations (c) Normalized standard deviations

(a)

Averaging time	u_*	H	LE	Fco_2
0.5h	0.33	76.72	13.22	1.17
1h	0.31	0.38	3.40	0.81
2h	0.30	0.34	0.73	0.62
4h	0.30	0.31	0.75	0.88
8h	0.29	0.30	0.74	0.46
20h	0.29	0.29	0.67	0.23
40h	0.29	0.28	0.58	0.30

(b)

Averaging time	σ_u	σ_w	σ_T	σ_q	σ_c
0.5h	0.10	0.09	0.12	0.20	0.27
1h	0.09	0.08	0.11	0.19	0.26
2h	0.08	0.07	0.10	0.18	0.24
4h	0.07	0.07	0.09	0.18	0.22
8h	0.06	0.07	0.08	0.17	0.21
20h	0.05	0.06	0.08	0.15	0.19
40h	0.05	0.06	0.07	0.15	0.18

(c)

Averaging time	L	σ_u/u_*	σ_w/u_*	σ_T/T_*	σ_q/q_*	σ_c/c_*
0.5h	1.33	0.40	0.38	0.57	2.18	1.76
1h	0.70	0.41	0.39	0.46	1.36	1.54
2h	0.62	0.42	0.39	0.33	1.48	1.31
4h	0.58	0.43	0.40	0.32	2.81	6.34
8h	0.53	0.43	0.40	0.24	4.19	1.23
20h	0.53	0.43	0.40	0.40	1.80	1.42
40h	0.51	0.43	0.40	0.30	0.67	2.66

Table 7 The temporal mean values of the relative coefficient of variance (RV) of turbulent statistics measured at tower B at 40m and 32m, and at tower A at 28m for daytime (am 9:00-pm 3:00). (a) Friction velocity (u_*) and fluxes (b) Standard deviations (c) Normalized standard deviations

(a)

Averaging time	u_*	H	LE	Fco_2
0.5h	0.10	0.12	0.22	0.12
1h	0.09	0.11	0.20	0.10
1.5h	0.08	0.10	0.18	0.09
2h	0.07	0.10	0.19	0.08
3h	0.07	0.10	0.18	0.07
6h	0.06	0.10	0.19	0.07
15h	0.06	0.10	0.18	0.06
30h	0.06	0.09	0.18	0.06

(b)

Averaging time	σ_u	σ_w	σ_T	σ_q	σ_c
0.5h	0.06	0.12	0.09	0.10	0.08
1h	0.05	0.12	0.09	0.09	0.08
1.5h	0.04	0.12	0.09	0.08	0.07
2h	0.04	0.12	0.09	0.08	0.07
3h	0.03	0.12	0.09	0.07	0.07
6h	0.02	0.12	0.09	0.07	0.07
15h	0.02	0.12	0.09	0.07	0.07
30h	0.02	0.12	0.09	0.07	0.07

(c)

Averaging time	L	σ_u/u_*	σ_w/u_*	σ_T/T_*	σ_q/q_*	σ_c/c_*
0.5h	0.19	0.10	0.14	0.20	0.26	0.16
1h	0.18	0.08	0.14	0.19	0.27	0.15
1.5h	0.16	0.09	0.14	0.19	0.33	0.14
2h	0.15	0.08	0.14	0.18	0.32	0.13
3h	0.13	0.08	0.14	0.19	0.33	0.12
6h	0.10	0.07	0.14	0.17	0.31	0.10
15h	0.09	0.06	0.15	0.12	0.31	0.06
30h	0.08	0.06	0.15	0.01	0.39	0.02

Table 8 The temporal mean values of the relative coefficient of variance (RV) of turbulent statistics measured at tower B at 40 m and at 32 m and at tower A at 28 m for nighttime (pm 9:00-am 5:00). (a) Friction velocity (u_*) and fluxes (b) Standard deviations (c) Normalized standard deviations.

(a)

Averaging time	u_*	H	LE	Fco_2
0.5h	0.24	0.28	0.41	0.40
1h	0.23	0.26	0.40	0.35
2h	0.23	0.24	0.37	0.34
4h	0.23	0.23	0.39	0.37
8h	0.23	0.23	0.40	0.31
20h	0.23	0.22	0.40	0.18
40h	0.22	0.22	0.37	0.23

(b)

Averaging time	σ_u	σ_w	σ_T	σ_q	σ_c
0.5h	0.09	0.08	0.10	0.16	0.21
1h	0.08	0.07	0.10	0.15	0.20
2h	0.07	0.07	0.09	0.15	0.19
4h	0.06	0.06	0.08	0.15	0.17
8h	0.06	0.06	0.07	0.14	0.17
20h	0.05	0.06	0.07	0.13	0.16
40h	0.05	0.05	0.07	0.13	0.16

(c)

Averaging time	L	σ_u/u_*	σ_w/u_*	σ_T/T_*	σ_q/q_*	σ_c/c_*
0.5h	0.38	0.27	0.26	0.21	0.40	0.43
1h	0.38	0.28	0.27	0.21	0.44	0.47
2h	0.36	0.28	0.27	0.19	0.47	0.50
4h	0.36	0.29	0.28	0.19	0.52	0.58
8h	0.34	0.29	0.28	0.16	0.52	0.54
20h	0.34	0.30	0.28	0.29	0.57	0.57
40h	0.34	0.30	0.29	0.23	0.40	0.73

Table 9 The spatial mean values of the coefficient of variance (CV) and the relative coefficient of variance (RV) of turbulent statistics measured at tower B at 40 m and 32 m, and at tower A at 28 m for daytime (am9:00 - pm3:00).

Flux	CV	RV
H	0.12	0.11
LE	0.17	0.10
Fco_2	0.13	0.14
u_*	0.13	0.11

Standard deviation	CV	RV
σ_u	0.06	0.06
σ_w	0.13	0.11
σ_T	0.12	0.10
σ_q	0.12	0.10
σ_c	0.11	0.09

Normalized standard deviation	CV	RV
σ_u/u_*	0.15	0.12
σ_w/u_*	0.19	0.15
σ_T/T_*	0.18	0.15
σ_q/q_*	0.24	0.18
σ_c/c_*	0.20	0.16

Table 10 The spatial mean values of the coefficient of variance (CV) and the relative coefficient of variance (RV) of turbulent statistics measured at tower B at 40 m and 32 m, and at tower A at 28 m for nighttime (pm9:00 - am5:00).

Flux	CV	RV
H	4.02	0.05
LE	2.16	0.41
Fco_2	4.13	0.39
u_*	0.30	0.22

Standard deviation	CV	RV
σ_u	0.12	0.10
σ_w	0.08	0.07
σ_T	0.13	0.11
σ_q	0.18	0.14
σ_c	0.26	0.20

Normalized standard deviation	CV	RV
σ_u/u_*	0.38	0.26
σ_w/u_*	0.34	0.24
σ_T/T_*	0.70	0.15
$\sigma q/q_*$	2.72	0.30
σ_c/c_*	1.74	0.42

Table 11 The spatial mean values of the coefficient of variance (CV) of turbulent statistics presented in previous studies.

(a)

	This study (daytime)	Katul et al., 1999 (daytime)	Wilson and Meyers, 2001 (all day)		
Variable	CV (6h)	CV (7h)	CV (48h) (a)	CV (48h) (b)	CV (48h) (c)
H	0.15 (0.11)	0.17 (0.12)	0.57 (0.07)	0.35 (0.13)	0.40 (0.20)
LE	0.32 (0.24)	0.33 (0.10)	0.53 (0.09)	0.38 (0.24)	0.31 (0.06)
Fco_2	0.14 (0.07)	0.22 (0.10)	0.57 (0.16)	0.34 (0.07)	0.33 (0.11)
u_*	0.12 (0.07)	0.16			
$\overline{w'u'}$			0.86 (0.14)	0.70 (0.56)	0.49 (0.18)

(b)

	This study (daytime)	Katul et al., 1999 (daytime)	Wilson and Meyers, 2001 (all day)		
Variable	CV (6h)	CV (7h)	CV (48h) (a)	CV (48h) (b)	CV (48h) (c)
σ_u	0.07 (0.03)	0.11	0.09 (0.03)	0.07 (0.03)	0.06 (0.03)
σ_w	0.14 (0.13)	0.06	0.16 (0.05)	0.20 (0.20)	0.18 (0.15)
σ_T	0.10 (0.10)	0.10	0.12 (0.02)	0.11 (0.02)	0.10 (0.03)
σ_q	0.11 (0.07)		0.21 (0.07)	0.12 (0.05)	0.19 (0.14)
σ_c	0.09 (0.07)		0.23 (0.08)	0.17 (0.07)	0.22 (0.20)

Table 12 Wind velocity and scalar similarity characteristic analysis results for daytime (under unstable condition). The similarity constants (C_1, C_2, and C_x), the standard error of estimate (SEE), the coefficient of determination (R^2) and the amount of data (N) for regression are shown. (a)The regression models of wind velocity are of the forms: $\sigma_u/u_* = C_1(1+C_2(-\zeta))^{1/3}$, and $\sigma_w/u_* = C_1(1+C_2(-\zeta))^{1/3}$. (b) The regression model of scalar is of the form: $\sigma_x/x_* = C_x(-\zeta)^{-1/3}$.

(a)

Variable	Site	C_1	C_2	SEE	R^2	N
σ_u/u_*	BT 40m	1.40	3.46	1.03	0.79	1176
	BT 32m	1.42	3.19	0.55	0.79	1176
	AT 28m	1.78	1.28	0.63	0.86	1176
σ_w/u_*	BT 40m	0.91	3.75	0.27	0.97	1176
	BT 32m	0.85	3.71	0.13	0.97	1176
	AT 28m	0.79	3.82	0.15	0.96	1176

(b)

Variable	Site	Cx	SEE	R^2	N
σ_T/T_*	BT 40m	1.21	0.38	0.61	586
	BT 32m	1.29	0.44	0.55	228
	AT 28m	1.46	0.55	0.50	287
σ_q/q_*	BT 40m	1.88	3.85	0.09	586
	BT 32m	1.69	2.97	0.13	228
	AT 28m	1.94	4.23	0.08	287
σ_c/c_*	BT 40m	2.79	2.02	0.16	586
	BT 32m	2.51	1.23	0.28	228
	AT 28m	1.96	0.92	0.34	287

Table 13 Wind velocity similarity constants presented in previous studies under unstable condition ($\zeta < 0$). z and h are in unit of meters.

Study	Description	z	h	z/h	σ_u/u_*	σ_w/u_*
Panofsky et al. (1984)					$2.29(1+0.04(-\zeta))^{1/3}$	$1.25(1+3(-\zeta))^{1/3}$
De Bruin et al. (1993)	Plain	11.3				
Andreas et al. (1998)	Flat grass land	4	0.25	16		$1.07(1+4.29(-\zeta))^{1/3}$
Choi et al. (2004)	Tibetan prairie	2.85	0.05	57	$3.13(1+8(-\zeta))^{1/3}$	$1.12(1+2.8(-\zeta))^{1/3}$
Detto et al. (2008)	Mediterranean	10	5	2		$1.2\ (1+2(-\zeta))^{1/3}$
Marques et al. (2008)	Wetland	25	7	3.57		$1.17(1+2.44(-\zeta))^{1/3}$
This Study	Mountainous forest	40	27	1.43	$1.40(1+3.46(-\zeta))^{1/3}$	$0.91(1+1.75(-\zeta))^{1/3}$
		32	27	1.14	$1.14(1+3.19(-\zeta))^{1/3}$	$0.85(1+3.71(-\zeta))^{1/3}$
		28	27	1.04	$1.78(1+1.28(-\zeta))^{1/3}$	$0.79(1+3.82(-\zeta))^{1/3}$

Table 14 Scalar similarity constants presented in previous studies under unstable condition ($\zeta < 0$). z and h are in unit of meters.

Study	Description	z	h	z/h	C_T	C_q	C_c
Lamaud and Irvine(2006)		40	19	2.1	0.95	1.3	
Cava et al.(2008)	Coniferous forest	32	29	1.1	1.09	1.61	
Hsieh et al.(2008)(a)	Grassland	10	0.45	22.2	1.1	1.1	0.95
Hsieh et al.(2008)(b)	Rice paddy	2	0.65	3.08	1.0	1.0	1.0
Hsieh et al.(2008)(c)	Cypress forest	23.8	10.3	2.31	1.25	1.5	1.7
Marques et al.(2008)	Wetland	25	7	3.57	1.15		
Guo et al.(2009)	Farmland	1.8	0.2	9	1.16	0.92	1.1
This Study	Mountainous forest	40	27	1.43	1.21	1.88	2.79
		32	27	1.14	1.29	1.69	2.51
		28	27	1.04	1.46	1.94	0.92

Table 15 Wind velocity similarity constants presented in previous studies under neutral condition ($\zeta \sim 0$). z and h are in unit of meters.

Study	Description	z	h	z/h	$C_1(u)$	$C_1(w)$
Panofsky et al.(1984)					2.39	1.30
Hogstrom(1990)					2.78	
Andreas et al.(1998)	Flat grass land	4	0.25	16	2.55	1.25
Moraes et al.(2005)					2.4	1.2
This Study	Mountainous forest	40	27	1.43	3	1
		32	27	1.14	2.5	1
		28	27	1.04	3	1

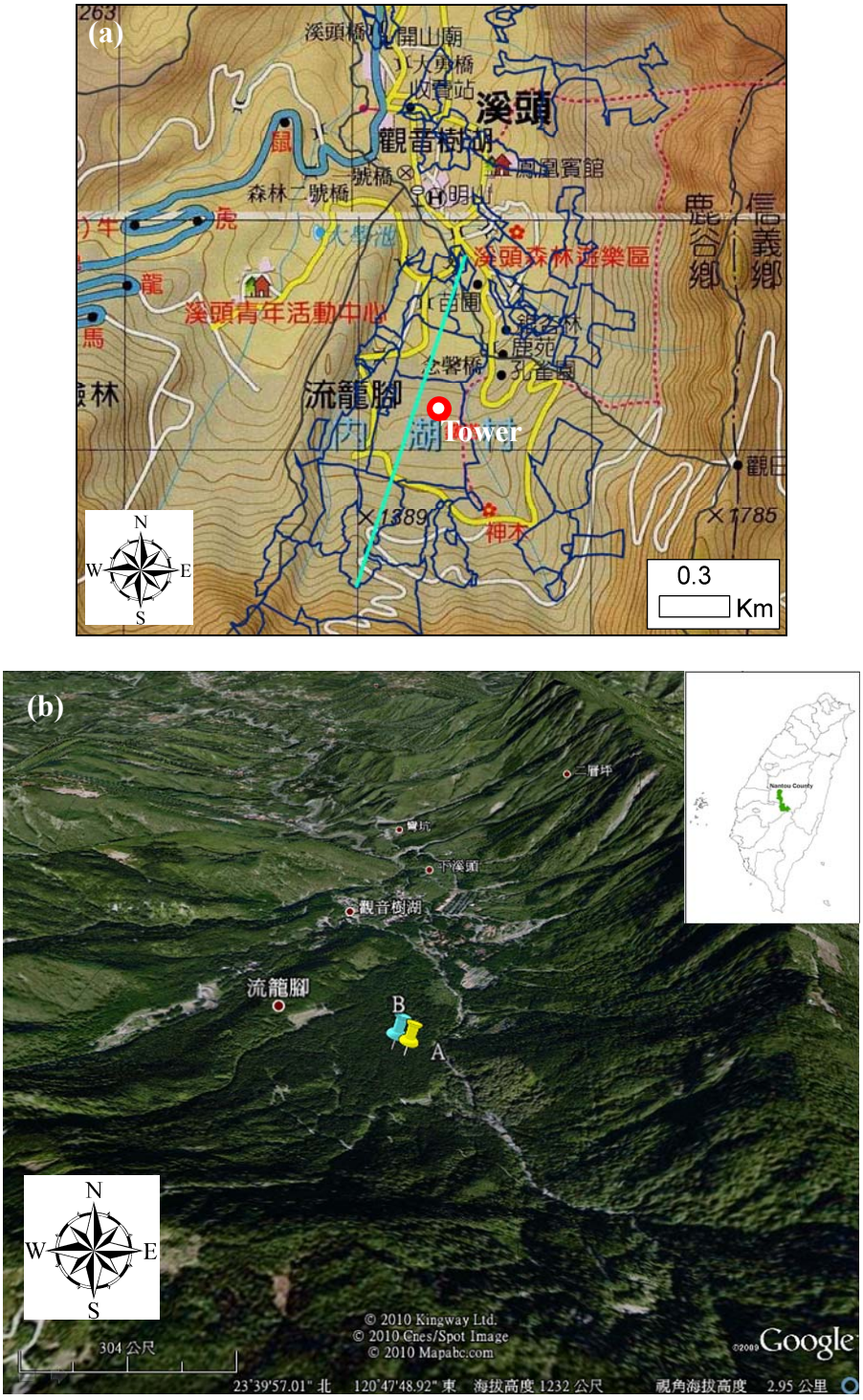
(a)
溪頭
觀音樹湖
溪頭森林遊樂區
溪頭青年活動中心
流籠腳
Tower
N
W
E
S
0.3
Km
(b)
觀音樹湖
流籠腳
B
A
© 2010 Kingway Ltd.
© 2010 Cnes/Spot Image
© 2010 Mapabc.com
Google
304 公尺
23°39'57.01" 北 120°47'48.92" 東 海拔高度 1232 公尺
視角海拔高度 2.95 公里

Figure 1

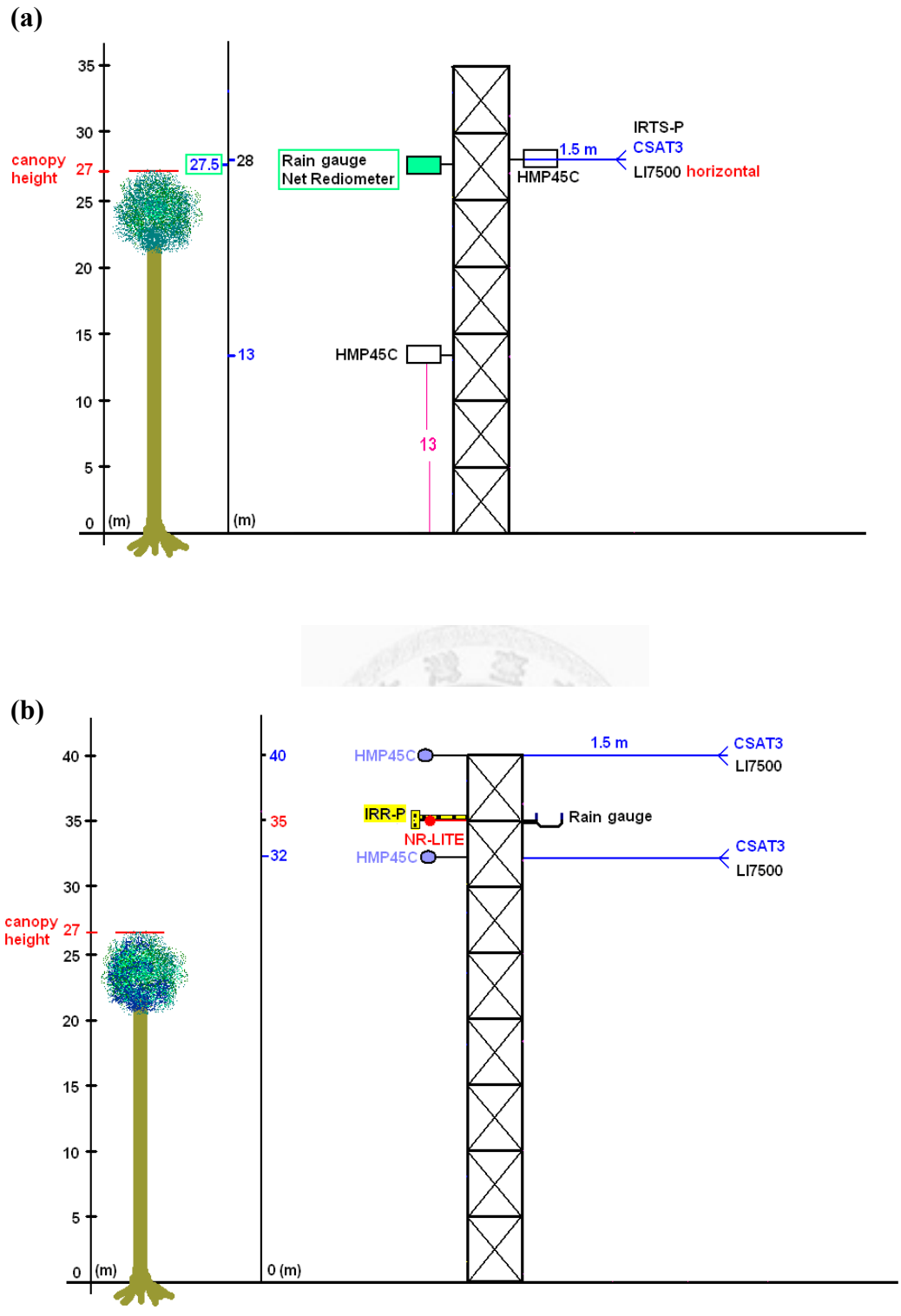
(a)
35
30
canopy
height
27
25
20
15
10
5
0
(m)
27.5
28
13
(m)
Rain gauge
Net Rediometer
HMP45C
13
1.5 m
IRTS-P
CSAT3
LI7500 horizontal
HMP45C
(b)
40
35
32
canopy
height
27
25
20
15
10
5
0
(m)
40
35
32
0 (m)
HMP45C
IRR-P
NR-LITE
HMP45C
1.5 m
CSAT3
LI7500
Rain gauge
CSAT3
LI7500

Figure 2

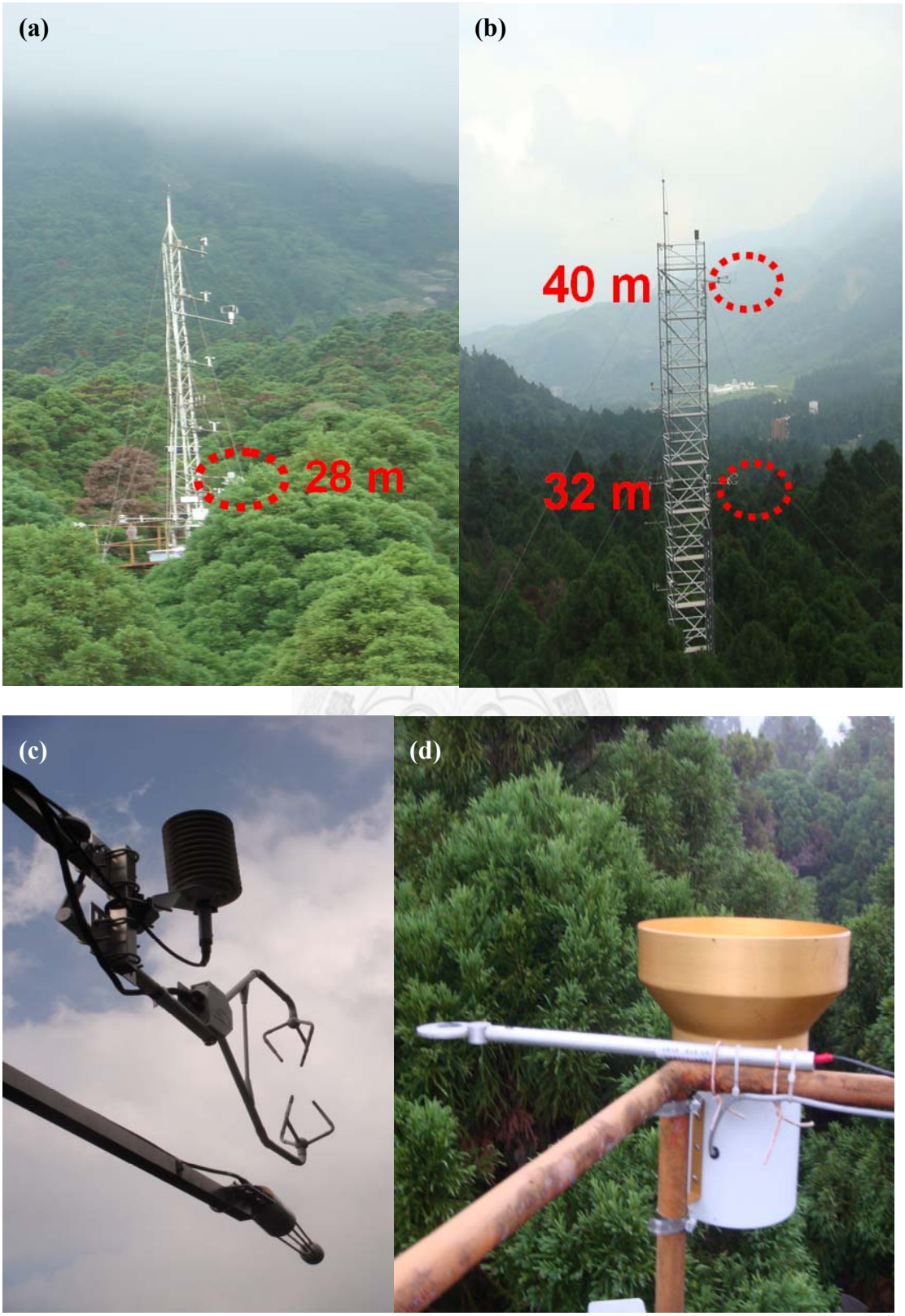

Figure 3

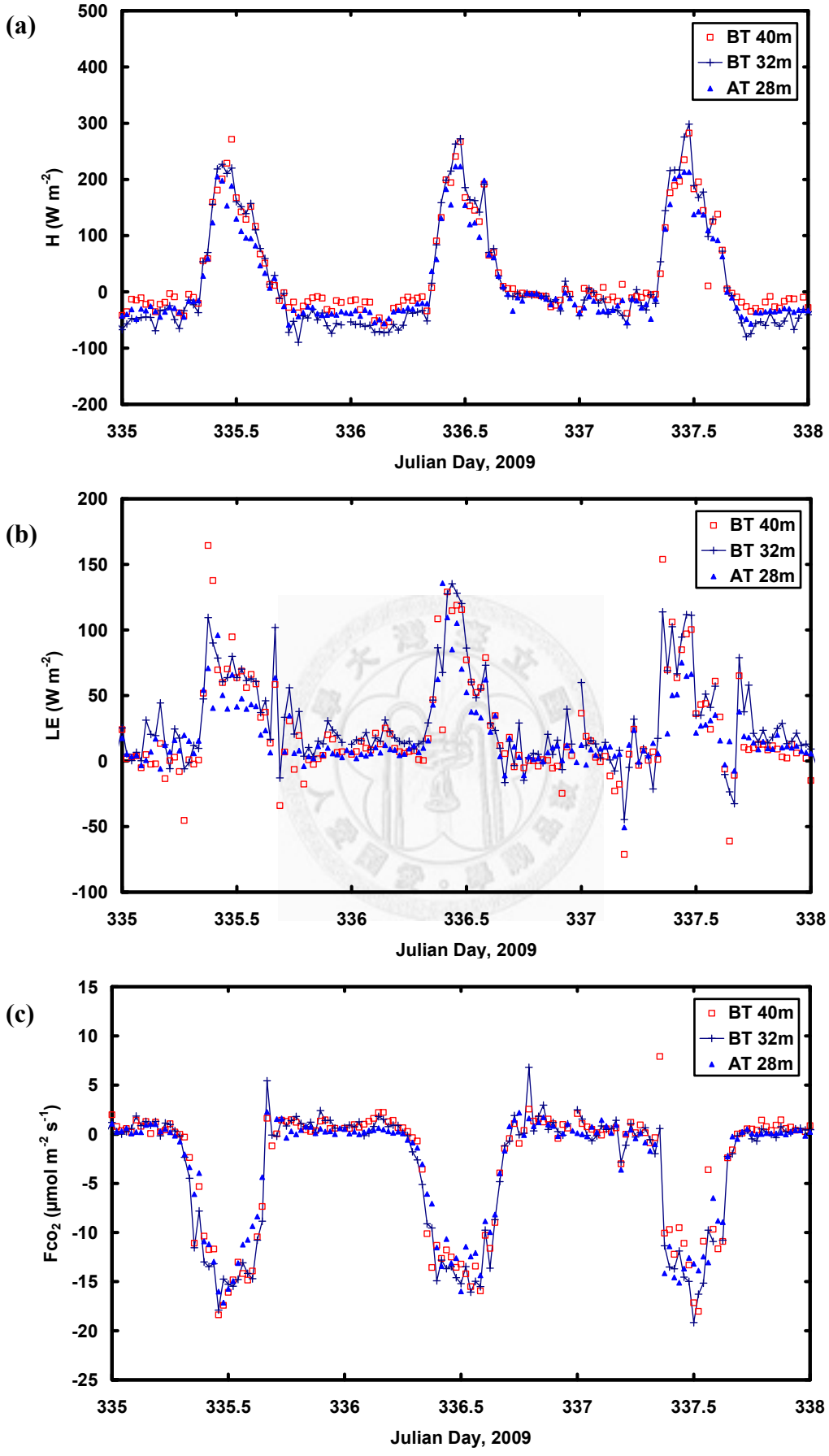
(a)
BT 40m
BT 32m
AT 28m
H (W m-2)
500
400
300
200
100
0
-100
-200
335
335.5
336
336.5
337
337.5
338
Julian Day, 2009
(b)
BT 40m
BT 32m
AT 28m
LE (W m-2)
200
150
100
50
0
-50
-100
335
335.5
336
336.5
337
337.5
338
Julian Day, 2009
(c)
BT 40m
BT 32m
AT 28m
Fco2 (μmol m-2 s-1)
15
10
5
0
-5
-10
-15
-20
-25
335
335.5
336
336.5
337
337.5
338
Julian Day, 2009

Figure 4

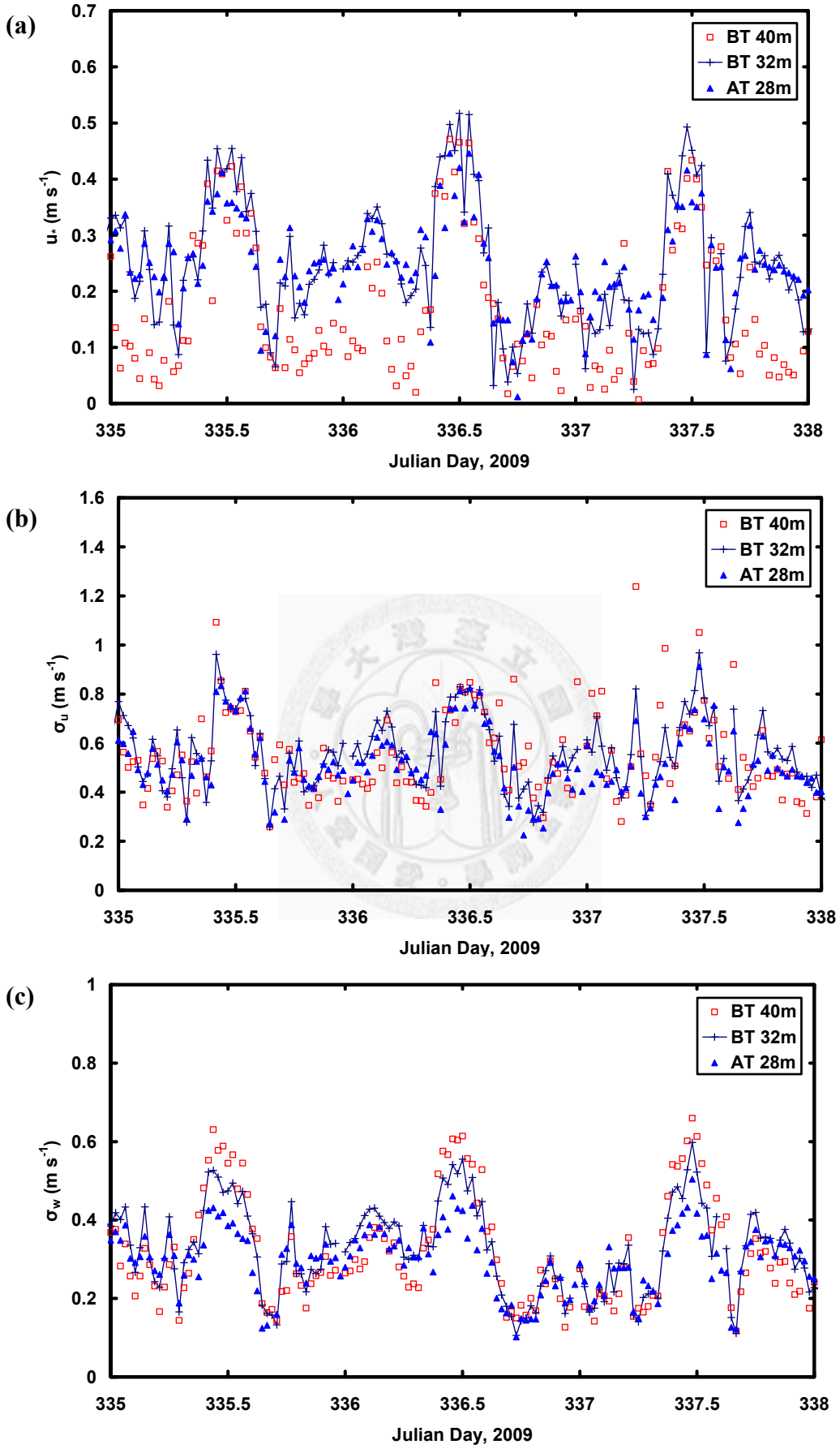
(a)
BT 40m
BT 32m
AT 28m
u* (m s-1)
0.7
0.6
0.5
0.4
0.3
0.2
0.1
0
335
335.5
336
336.5
337
337.5
338
Julian Day, 2009
(b)
BT 40m
BT 32m
AT 28m
σu (m s-1)
1.6
1.4
1.2
1
0.8
0.6
0.4
0.2
0
335
335.5
336
336.5
337
337.5
338
Julian Day, 2009
(c)
BT 40m
BT 32m
AT 28m
σw (m s-1)
1
0.8
0.6
0.4
0.2
0
335
335.5
336
336.5
337
337.5
338
Julian Day, 2009

Figure 5

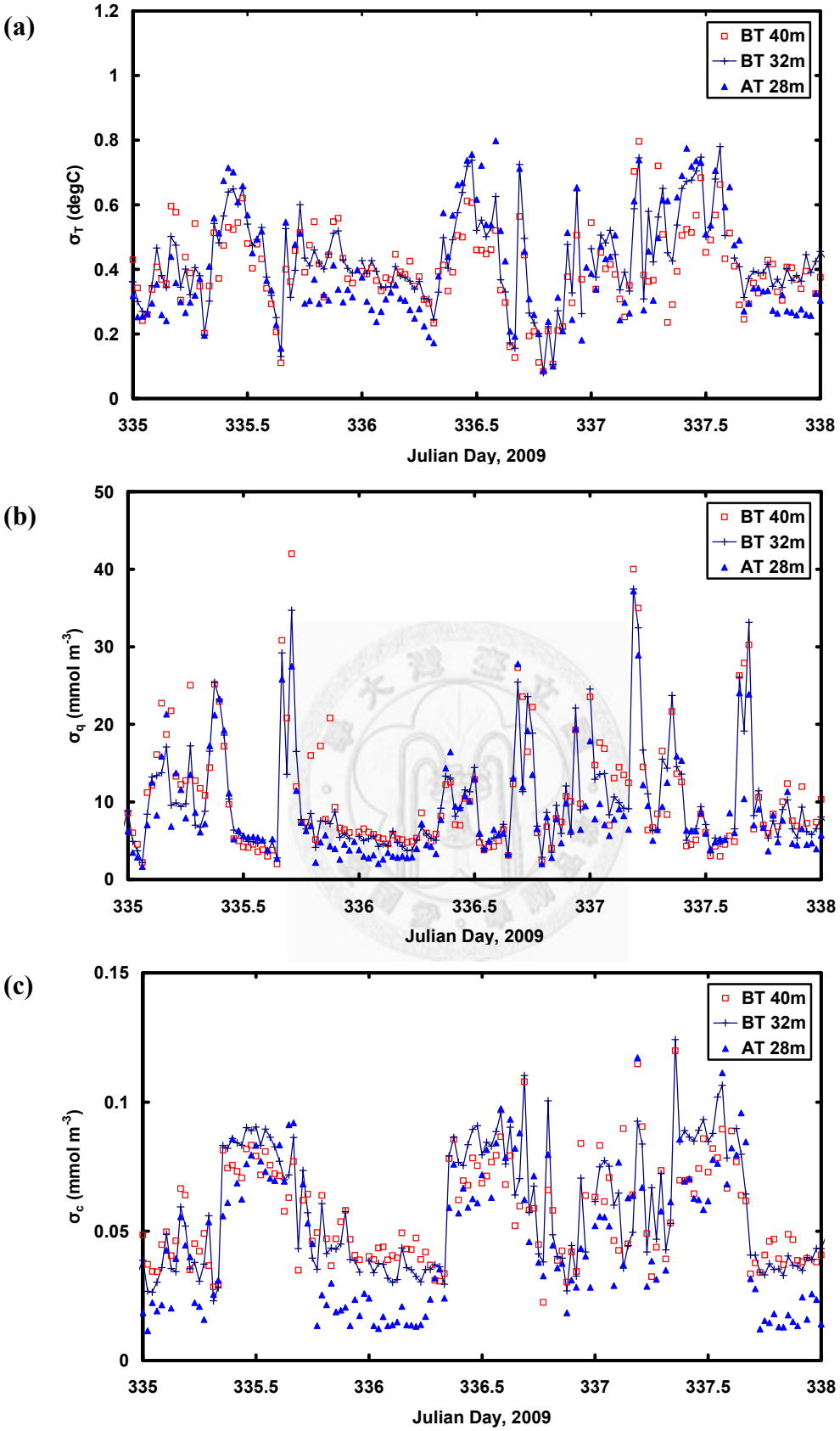
(a)
BT 40m
BT 32m
AT 28m
σT (degC)
Julian Day, 2009
(b)
σq (mmol m-3)
(c)
σc (mmol m-3)

Figure 6

(a)

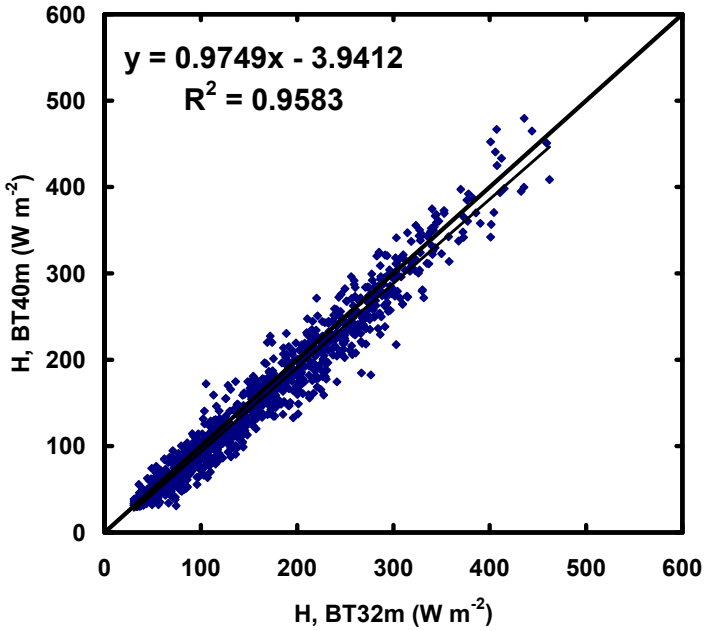
y = 0.9749x - 3.9412
R2 = 0.9583
H, BT40m (W m-2)
H, BT32m (W m-2)
0
100
200
300
400
500
600

(b)

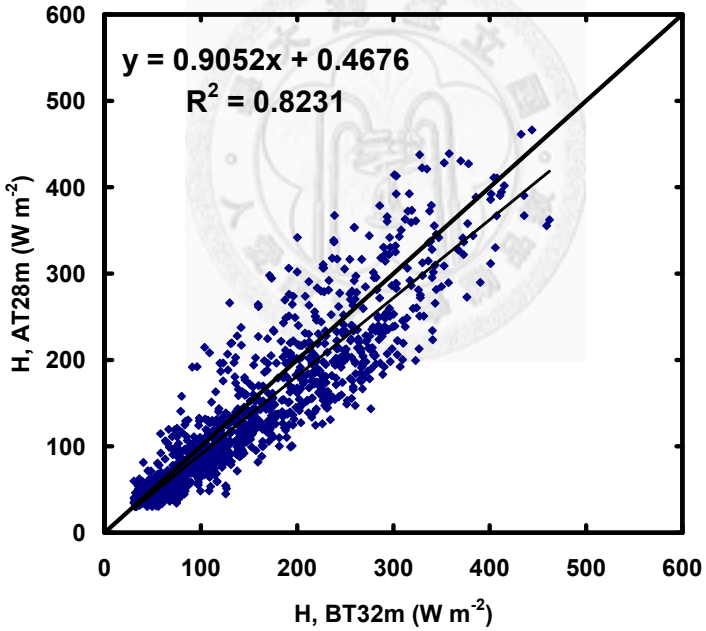
y = 0.9052x + 0.4676
R2 = 0.8231
H, AT28m (W m-2)
H, BT32m (W m-2)
0
100
200
300
400
500
600

Figure 7

(a)

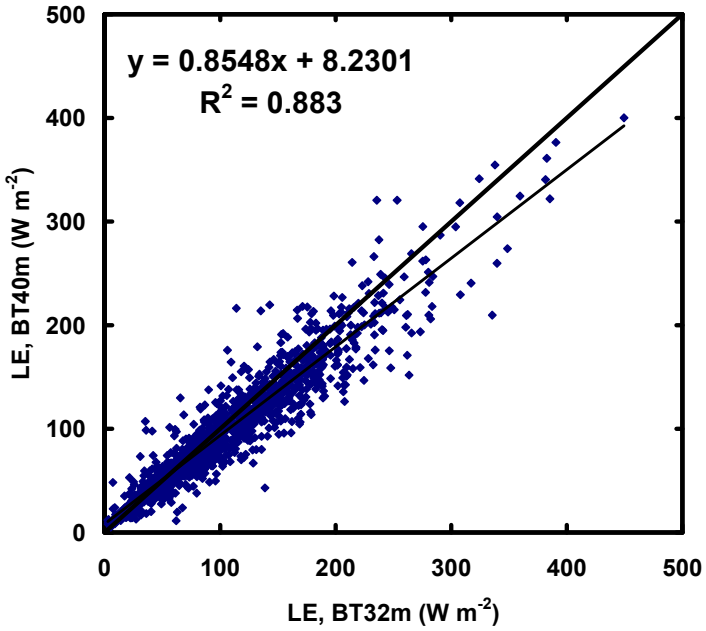
y = 0.8548x + 8.2301
R2 = 0.883
LE, BT40m (W m-2)
LE, BT32m (W m-2)
0
100
200
300
400
500

(b)

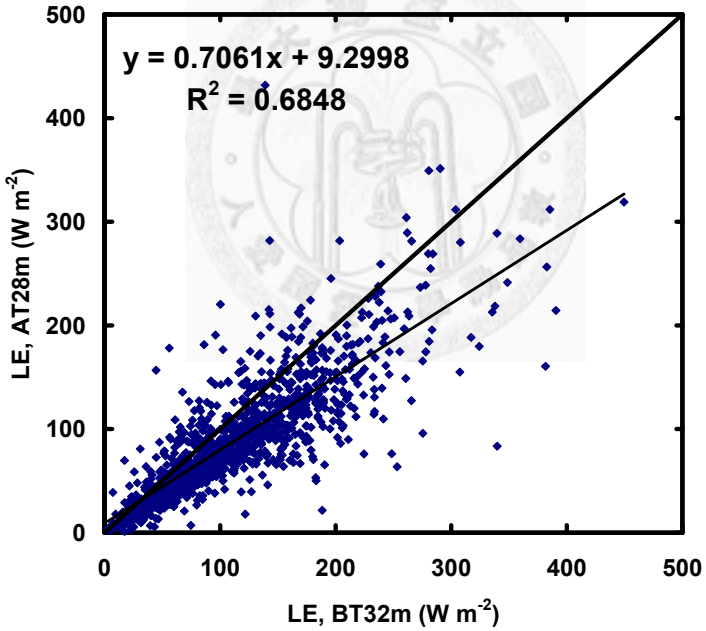
y = 0.7061x + 9.2998
R2 = 0.6848
LE, AT28m (W m-2)
LE, BT32m (W m-2)
0
100
200
300
400
500

Figure 8

(a)

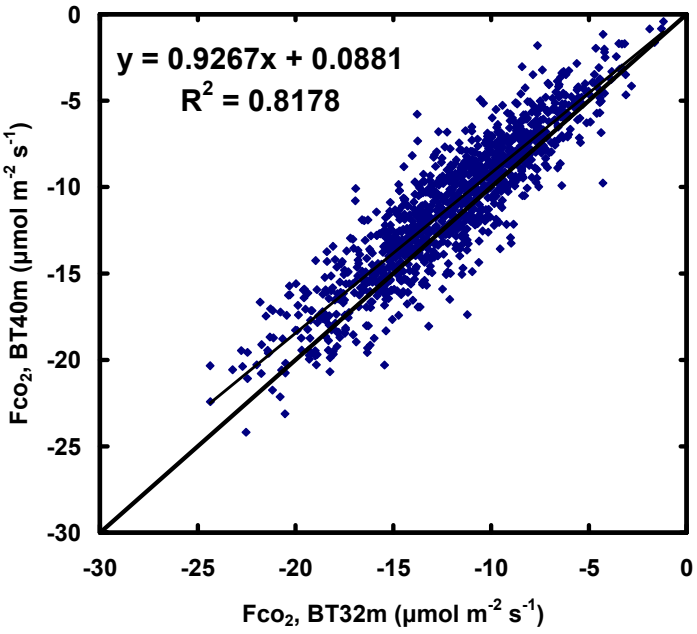
y = 0.9267x + 0.0881
R2 = 0.8178
Fco2, BT40m (μmol m-2 s-1)
Fco2, BT32m (μmol m-2 s-1)
0
-5
-10
-15
-20
-25
-30

(b)

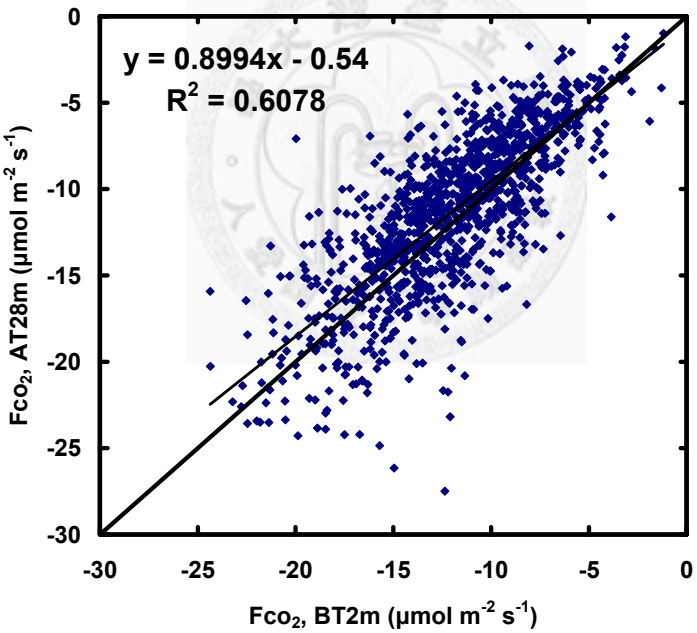
y = 0.8994x - 0.54
R2 = 0.6078
Fco2, AT28m (μmol m-2 s-1)
Fco2, BT2m (μmol m-2 s-1)
0
-5
-10
-15
-20
-25
-30

Figure 9

(a)

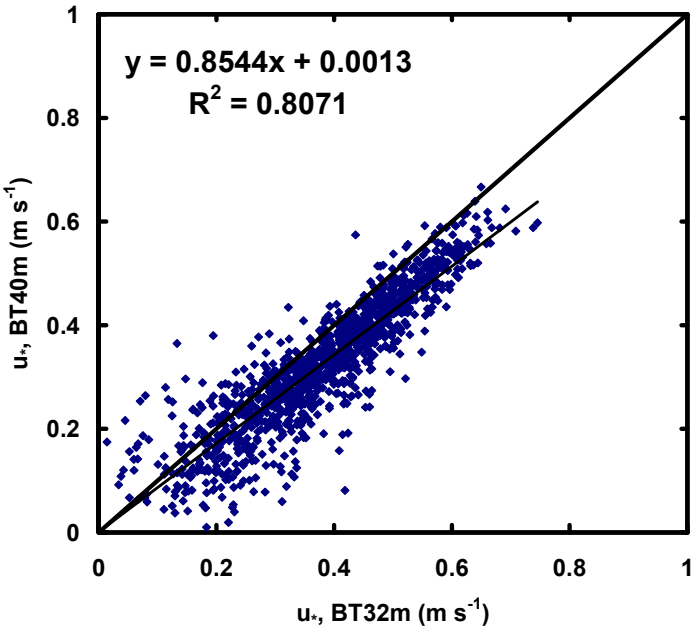
y = 0.8544x + 0.0013
R2 = 0.8071
u*, BT40m (m s-1)
u*, BT32m (m s-1)
0
0.2
0.4
0.6
0.8
1

(b)

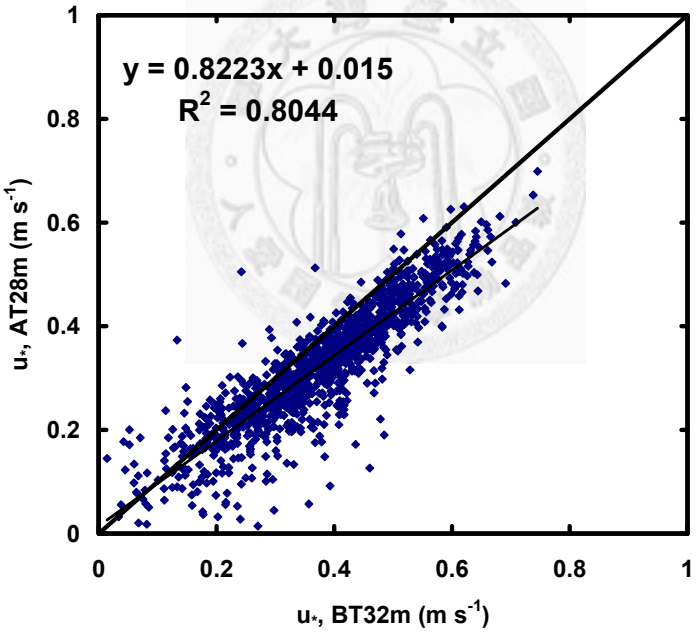
y = 0.8223x + 0.015
R2 = 0.8044
u*, AT28m (m s-1)
u*, BT32m (m s-1)
0
0.2
0.4
0.6
0.8
1

Figure 10

(a)

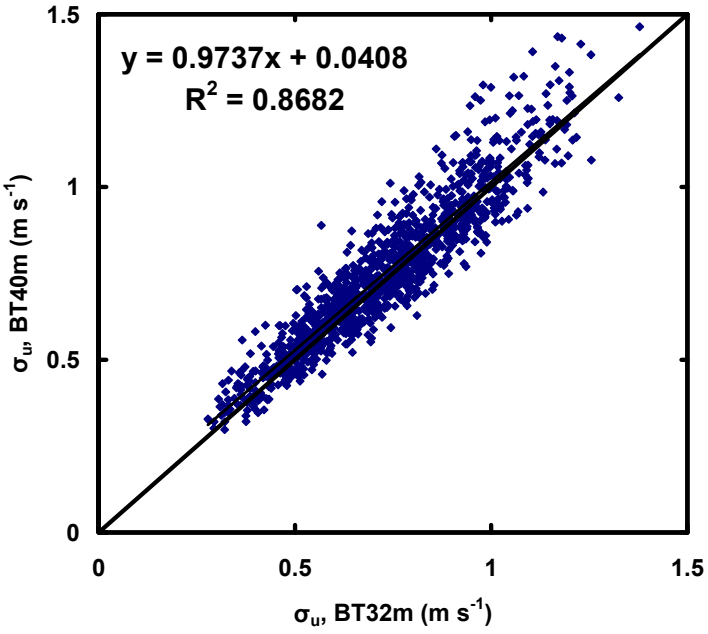
y = 0.9737x + 0.0408
R2 = 0.8682
σu, BT40m (m s-1)
σu, BT32m (m s-1)
0
0.5
1
1.5

(b)

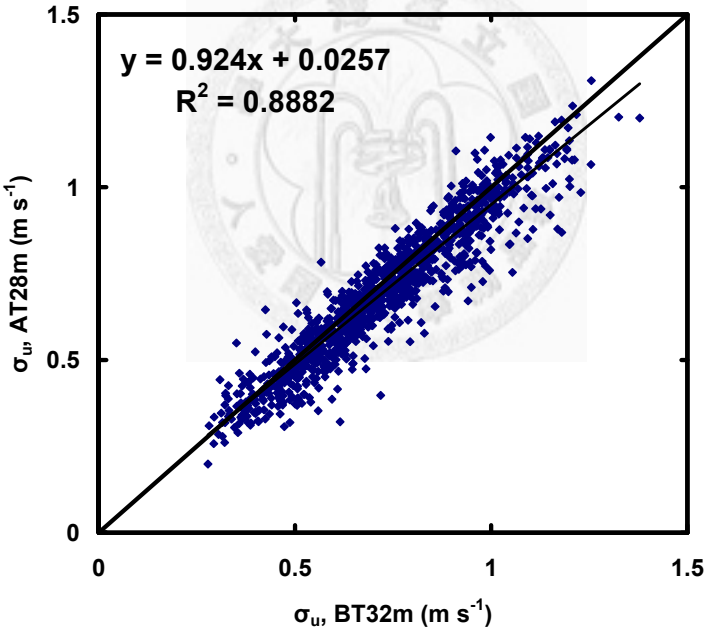
y = 0.924x + 0.0257
R2 = 0.8882
σu, AT28m (m s-1)
σu, BT32m (m s-1)
0
0.5
1
1.5

Figure 11

(a)

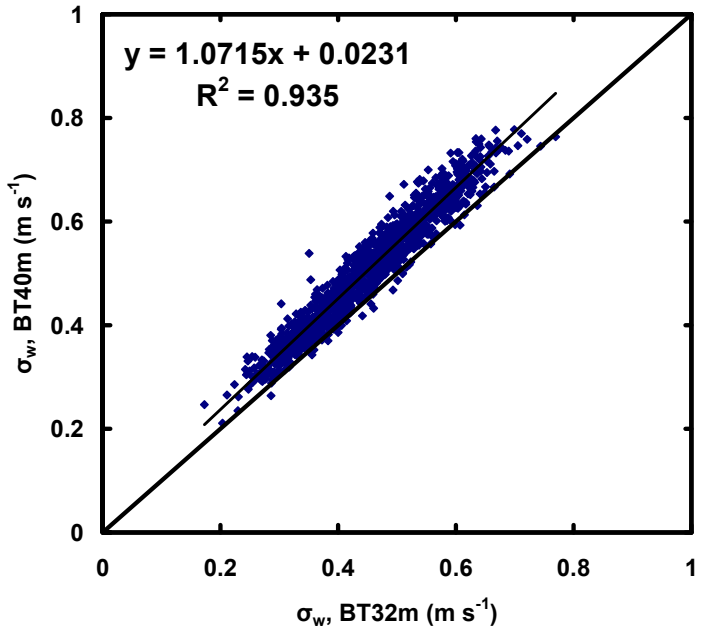
y = 1.0715x + 0.0231
R2 = 0.935
σw, BT40m (m s-1)
σw, BT32m (m s-1)
0
0.2
0.4
0.6
0.8
1

(b)

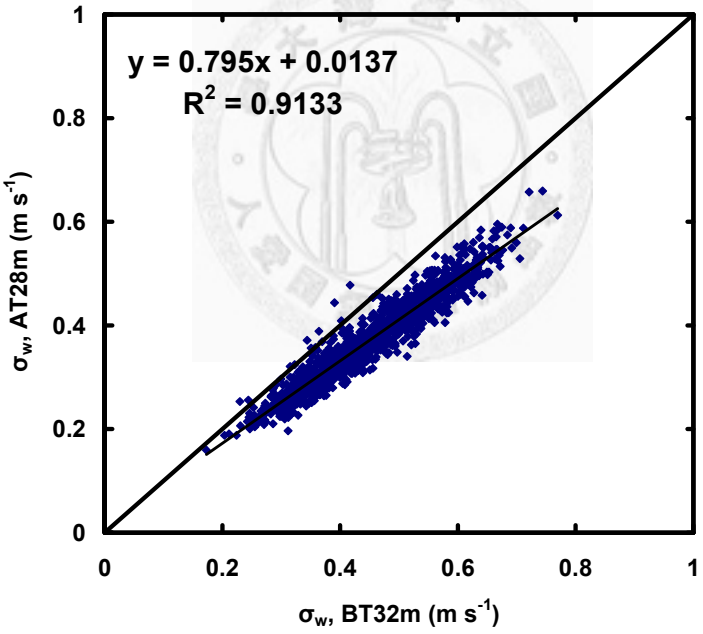
y = 0.795x + 0.0137
R2 = 0.9133
σw, AT28m (m s-1)
σw, BT32m (m s-1)
0
0.2
0.4
0.6
0.8
1

Figure 12

(a)

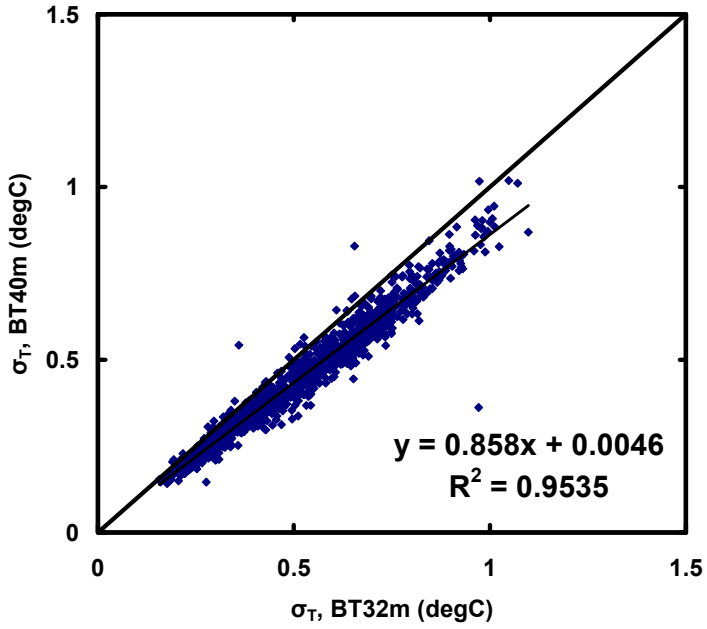
1.5
1
0.5
0
0
0.5
1
1.5
σT, BT40m (degC)
σT, BT32m (degC)
y = 0.858x + 0.0046
R2 = 0.9535

(b)

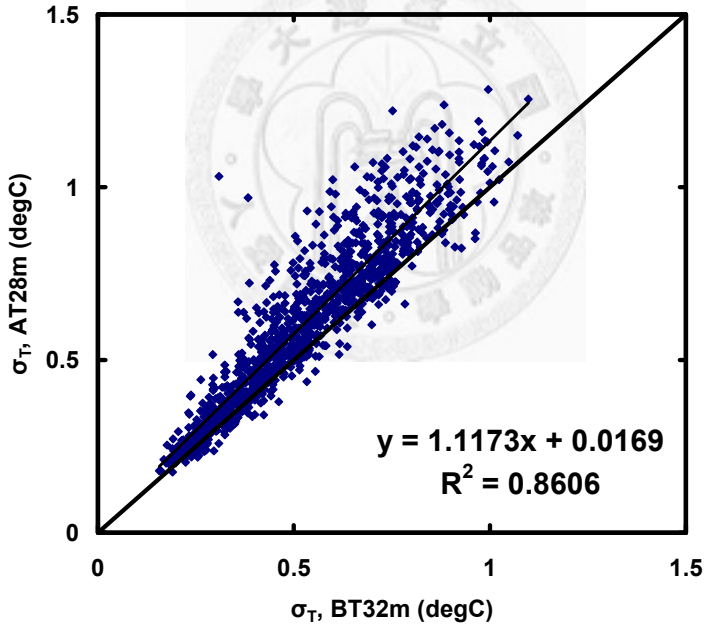
1.5
1
0.5
0
0
0.5
1
1.5
σT, AT28m (degC)
σT, BT32m (degC)
y = 1.1173x + 0.0169
R2 = 0.8606

Figure 13

(a)

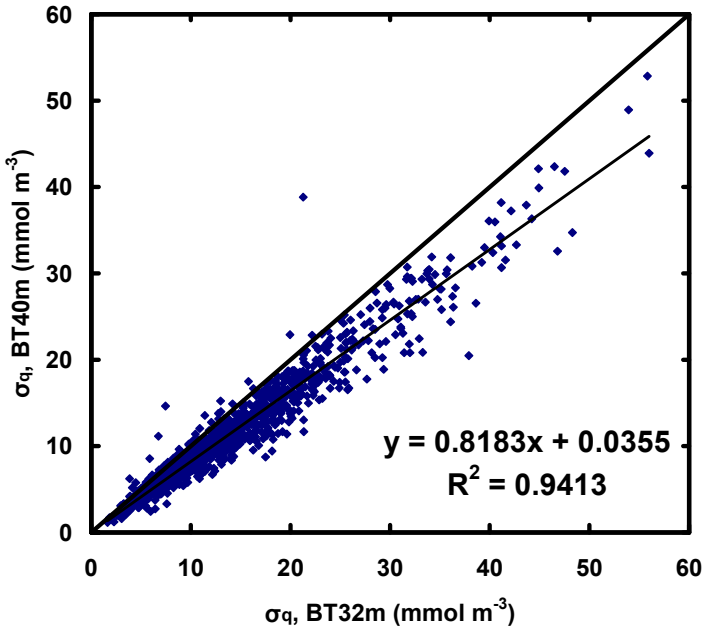
σq, BT40m (mmol m-3)
σq, BT32m (mmol m-3)
y = 0.8183x + 0.0355
R2 = 0.9413
0
10
20
30
40
50
60

(b)

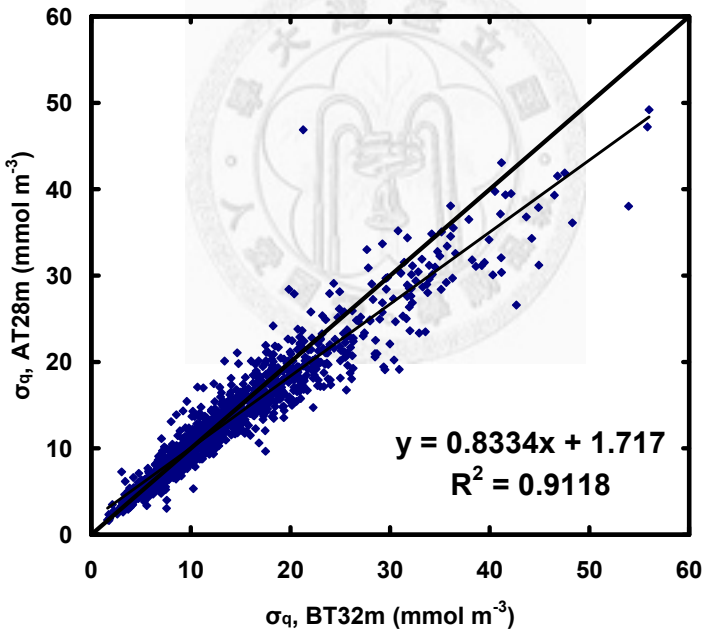
σq, AT28m (mmol m-3)
σq, BT32m (mmol m-3)
y = 0.8334x + 1.717
R2 = 0.9118
0
10
20
30
40
50
60

Figure 14

(a)

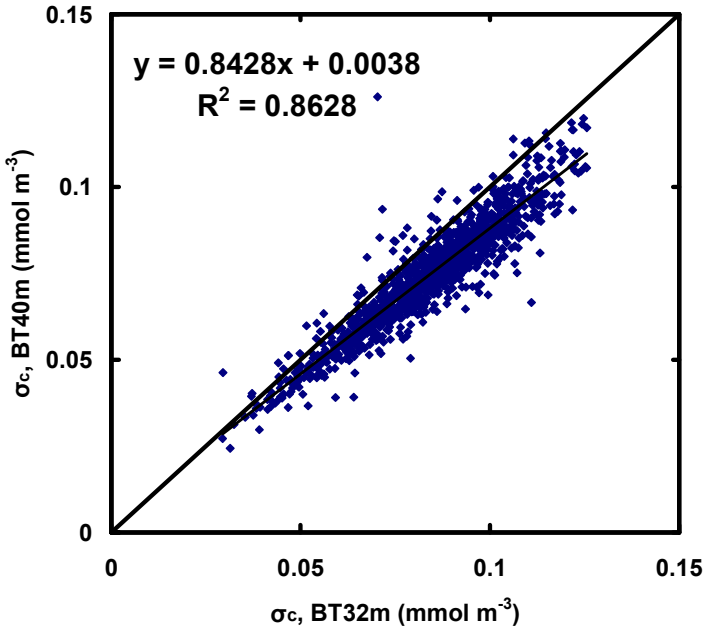
y = 0.8428x + 0.0038
R2 = 0.8628
σc, BT40m (mmol m-3)
σc, BT32m (mmol m-3)
0
0.05
0.1
0.15

(b)

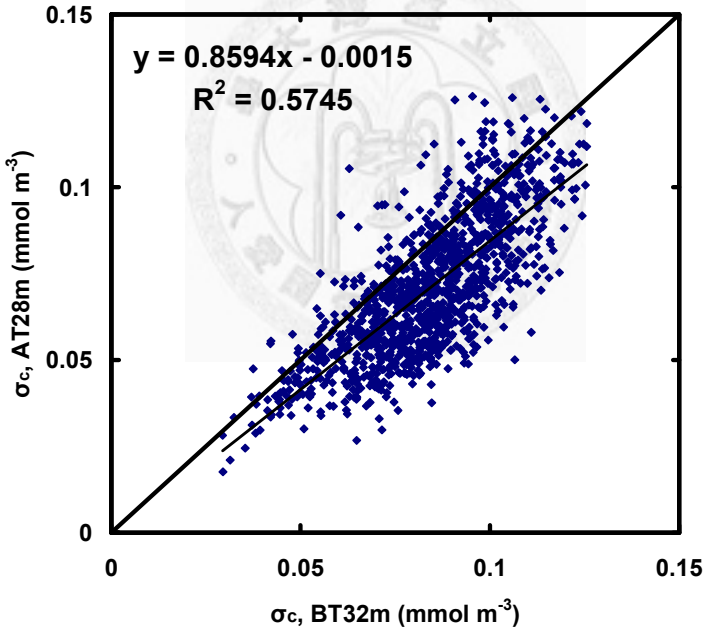
y = 0.8594x - 0.0015
R2 = 0.5745
σc, AT28m (mmol m-3)
σc, BT32m (mmol m-3)
0
0.05
0.1
0.15

Figure 15

(a)

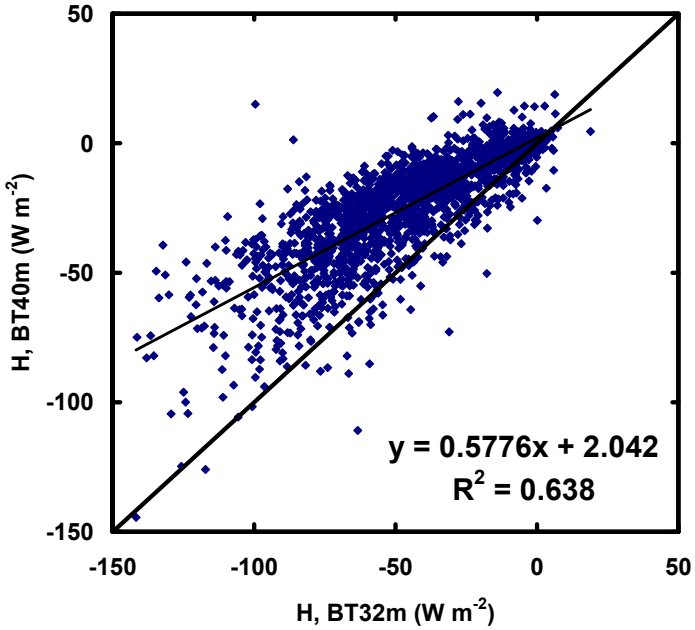
50
0
-50
-100
-150
-150
-100
-50
0
50
H, BT40m (W m-2)
H, BT32m (W m-2)
y = 0.5776x + 2.042
R2 = 0.638

(b)

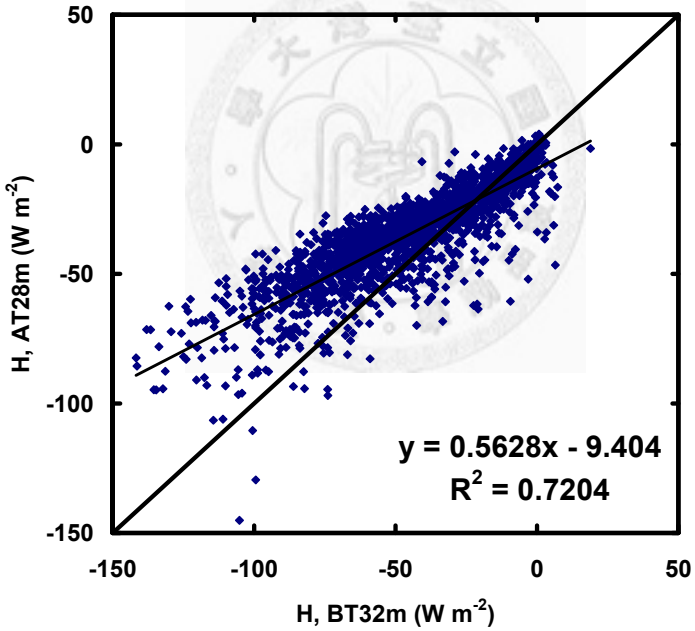
50
0
-50
-100
-150
-150
-100
-50
0
50
H, AT28m (W m-2)
H, BT32m (W m-2)
y = 0.5628x - 9.404
R2 = 0.7204

Figure 16

(a)

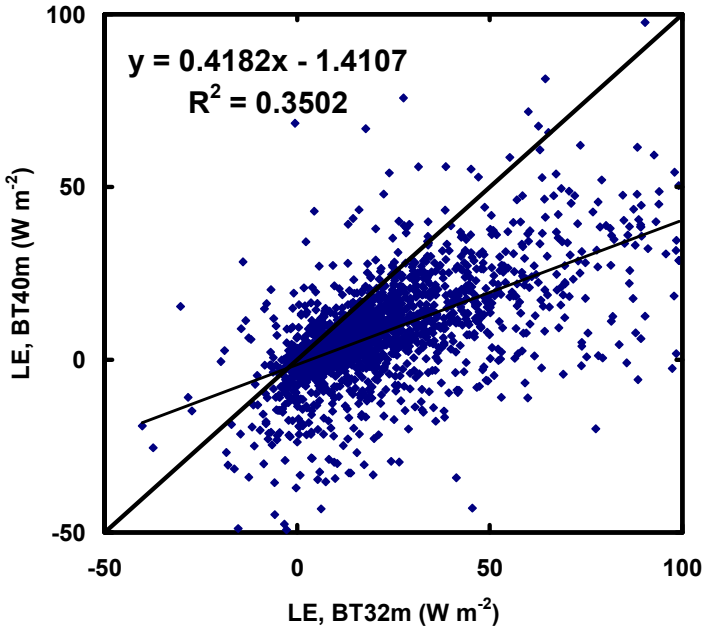
y = 0.4182x - 1.4107
R2 = 0.3502
LE, BT40m (W m-2)
LE, BT32m (W m-2)
100
50
0
-50
-50
0
50
100

(b)

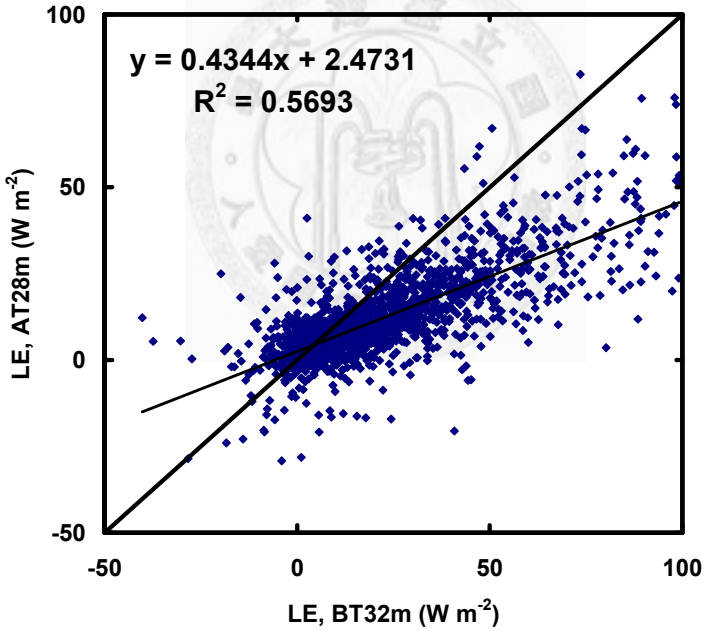
y = 0.4344x + 2.4731
R2 = 0.5693
LE, AT28m (W m-2)
LE, BT32m (W m-2)
100
50
0
-50
-50
0
50
100

Figure 17

(a)

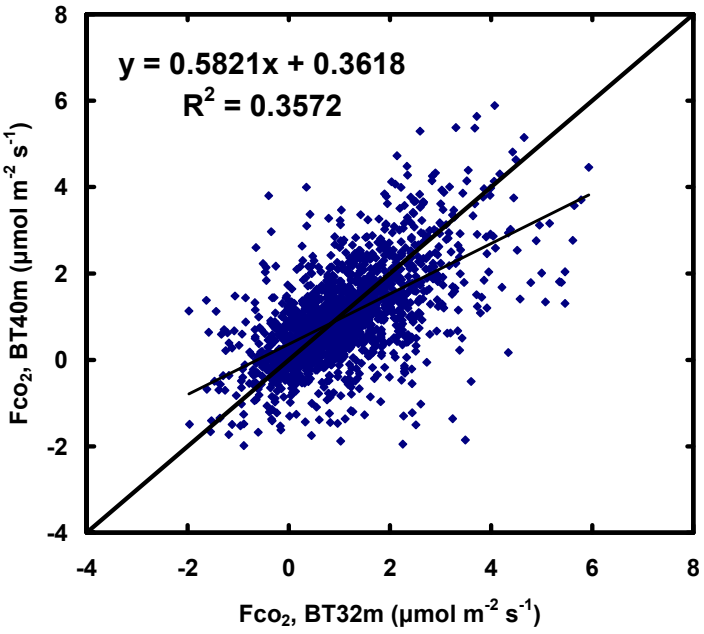
y = 0.5821x + 0.3618
R2 = 0.3572
Fco2, BT40m (μmol m-2 s-1)
Fco2, BT32m (μmol m-2 s-1)
8
6
4
2
0
-2
-4
-4
-2
0
2
4
6
8

(b)

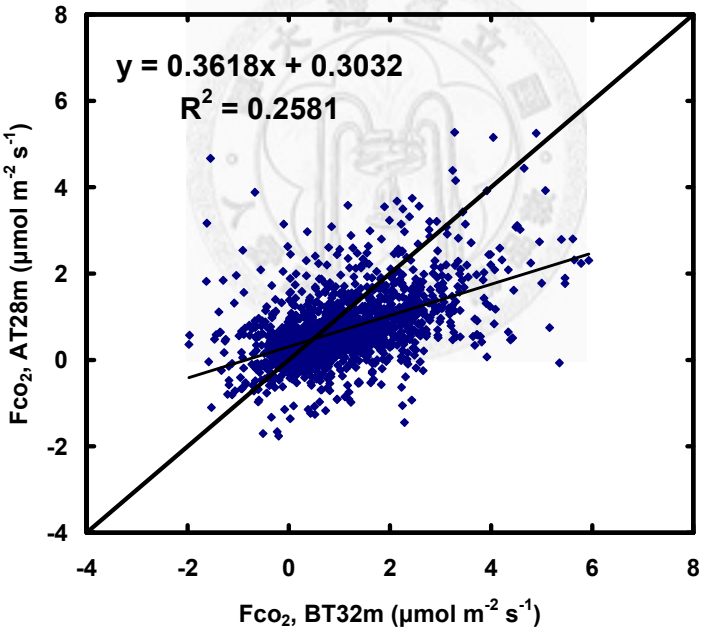
y = 0.3618x + 0.3032
R2 = 0.2581
Fco2, AT28m (μmol m-2 s-1)
Fco2, BT32m (μmol m-2 s-1)
8
6
4
2
0
-2
-4
-4
-2
0
2
4
6
8

Figure 18

(a)

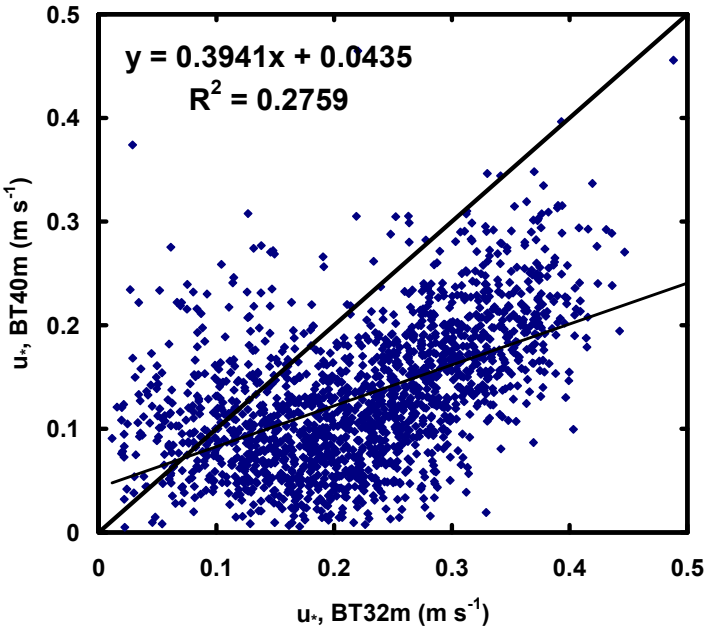
y = 0.3941x + 0.0435
R2 = 0.2759
u*, BT40m (m s-1)
u*, BT32m (m s-1)
0
0.1
0.2
0.3
0.4
0.5

(b)

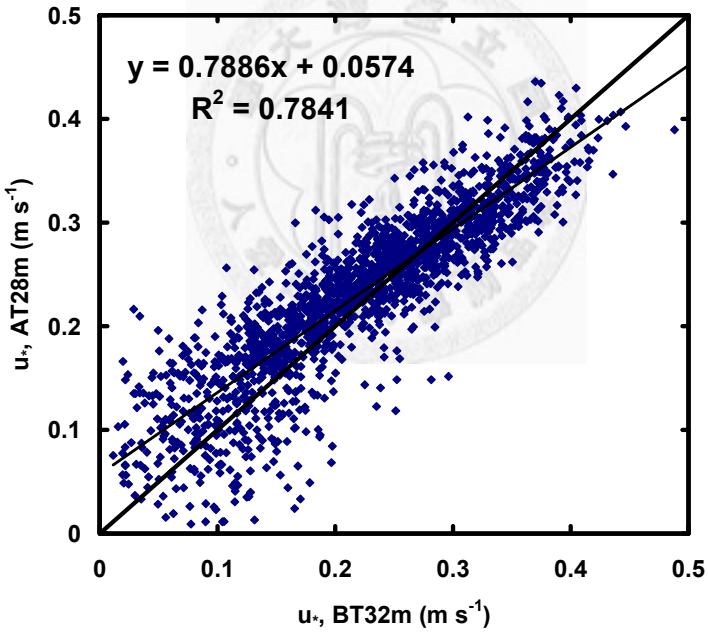
y = 0.7886x + 0.0574
R2 = 0.7841
u*, AT28m (m s-1)
u*, BT32m (m s-1)
0
0.1
0.2
0.3
0.4
0.5

Figure 19

(a)

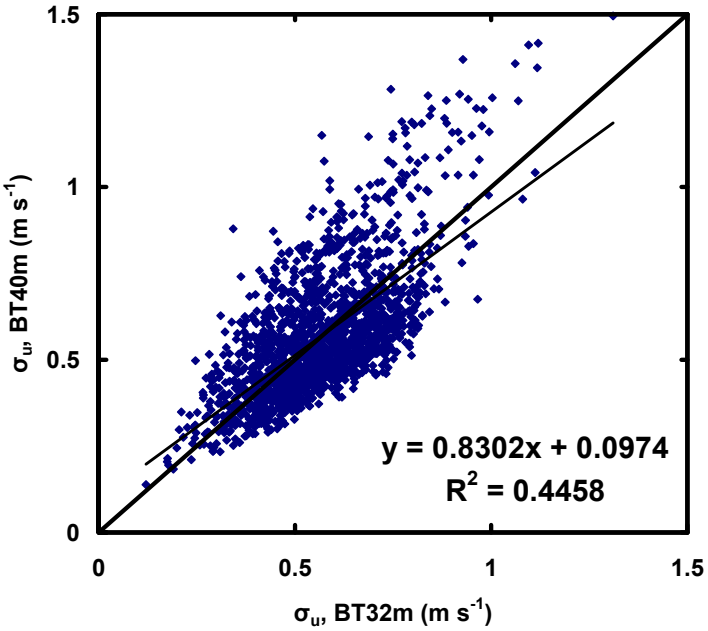
1.5
1
0.5
0
0
0.5
1
1.5
σu, BT40m (m s-1)
σu, BT32m (m s-1)
y = 0.8302x + 0.0974
R2 = 0.4458

(b)

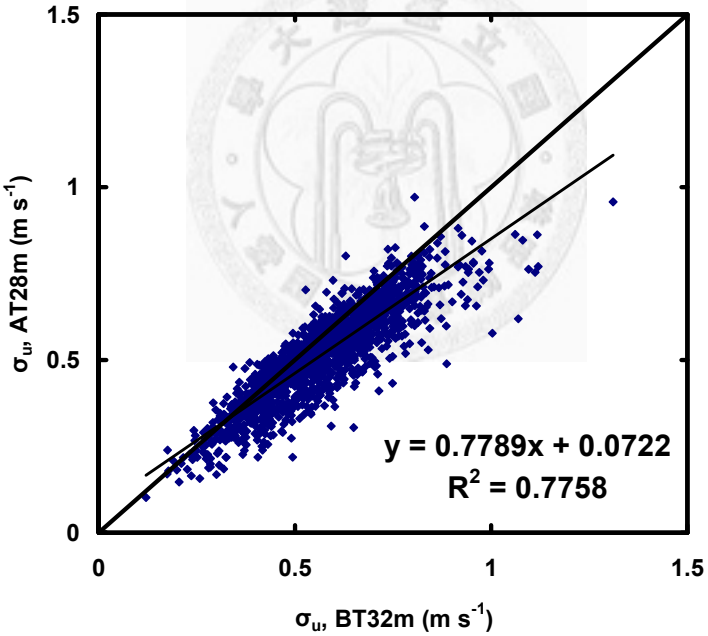
1.5
1
0.5
0
0
0.5
1
1.5
σu, AT28m (m s-1)
σu, BT32m (m s-1)
y = 0.7789x + 0.0722
R2 = 0.7758

Figure 20

(a)

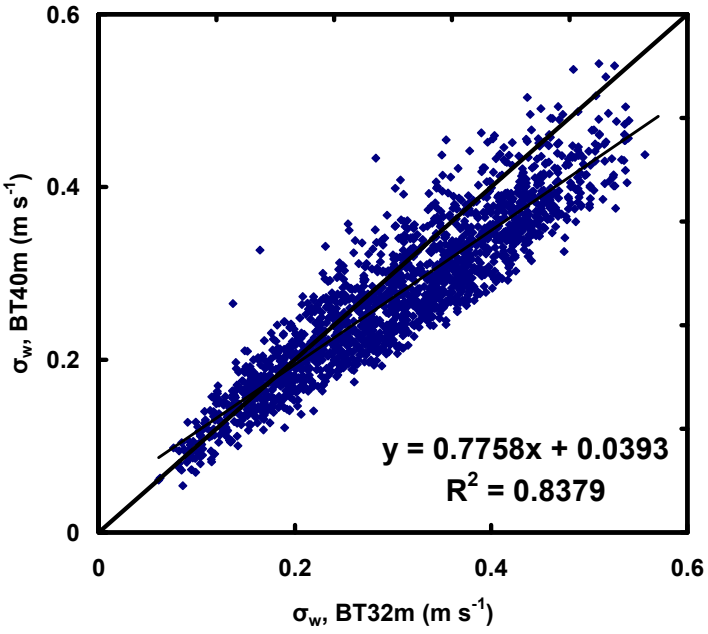
0.6
0.4
0.2
0
0
0.2
0.4
0.6
σw, BT40m (m s-1)
σw, BT32m (m s-1)
y = 0.7758x + 0.0393
R2 = 0.8379

(b)

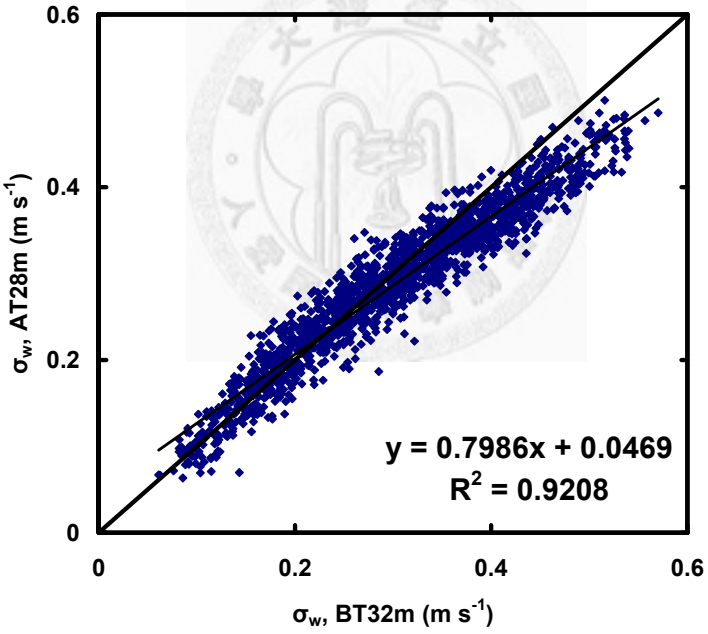
0.6
0.4
0.2
0
0
0.2
0.4
0.6
σw, AT28m (m s-1)
σw, BT32m (m s-1)
y = 0.7986x + 0.0469
R2 = 0.9208

Figure 21

(a)

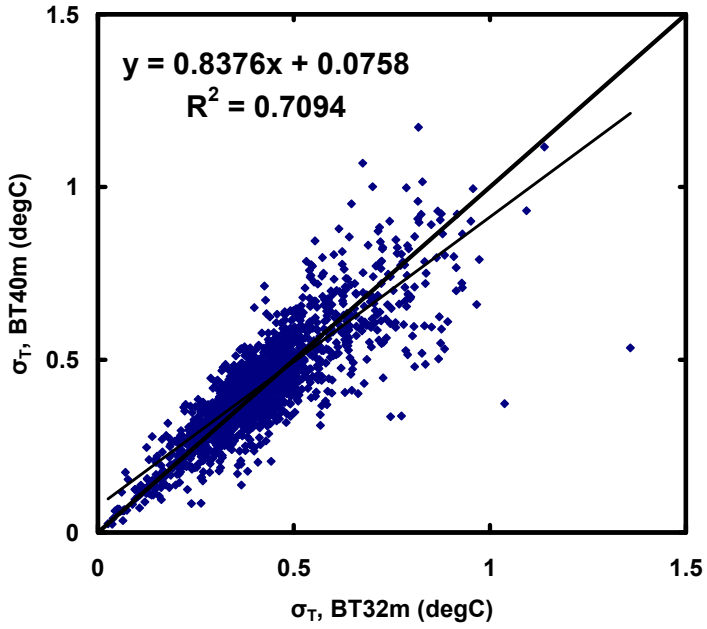
y = 0.8376x + 0.0758
R2 = 0.7094
σT, BT40m (degC)
σT, BT32m (degC)
0
0.5
1
1.5

(b)

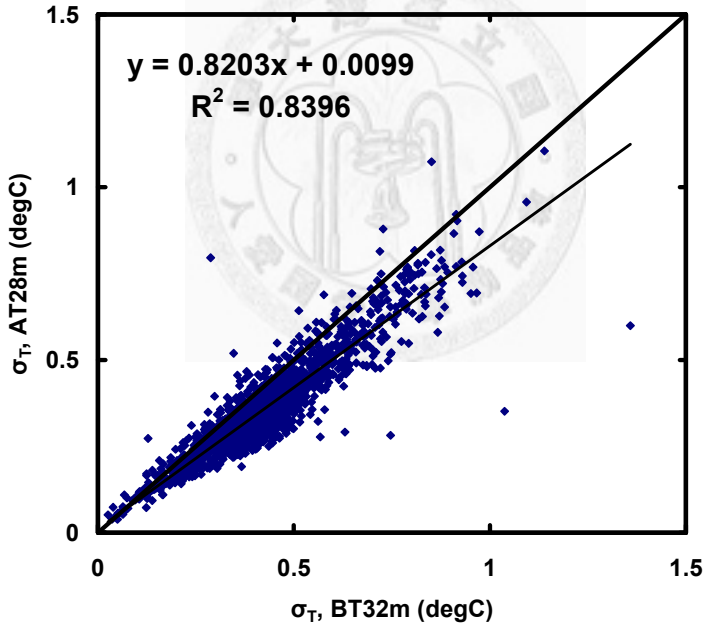
y = 0.8203x + 0.0099
R2 = 0.8396
σT, AT28m (degC)
σT, BT32m (degC)
0
0.5
1
1.5

Figure 22

(a)

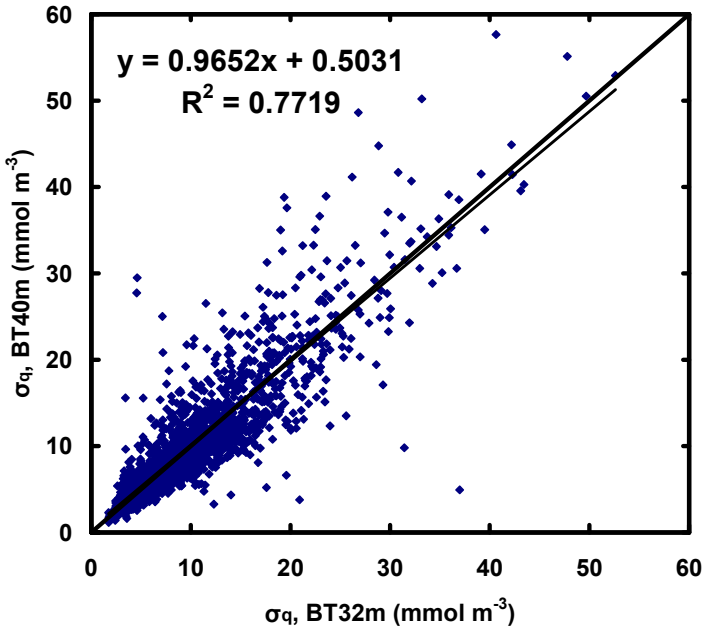
y = 0.9652x + 0.5031
R2 = 0.7719
σq, BT40m (mmol m-3)
σq, BT32m (mmol m-3)
0
10
20
30
40
50
60

(b)

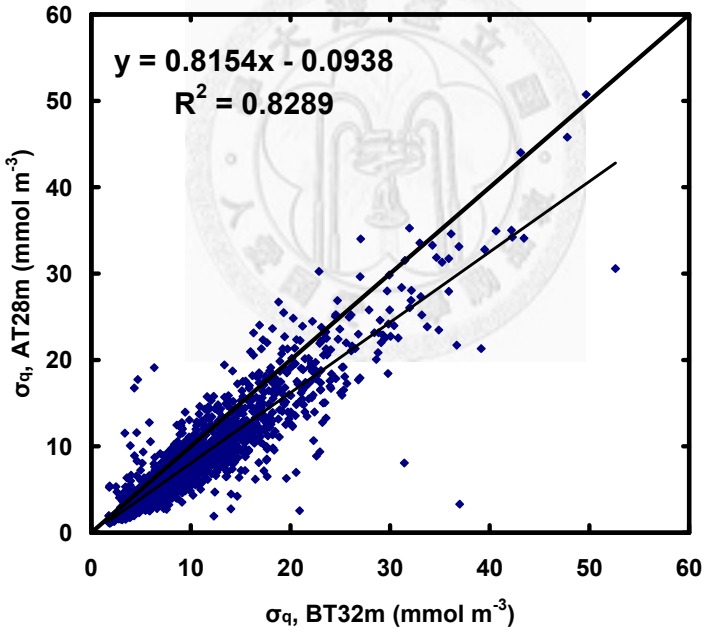
y = 0.8154x - 0.0938
R2 = 0.8289
σq, AT28m (mmol m-3)
σq, BT32m (mmol m-3)
0
10
20
30
40
50
60

Figure 23

(a)

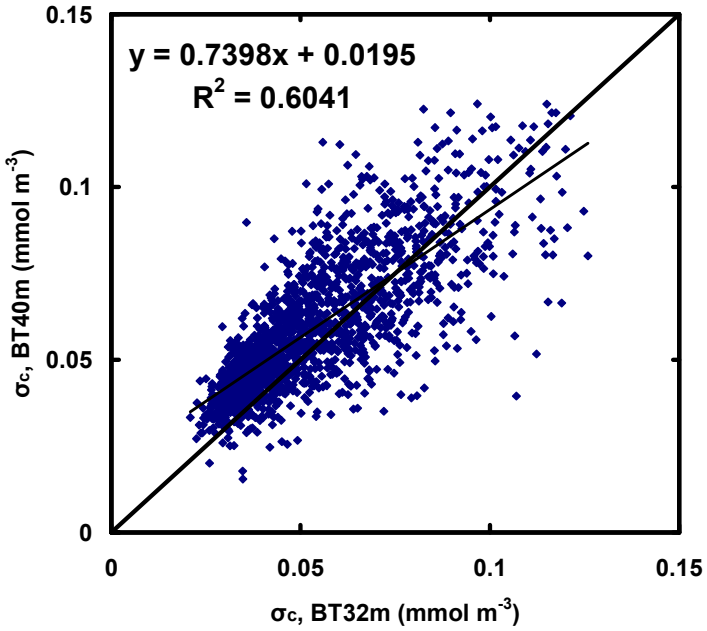
y = 0.7398x + 0.0195
R2 = 0.6041
σc, BT40m (mmol m-3)
σc, BT32m (mmol m-3)
0
0.05
0.1
0.15

(b)

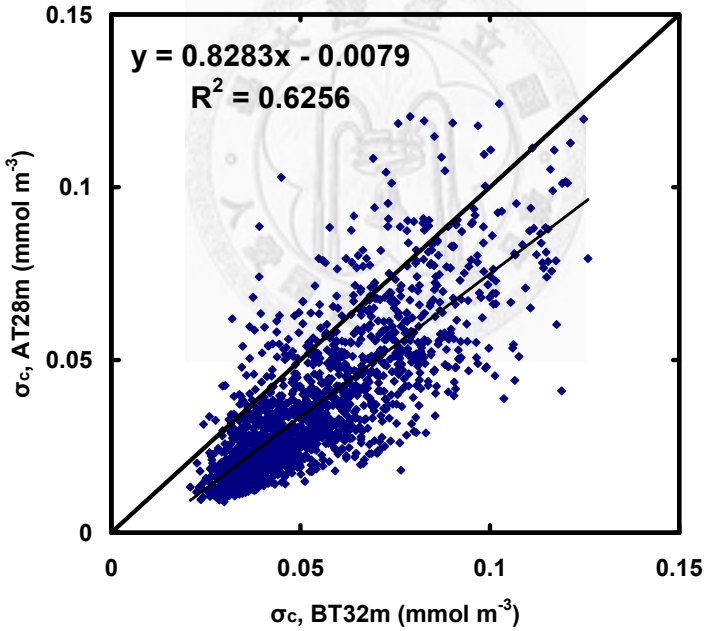
y = 0.8283x - 0.0079
R2 = 0.6256
σc, AT28m (mmol m-3)
σc, BT32m (mmol m-3)
0
0.05
0.1
0.15

Figure 24

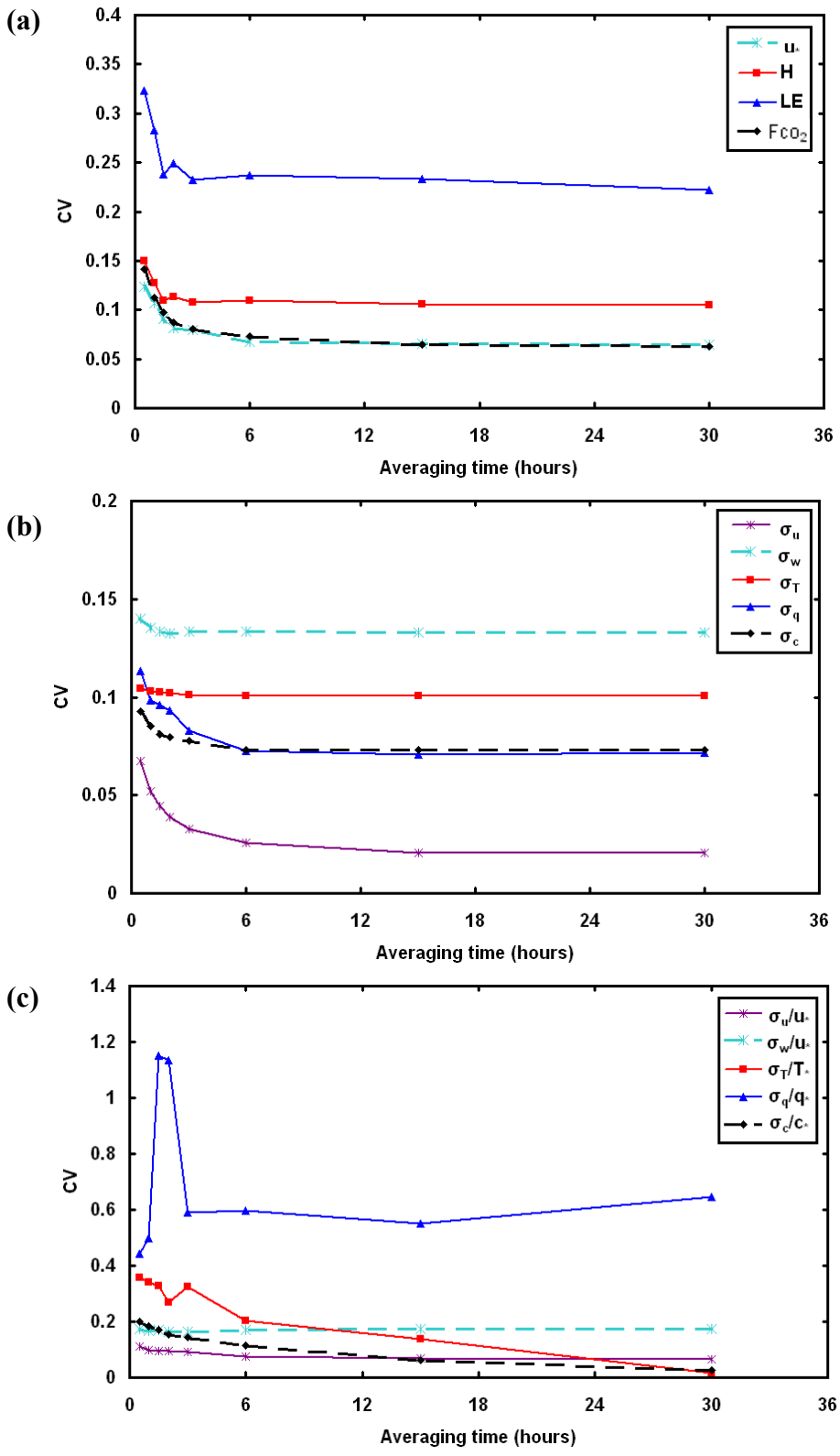
(a)
CV
Averaging time (hours)
u*
H
LE
Fco2
(b)
CV
Averaging time (hours)
σu
σw
σT
σq
σc
(c)
CV
Averaging time (hours)
σu/u*
σw/u*
σT/T*
σq/q*
σc/c*

Figure 25

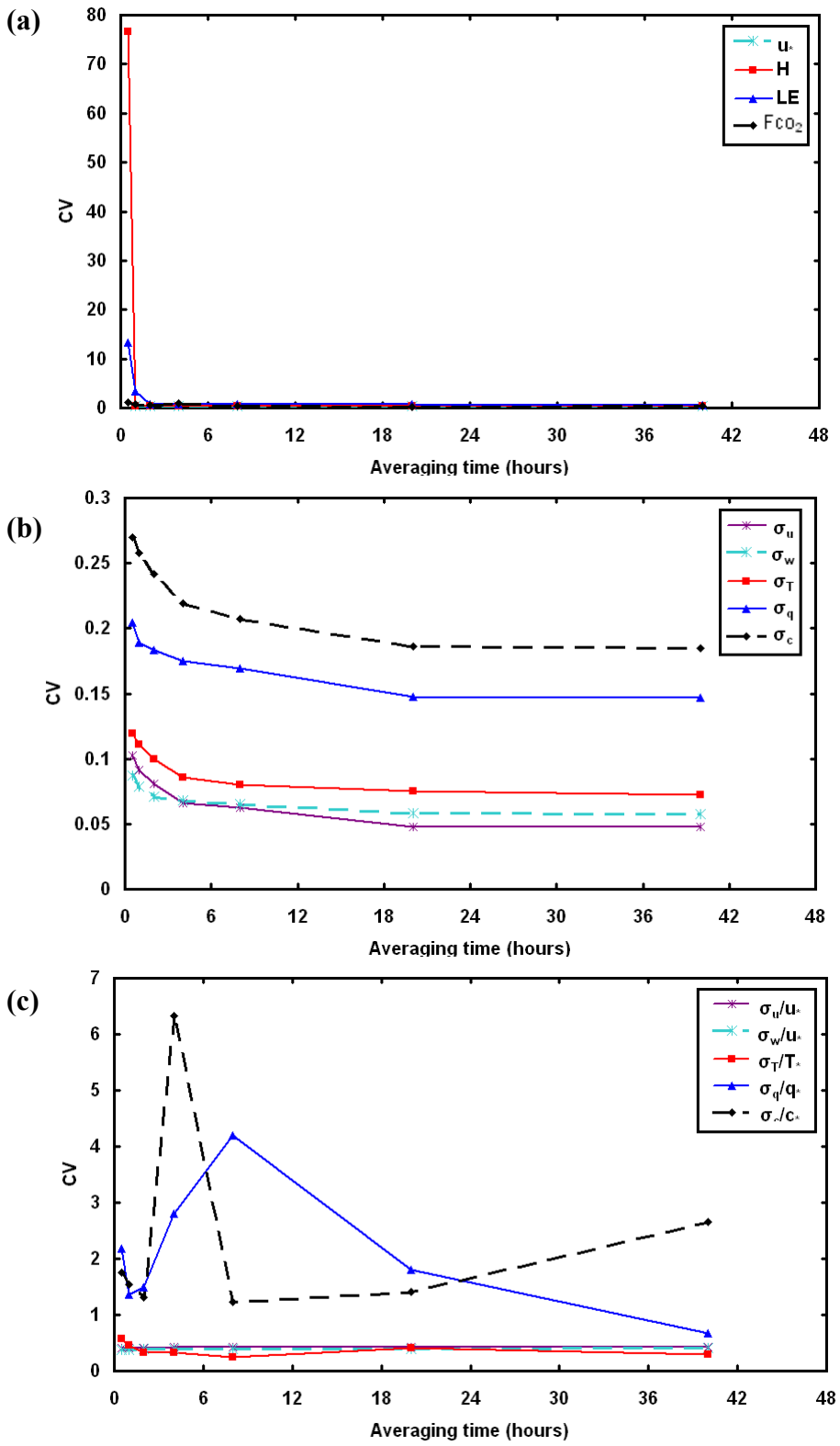
(a)
CV
Averaging time (hours)
u*
H
LE
Fco2
(b)
CV
Averaging time (hours)
σu
σw
σT
σq
σc
(c)
CV
Averaging time (hours)
σu/u*
σw/u*
σT/T*
σq/q*
σc/c*

Figure 26

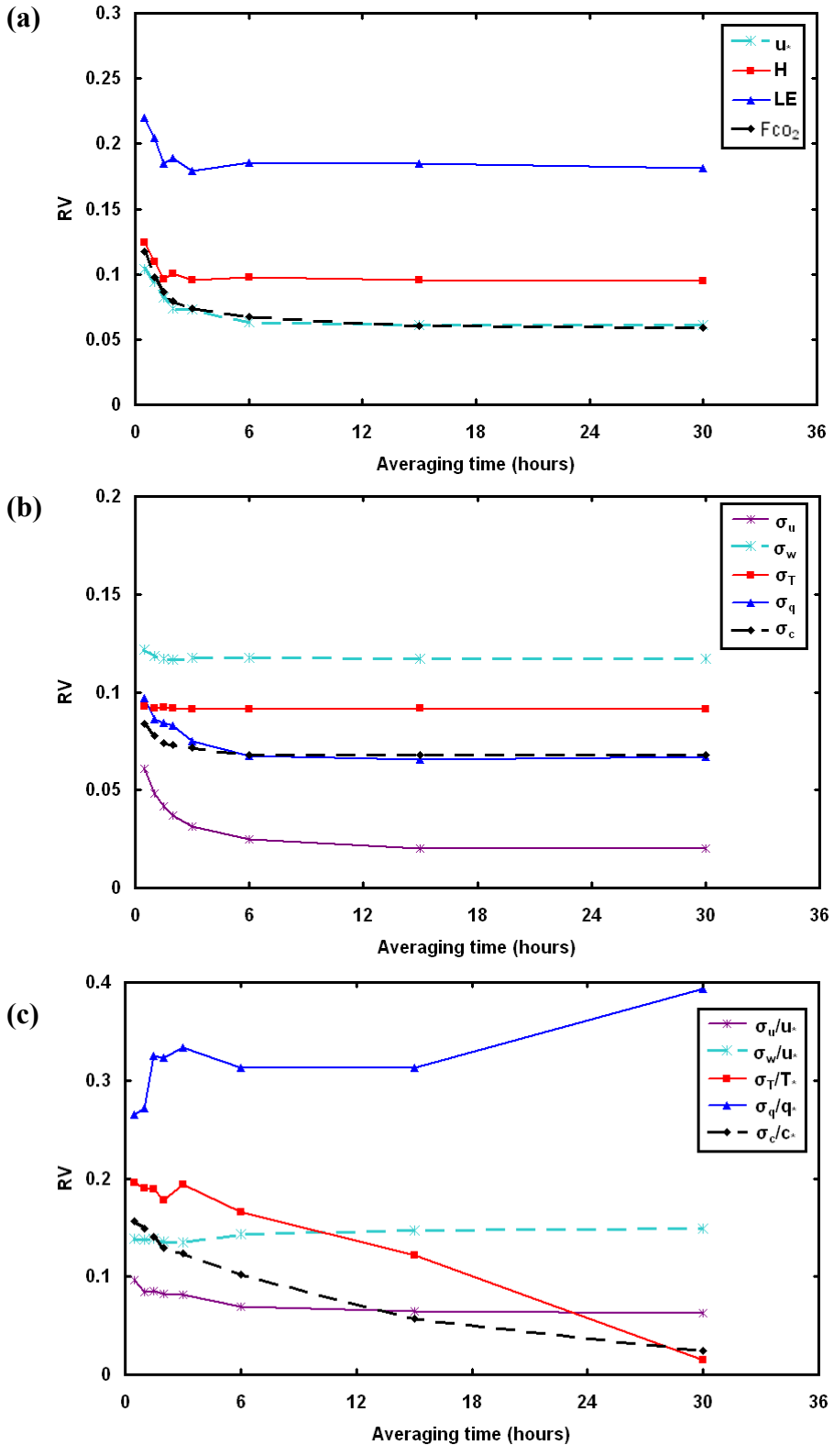
(a)
RV
Averaging time (hours)
u*
H
LE
Fco2
(b)
RV
Averaging time (hours)
σu
σw
σT
σq
σc
(c)
RV
Averaging time (hours)
σu/u*
σw/u*
σT/T*
σq/q*
σc/c*

Figure 27

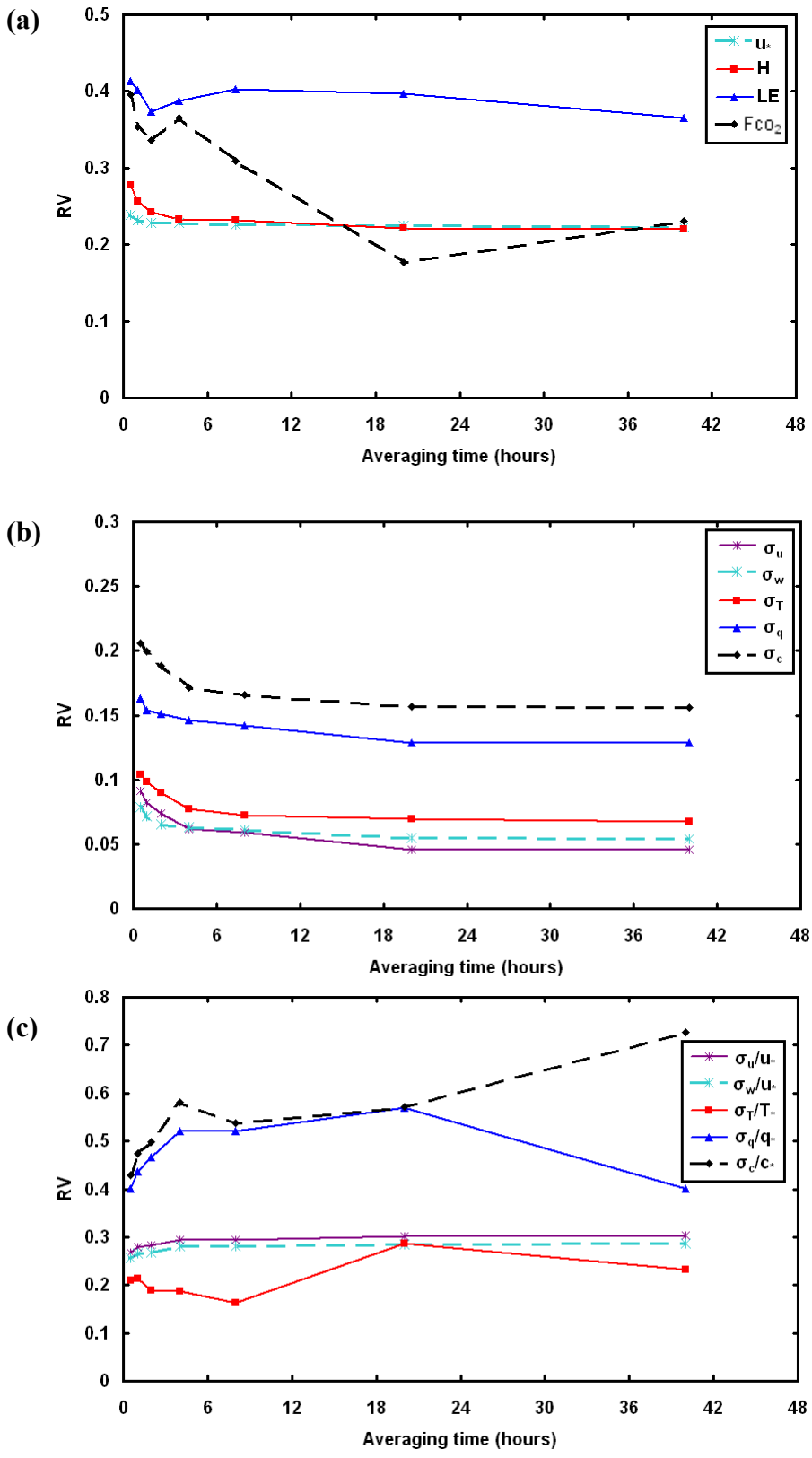
(a)
RV
Averaging time (hours)
u*
H
LE
Fco2
(b)
RV
Averaging time (hours)
σu
σw
σT
σq
σc
(c)
RV
Averaging time (hours)
σu/u*
σw/u*
σT/T*
σq/q*
σc/c*

Figure 28

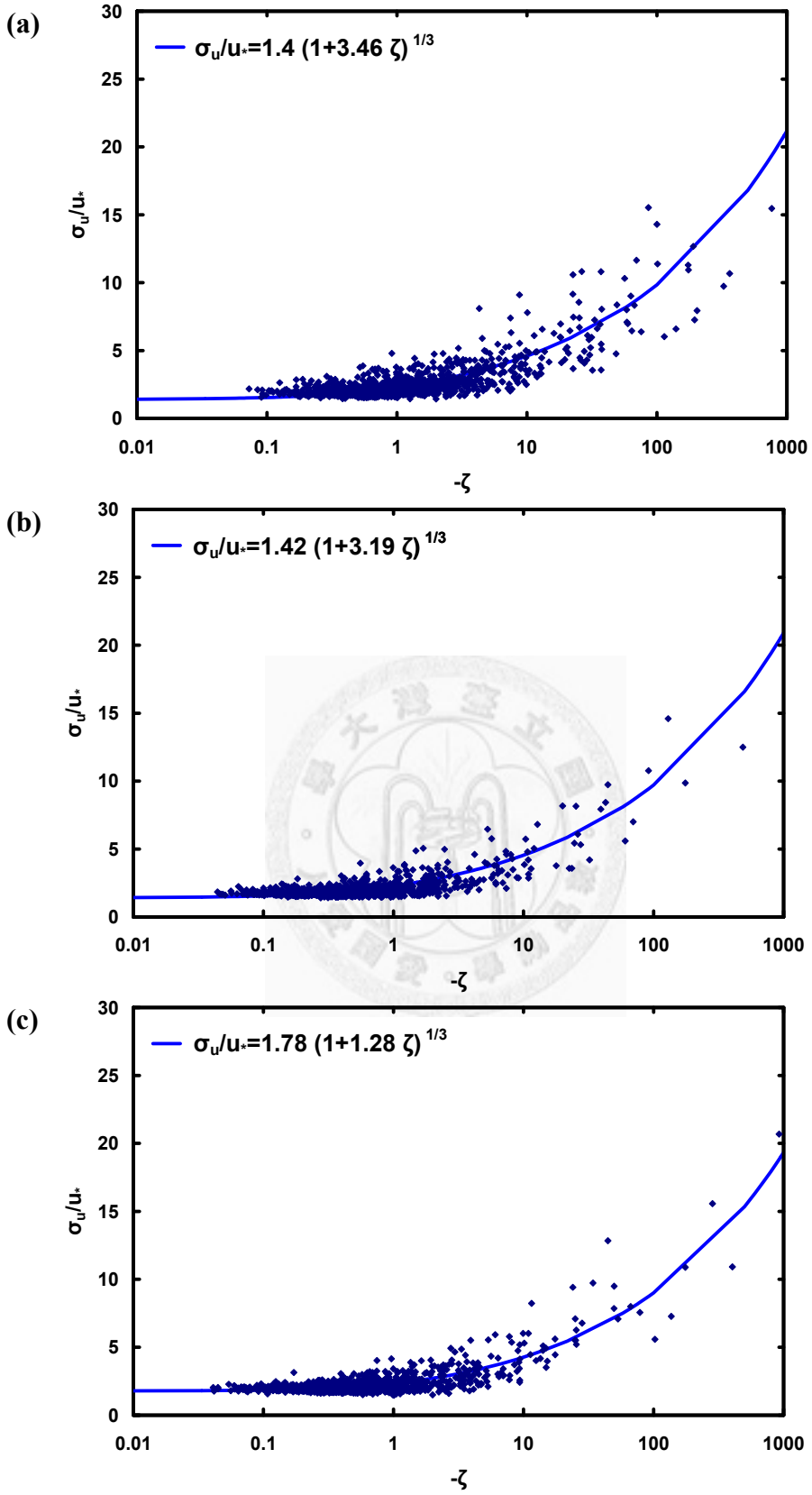
(a)
σu/u*=1.4 (1+3.46 ζ) 1/3
σu/u*
-ζ
(b)
σu/u*=1.42 (1+3.19 ζ) 1/3
σu/u*
-ζ
(c)
σu/u*=1.78 (1+1.28 ζ) 1/3
σu/u*
-ζ

Figure 29

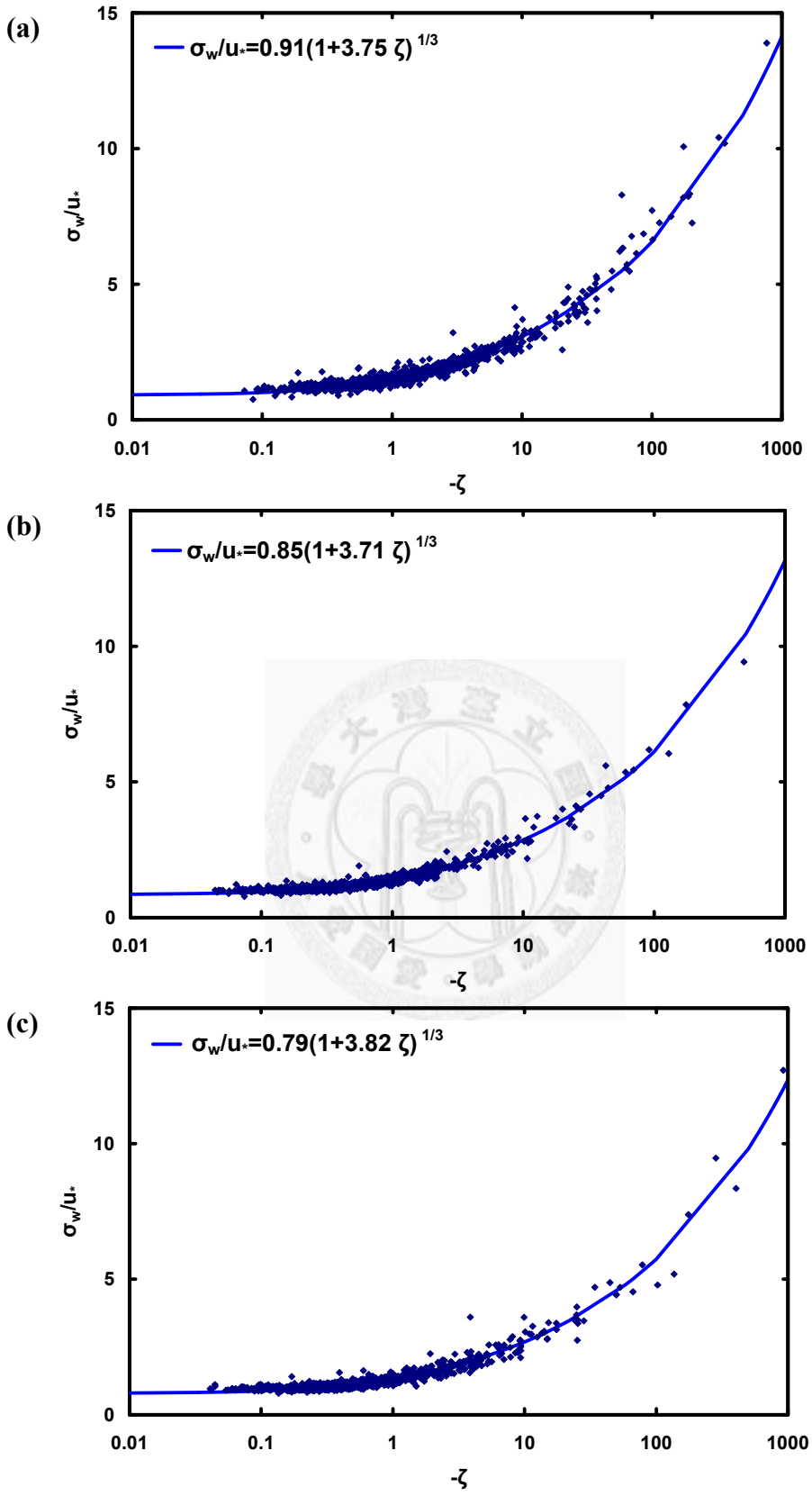
(a)
σw/u*=0.91(1+3.75 ζ) 1/3
σw/u*
-ζ
(b)
σw/u*=0.85(1+3.71 ζ) 1/3
σw/u*
-ζ
(c)
σw/u*=0.79(1+3.82 ζ) 1/3
σw/u*
-ζ

Figure 30

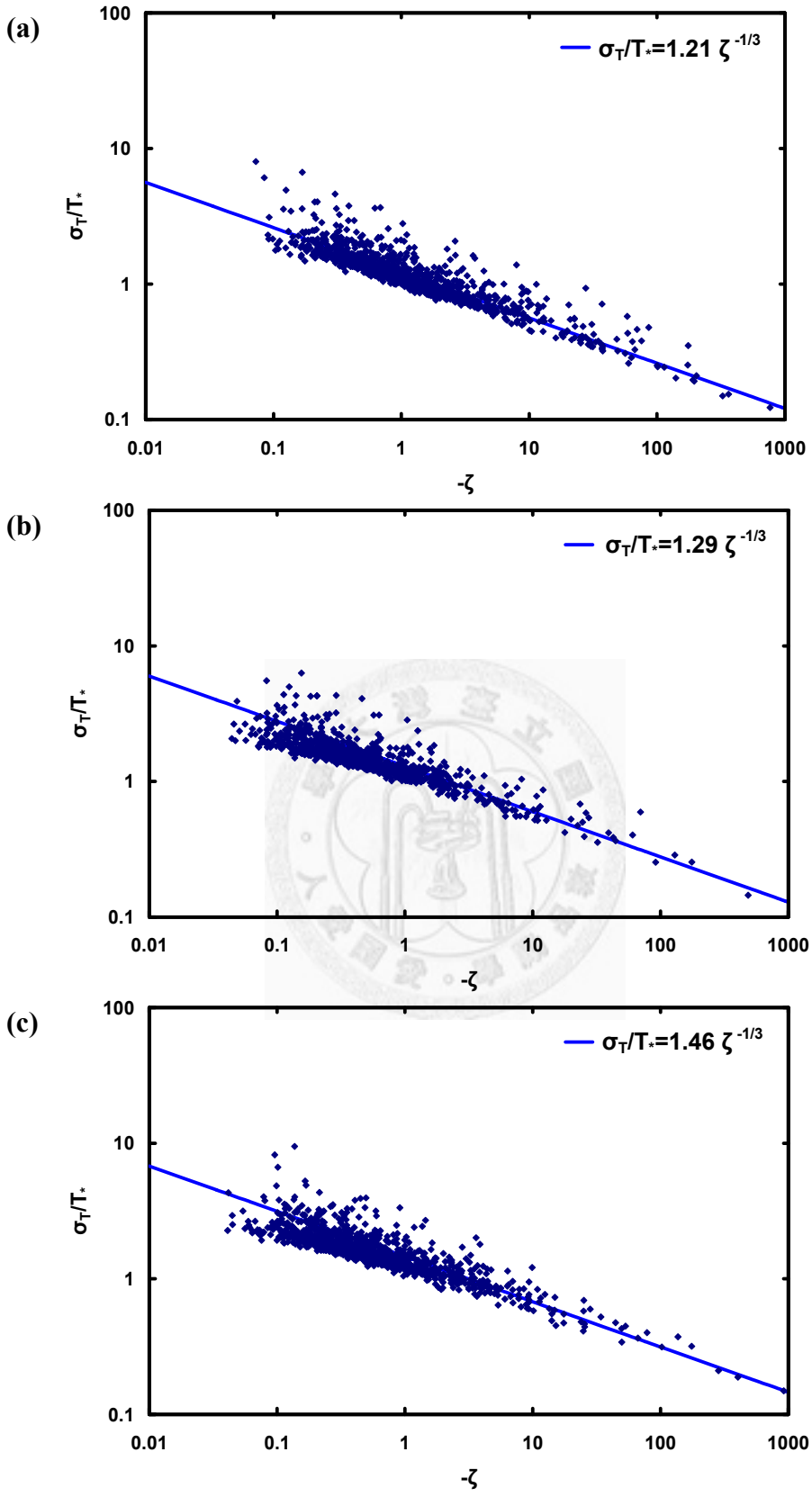
(a)
σT/T*=1.21 ζ -1/3
σT/T*
-ζ
(b)
σT/T*=1.29 ζ -1/3
σT/T*
-ζ
(c)
σT/T*=1.46 ζ -1/3
σT/T*
-ζ
100
10
1
0.1
0.01
0.1
1
10
100
1000

Figure 31

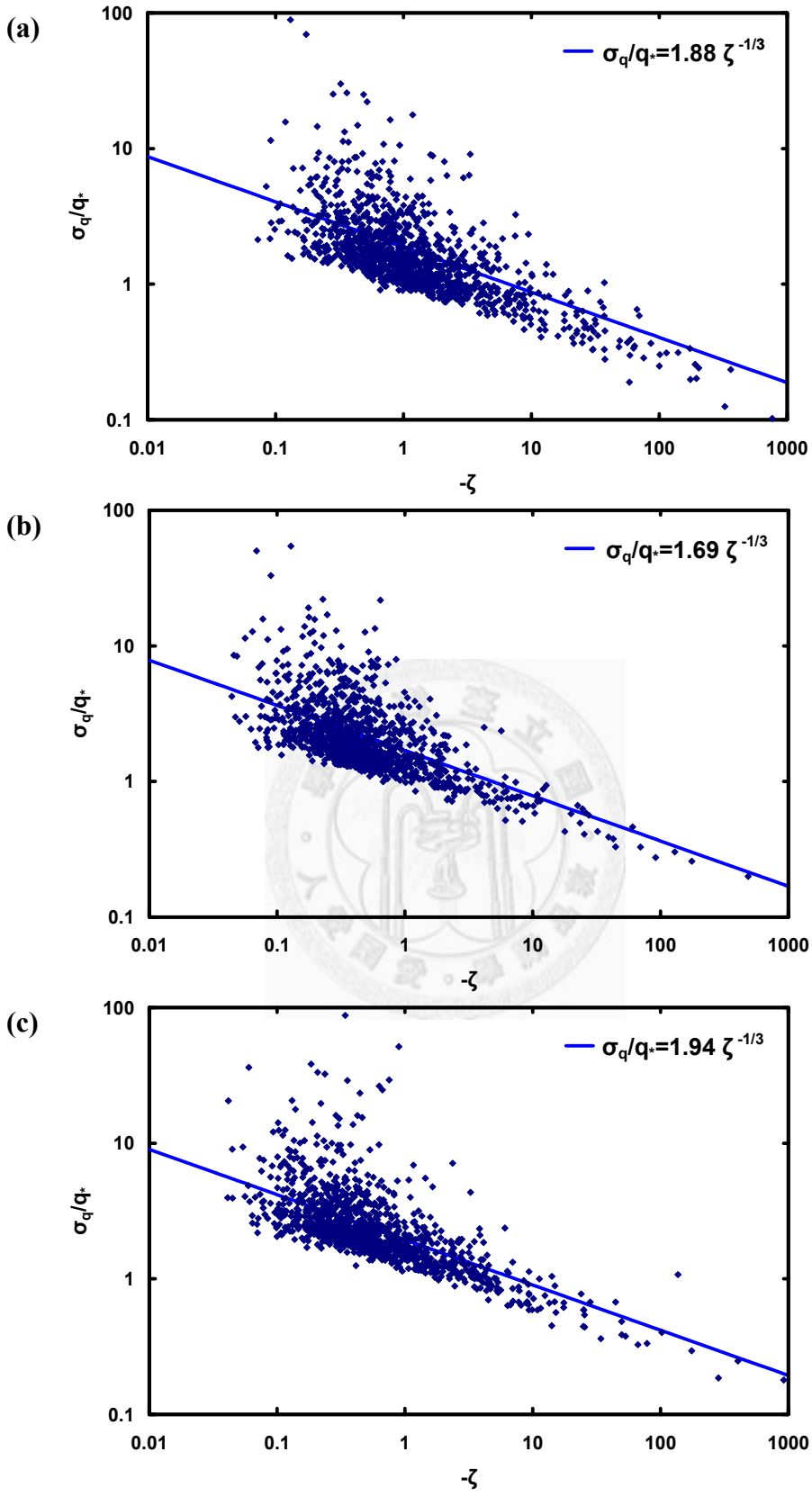
(a)
σq/q*=1.88 ζ -1/3
σq/q*
-ζ
(b)
σq/q*=1.69 ζ -1/3
σq/q*
-ζ
(c)
σq/q*=1.94 ζ -1/3
σq/q*
-ζ
100
10
1
0.1
0.01
0.1
1
10
100
1000

Figure 32

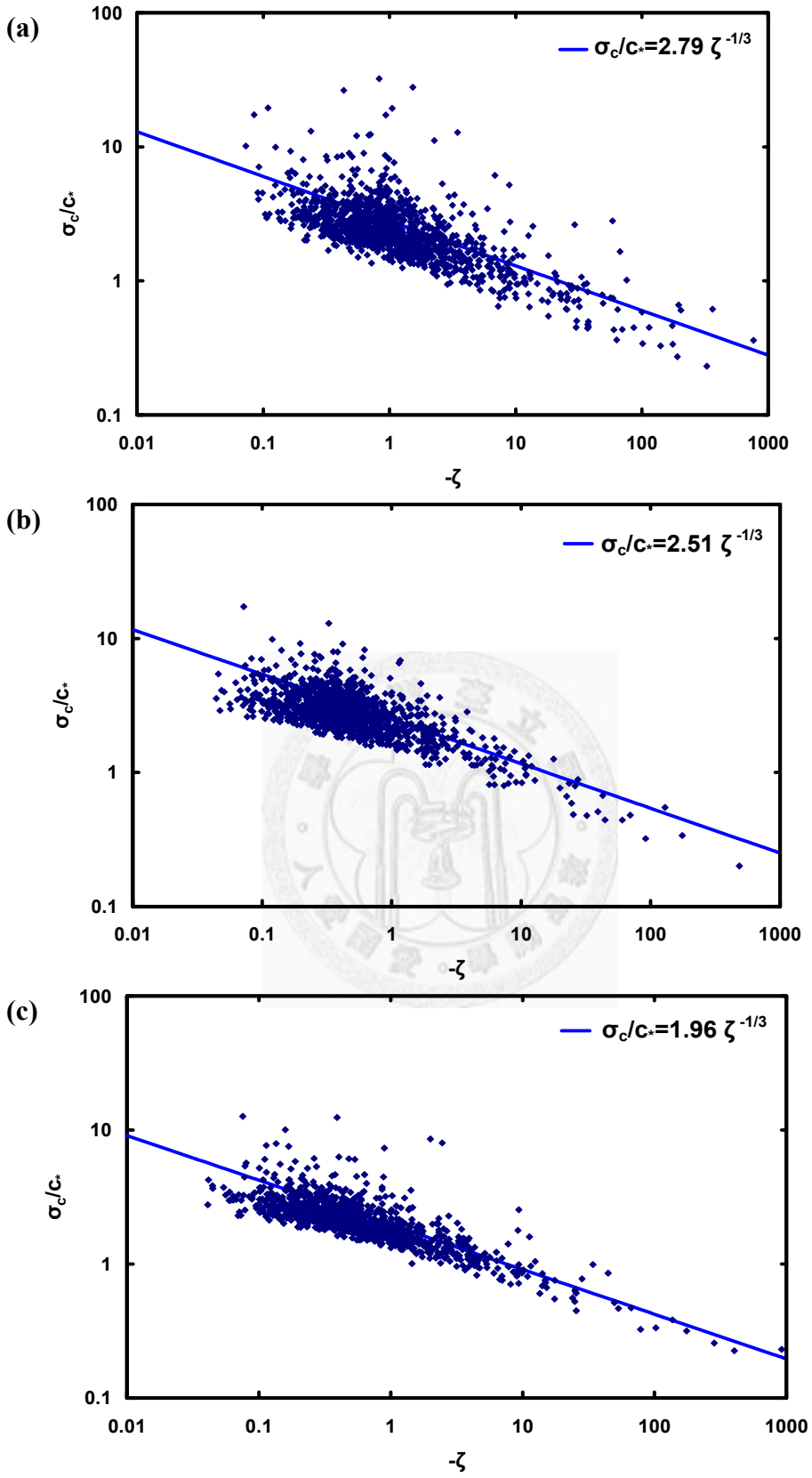
(a)
σc/c*=2.79 ζ -1/3
σc/c*
-ζ
(b)
σc/c*=2.51 ζ -1/3
σc/c*
-ζ
(c)
σc/c*=1.96 ζ -1/3
σc/c*
-ζ
100
10
1
0.1
0.01
0.1
1
10
100
1000

Figure 33

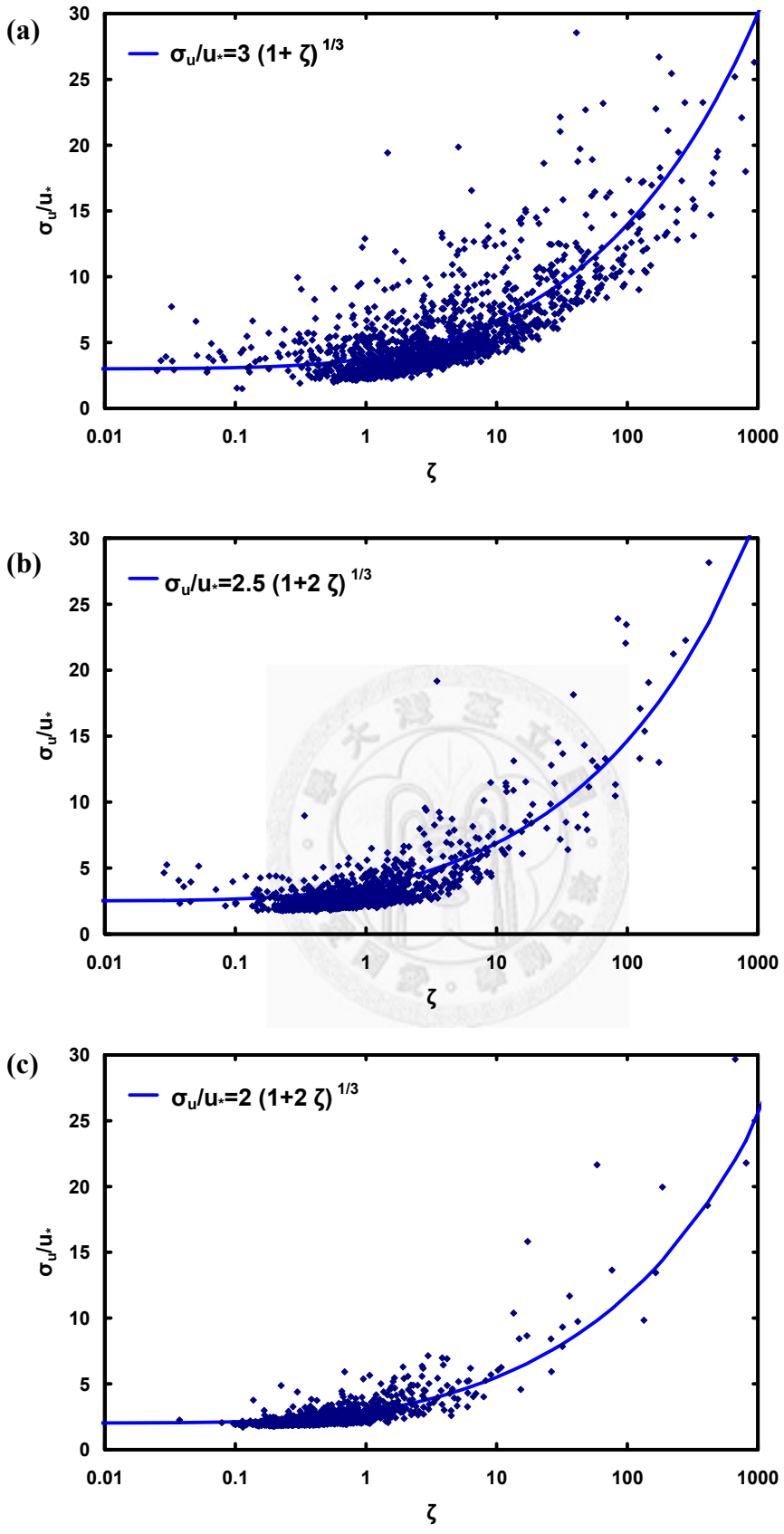
(a)
σu/u*=3 (1+ ζ) 1/3
σu/u*
ζ
(b)
σu/u*=2.5 (1+2 ζ) 1/3
σu/u*
ζ
(c)
σu/u*=2 (1+2 ζ) 1/3
σu/u*
ζ
0
5
10
15
20
25
30
0.01
0.1
1
10
100
1000

Figure 34

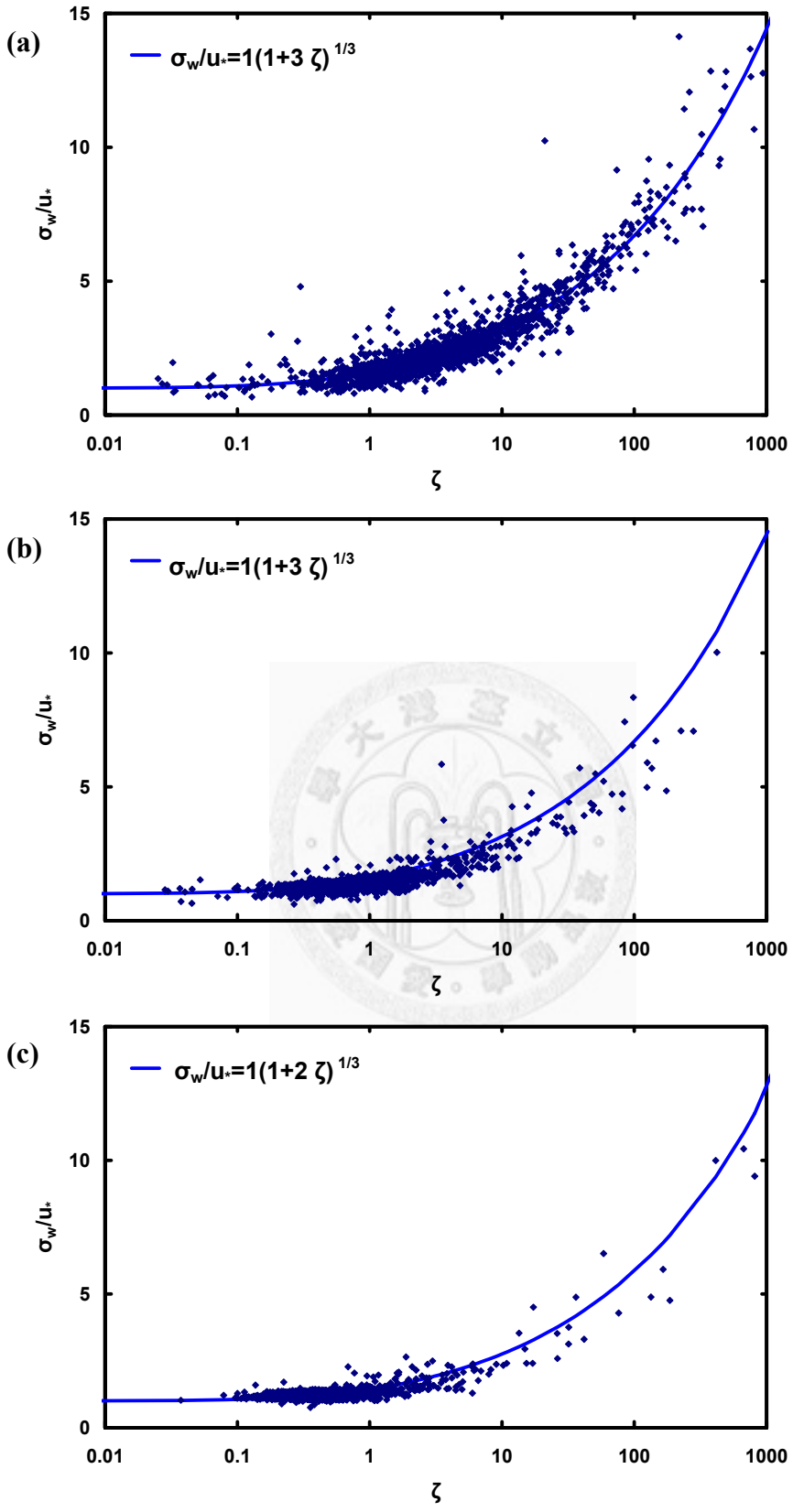
(a)
σw/u*=1(1+3 ζ) 1/3
σw/u*
ζ
0
5
10
15
0.01
0.1
1
10
100
1000
(b)
σw/u*=1(1+3 ζ) 1/3
σw/u*
ζ
(c)
σw/u*=1(1+2 ζ) 1/3
σw/u*
ζ

Figure 35

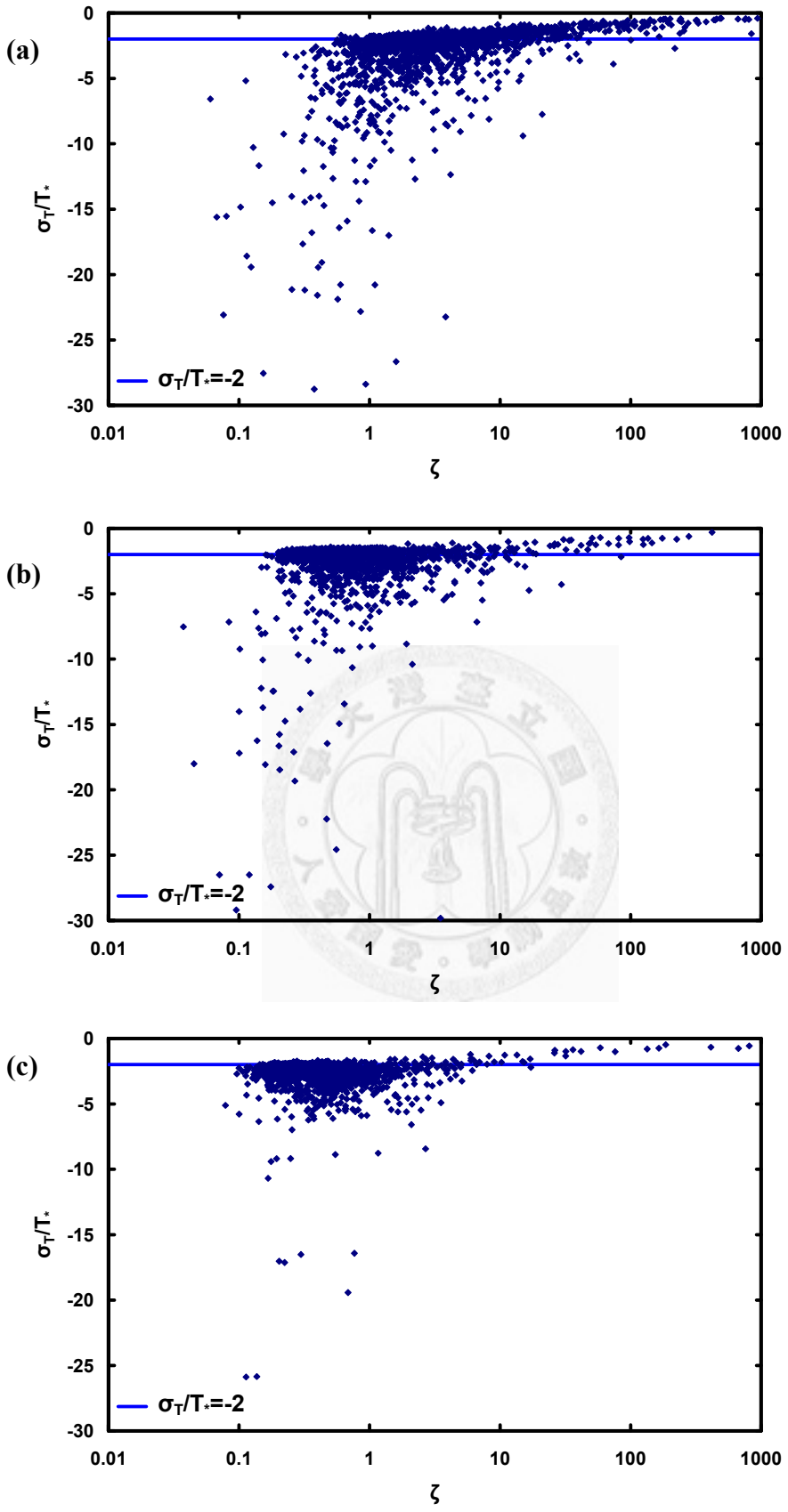

Figure 36

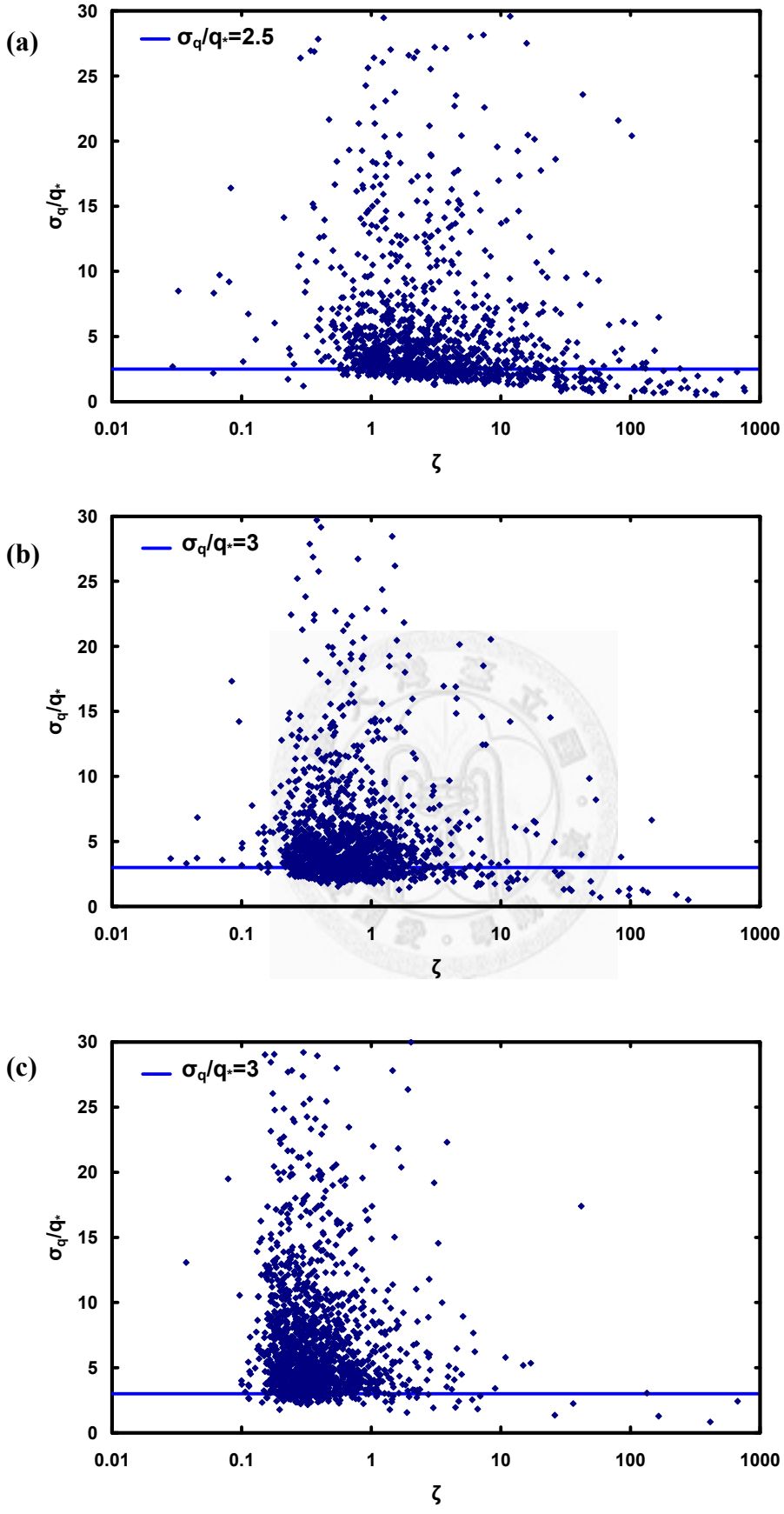
(a)
σq/q*=2.5
σq/q*
ζ
(b)
σq/q*=3
σq/q*
ζ
(c)
σq/q*=3
σq/q*
ζ
0
5
10
15
20
25
30
0.01
0.1
1
10
100
1000

Figure 37

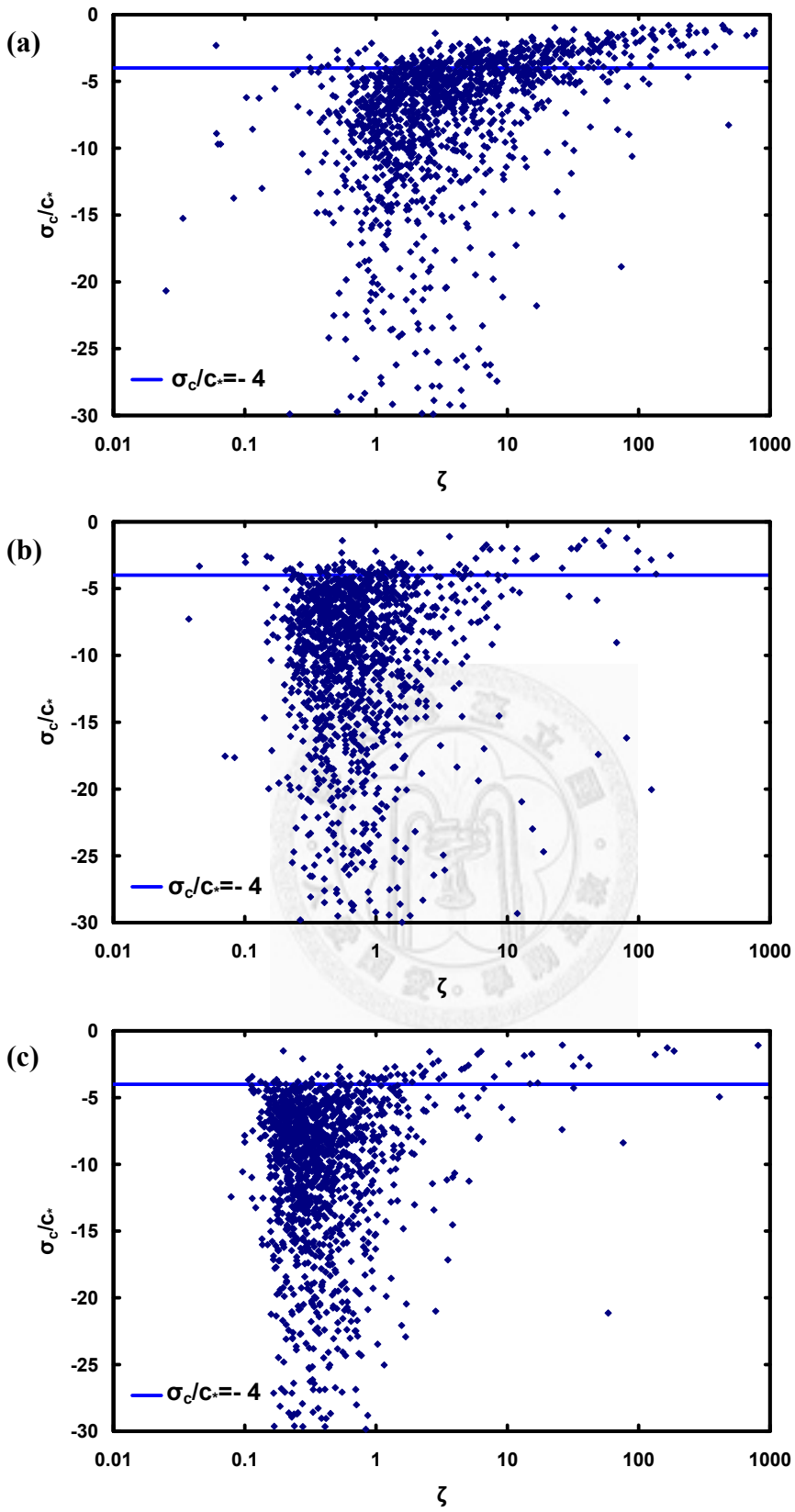

Figure 38

附錄 A 渦流相關法

在量測大氣-地表能量與物質交換的方式中，渦流相關法 (Eddy Covariance method, EC) 是目前國內外通量觀測上常使用、也具效力的方法之一，此方法可用於連續且長期觀測，並具有大範圍之代表性。

在大氣邊界層中，熱、水氣或是其他物質量的傳輸幾乎完全由紊流主導，因此渦流相關法利用高頻率的儀器同時量測風速與純量 (如:溫度、水氣濃度或是二氧化碳濃度等)，獲得兩者間的共變異數，經計算得到通量。

渦流相關法 (Eddy Covariance method, EC)是建立在advection-diffusion equation上:

$$\frac{\partial C}{\partial t} + U_j \frac{\partial C}{\partial x_j} = \frac{\upsilon \partial^2 C}{\partial x_j^2} + S - \frac{\partial \overline{u_j c}}{\partial x_j} \qquad (A.1)$$

式(A.1)中下標j = 1.2. or 3，t及 x_j分別代表時間及空間軸 ($x_1 = x, x_2 = y, x_3 = z$)，C為純量 (scalar，如溫度、水氣、或$CO_2$)之平均值，υ為純量C的分子擴散係數 (molecular diffusivity)，U_j為平均風速(U_1.U_2及U_3分別為x. y及z方向之平均風速,U_1=U.U_2=V.U_3=W)，S為C之源或匯項 (source/sink term)，小寫u_j, c分別是U_j, C的擾動項 (fluctuation term)，$\overline{u_j c}$ 為紊流通量 (flux)。

若地形植被為水平且均勻 (horizontal homogeneity)，因在不同位置量測純量差異極小，在水平方向的濃度梯度變化量可忽略不計，又分子擴散項通常遠小於風帶動的流動通量，也忽略不計，由上述方程式得知純量C之大氣與地表的交換通量 (Fco_2) 為

$$Fco_2 = \overline{u_3 c(h)} + \int_0^h \frac{\partial C}{\partial t} \partial x_3 = \overline{wc(h)} + \int_0^h \frac{\partial C}{\partial t} \partial z \qquad (A.2)$$

I　　II

式(2)中積分的邊界值h為植被冠層高度，項I為垂直紊流通量項，項Ⅱ為暫存項 (storage term)，若在某一時段流況穩定的條件下，紊流發展良好，氣體得充分混合，純量在統計性質並不隨時間變化，暫存量也可忽略。因此根據式(A.2)，

只要在冠層以上的一固定高度，能同步 (simultaneously) 直接量測風速及純量的擾動量及冠層內純量的分佈剖面，即能計算出Fco_2。

根據熱守恆 (First law of thermodynamics) 、水氣 (conservation of moisture) 及質量守恆 (conservation of a scalar quantity) 方程式，在某一時段流況穩定且地表平坦均值的條件下，可推導出以下可感熱、潛熱以及二氧化碳通量之計算式:

$$H = \rho \cdot Cp \cdot \overline{wt} \quad (A.3)$$

$$LE = Lv \cdot \overline{wq} \quad (A.4)$$

$$F_{CO_2} = \overline{wc} \quad (A.5)$$

上式中，H為可感熱通量 (Sensible heat flux) [W m^{-2}]，LE為潛熱通量 (Latent heat flux) [W m^{-2}]，Fco_2為二氧化碳通量 (Carbon dioxide flux) [μmol m^{-2} s^{-1}]，ρ為空氣密度 [kg m^{-3}]，Cp為比熱容 [J kg^{-1} K^{-1}]，Lv為水的汽化熱 [J kg^{-1}]，而 $\overline{wt}$.$\overline{wq}$ 及 $\overline{wc}$ 分別代表溫度、水氣及二氧化碳的垂直紊流通量。

通量計算式中所使用的水汽化熱 Lv，比熱容 Cp 及空氣密度 ρ，會受空氣溫度、濕度及壓力變化而不同，下式為各項的修正式:

$$Lv = (2.501 - 0.00237 \cdot T) \times 10^6 \quad (A.6)$$

式中T 為空氣溫度[℃]。

$$Cp = Cpd \cdot (1 + 0.84\, q) \quad (A.7)$$

上式中$Cpd = 1004.67$ [J kg^{-1} K^{-1}]為在固定壓力下之乾空氣的比熱容，q 為比濕，表示水氣在濕空氣中的質量比 [g g^{-1}]，而q 可以水蒸氣壓e [kPa]及大氣壓力P [kPa]求得:

$$q = 0.622 \frac{e}{P - 0.378\, e} \quad (A.8)$$

其中 0.622 為水比上乾空氣的莫耳比重 (18.016 [g mol^{-1}]/ 28.966 [g mol^{-1}])。

$$e = 1.61 \cdot \rho_v \cdot R \cdot Tk \quad (A.9)$$

1.61 為乾空氣比上水的莫耳比重 (28.966 [g mol^{-1}]/ 18.016 [g mol^{-1}])，ρ_v 為當時水的密度 [kg m^{-3}]，得自水氣分析儀，$R = 0.287$ [kPa m^3 K^{-1} kg^{-1}]為乾燥空氣之氣體常數，Tk 為以絕對溫度單位[K]表示的空氣溫度。

空氣密度 ρ 為乾空氣密度 ρ_d 與當時水密度 ρ_v 的總和:

$$\rho = \rho_d + \rho_v \tag{A.10}$$

而 ρ_d 可自理想氣體方程式求得:

$$\rho_d = \frac{P_d}{R_d \cdot T} = \frac{P - e}{R_d \cdot T} \tag{A.11}$$

附錄 B 資料處理

B.1 時間變異性分析(Temporal Variability of Flow Statistics)

當檢測空間變異性時，所取的平均時間間距長短會影響其值的大小，此實驗就針對不同的平均時間間距做計算，取 2009 年 334 至 338 天，共 5 天計算，但白天和晚上影響機制有不同，需要將這兩部份分別作計算。在白天部份，是取早上九點至下午三點(取起始時間 9~14.5)，共六小時(12 個 30 分鐘)計算，平均時間間距共有 0.5, 1, 1.5, 2, 3, 6, 15 及 30 小時，而晚上時間是取晚上九點至隔日早上五點(取起始時間 21~4.5)，共計八小時，平均時間間距共有 0.5, 1, 2, 4, 8, 20 及 40 小時。

B.2 MOST 之迴歸方式

MOST 對於純量之溫度、水氣及二氧化碳等迴歸，在不同大氣穩定度下有不同的形式，在不穩定的狀態下(Unstable condition, H>30 W m-2)，先取 $-\zeta>1$ 的值作截距為零的線性迴歸 $y=a\,x$，以 $-\zeta$ 為x值，σ_c/c_* 為y 值，得迴歸a值為係數 [$\sigma_c/c_* = Cc\,(-\zeta)^{-1/3}$, $a = Cc$]，再將所取得的迴歸式套用至全部的數據，以 $-\zeta$ 為x值，使用迴歸a值作係數得推估的 σ_c/c_*，將推估的 σ_c/c_* 數據和原數據作線性迴歸 $y=ax+b$，以原 σ_c/c_* 數據作x值，推估的 σ_c/c_* 數據作y值，得 R^2，用以檢查迴歸式的可信度，通常以 R^2 大於 0.7 為具高度相關性。

B.3 資料合理範圍

為確保用以分析之資料的正確性，訂定合理範圍過濾掉不正確之資料，晚上時間的界定為晚間八點至隔日早上五點鐘，而訂定範圍如下：可感熱通量(H) -150~20 (W m-2)，潛熱通量(LE) -50~100 (W m-2)以及二氧化碳通量(Fco_2) -2 ~6 (μmol m-2 s-1)。

B.4 數據時間紀錄

數據紀錄器 CR3000(CR23X)的時間紀錄，10Hz(30s)資料是使用 Scan 的指令，每 100 mSec 紀錄一次，分段平均與作共變異數是以 DataInterval 的指令設定，這裏使用 30 分鐘為一平均分段，紀錄的.dat 檔中顯示的時間，是紀錄結束時間，也就是此時間往前推的 30 分鐘計算資料，例如 00:30 表示 00:00-00:30 這段時間，16:30 是表示 16:00-16:30 這段時間。而 10Hz 資料經過 Fortran 程式切割分段為 30 分鐘一段時，是紀錄起始時間，就是此時間往後推的 30 分鐘計算資料，例如 00:30 表示 00:30-01:00 這段時間，16:30 是表示 16:30-17:00 這段時間。

當資料整合至 Excel 中時，時間[16]代表 16:00-16:30，[23.5] 代表 23:30-24:00 (00:00)，又將月、日轉以 Julian day 表示，1/1 的 12:00-12:30 是以 Julian day 1.5 表示，1/2 的 7:30~8:00 是以 Julian day 2.3125[7.5hr/24hr]表示。

B.5 實驗紀錄

資料自2009年5月22日開始收集，試運於2009年7月底完成，其後因八八風災(2009/8/8)造成系統停擺，於2009年10月底起恢復穩定運作，塔A實驗進行至2010年5月19日結束。實驗期間，塔A初期將資料紀錄器放置於塔上平台處，有時因紀錄器和電腦連線中斷而無法完整紀錄10Hz資料，故於2009年10月20日將紀錄器都移至塔下小屋內，所有儀器也自塔上延長接線至塔下小屋；儀器中，塔A以LI7000狀況不穩定，於2009年10月26日帶回維修，2010年1月5日收回；LI840因變壓器故障，可使用資料僅自2009年7月至2010年3月。

附錄 C 座標轉軸

C.1 平面擬合法(Planer Fit Method)

平面擬合法基本概念為: (1)尋找一直角座標，此直角座標之z軸垂直於由平均流線構成的假想平面，使得長期垂直方向的平均風速$\overline{w}$為 0。(2)此假想平面須由數個星期以上所有風向的數據進行迴歸得到。(3)此直角座標之y軸會垂直於由z軸與每 30 分鐘的平均風速向量$\vec{\vec{u}}$構成的平面(30 分鐘平均側向風速V=0) (Wilczak et al., 2001)。

根據基本概念，首先確定由儀器量測構成的座標系統(X、Y及Z軸)，如圖C.1所示，風速向量在儀器量測構成的座標系統(X、Y及Z軸組成之直角座標)中表示為:

$$\begin{aligned}\vec{\vec{u}}\cdot\vec{X}&=\overline{u_1}\\ \vec{\vec{u}}\cdot\vec{Y}&=\overline{v_1}\\ \vec{\vec{u}}\cdot\vec{Z}&=\overline{w_1}-b_0\end{aligned}\qquad\text{(C.1)}$$

也可表示為$\vec{\vec{u}}=(\overline{u_1},\overline{v_1},\overline{w_1}-b_0)$，其中$\vec{\vec{u}}$為風速向量，$\overline{u_1}$、$\overline{v_1}$、$\overline{w_1}$分別為X方向、Y方向與Z方向之每 30 分鐘平均風速，b_0為垂直風速因儀器量測誤差所造成的偏差值。

接著在上述座標系統中，以一組單位向量$\{\vec{i},\vec{j},\vec{k}\}$定義欲求之直角座標，$\vec{i}=(i_1,i_2,i_3)$、$\vec{j}=(j_1,j_2,j_3)$和$\vec{k}=(k_1,k_2,k_3)$可分別以X、Y及Z軸座標系統表示，如圖C.2 所示。在假設的$\{\vec{i},\vec{j},\vec{k}\}$座標中，垂直方向(k方向)的平均風速$\overline{w}$將表示為:

$$\overline{w}=\vec{\vec{u}}\cdot\vec{k}=(\overline{u_1},\overline{v_1},\overline{w_1}-b_0)\cdot(k_1,k_2,k_3)\qquad\text{(C.2)}$$

將上式展開，得出每 30 分鐘垂直平均風速$\overline{w_1}$:

$$\overline{w_1} = b_0 - \frac{k_1}{k_3}\overline{u_1} - \frac{k_2}{k_3}\overline{v_1} + \frac{1}{k_3}\overline{w} \tag{C.3}$$

其中令$-\frac{k_1}{k_3} = b_1$，$-\frac{k_2}{k_3} = b_2$，又因假設長期平均垂直風速$\overline{w}$為 0 :

$$\overline{w_1} = b_0 + b_1\overline{u_1} + b_2\overline{v_1} \tag{C.4}$$

係數b_0、b_1、b_2可由收集到所有之每 30 分鐘的平均風速$\overline{u_1}$、$\overline{v_1}$、$\overline{w_1}$作最小平方線性迴歸求得，加上$\vec{k}$為單位向量($\sqrt{k_1^{\,2} + k_2^{\,2} + k_3^{\,2}} = 1$)，可進而求得假想平面之$\vec{k}$座標:

$$\begin{aligned} k_3 &= \sqrt{b_1^{\,2} + b_2^{\,2} + 1} \\ k_2 &= -b_2 k_3 \\ k_1 &= -b_1 k_3 \end{aligned} \tag{C.5}$$

又因為欲求之直角座標中$\vec{j}$座標會垂直於由$\vec{k}$座標與每 30 分鐘的平均風速向量$\vec{\vec{u}}$構成的平面，所以新的直角座標系中$\vec{j}$座標可由下列式子求得:

$$\vec{j} = \vec{k} \times \vec{\vec{u}} \,/\, \left|\vec{k} \times \vec{\vec{u}}\right| \tag{C.6}$$

因此每 30 分鐘橫向風速經過新的座標轉換後會等於 0。

最後，根據右手直角座標系之定義可計算得新的座標系統中$\vec{i}$座標:

$$\vec{i} = \vec{j} \times \vec{k} \tag{C.7}$$

當求得$\vec{i}$後，可得平均風速在新座標軸上之表示。

獲得$\vec{i}, \vec{j}, \vec{k}$三項單位向量後，可以得出與地貌較相近之假想風速平面，特別需注意計算期間風速計位置不可移動，因會改變量測系統的座標系統。

C.2 二次轉軸(Double Rotation) (10 Hz)

當利用渦流相關法量測通量時，Lee et al.(2004)建議，以流線方向建立的座標系統是敘述在一般地形時質量守恆之最佳架構，又渦流相關系統之假設是在某一時段，流況穩定且地表平坦均質的條件下，但實際上，儀器架設並無法完全垂直於地表，量測區域也可能有坡度，因此使用 Tanner 和 Thurtell 於 1969 年定義的自然風向座標系統，使 X 軸經轉動而平行於風的平均流動方向，強迫$\overline{V}$ 、$\overline{W}$ 為 0，而 X 軸方向可代表流線方向，藉此座標系統的轉換，也可比較在不同場址以渦流相關系統量測的結果。

為強迫橫向風速$\overline{V}$ 和垂直風速$\overline{W}$ 為 0，先使 X-Y 平面繞 Z 軸旋轉一角度θ：

$$\theta = \tan^{-1}\left(\frac{\overline{V_0}}{\overline{U_0}}\right) \tag{C.8}$$

$$\begin{aligned} U_1 &= U_0\cos\theta + V_0\sin\theta \\ V_1 &= V_0\cos\theta - U_0\sin\theta \\ W_1 &= W_0 \end{aligned} \tag{C.9}$$

式(8.1)中$\overline{U_0}$ 、$\overline{V_0}$ 為計算期間(30 分鐘)內沿 X 及 Y 方向的平均風速，式(C.9)中W_0 為沿 Z 方向的平均風速。第一次轉軸得出的平均風速$\overline{V_1}$=0，再將 X-Z 平面繞 Y 軸旋轉一角度α：

$$\alpha = \tan^{-1}\left(\frac{\overline{W_0}}{\sqrt{\overline{U_0}^2 + \overline{V_0}^2}}\right) = \tan^{-1}\left(\frac{\overline{W_1}}{\overline{U_1}}\right) \tag{C.10}$$

$$\begin{aligned} U_2 &= U_1\cos\alpha + W_1\sin\alpha \\ V_2 &= V_1 \\ W_2 &= W_1\cos\alpha - U_1\sin\alpha \end{aligned} \tag{C.11}$$

式(C.10)中$\overline{U_1}$ 和$\overline{W_1}$ 為第一次轉軸得出的平均風速，當轉完第二次轉軸後，平均風速$\overline{W_2}$=0。當得旋轉座標軸迫使$\overline{V_2}$ 和$\overline{W_2}$ 為 0，U_2 方向可表為流線方向。

C.3 二次平均轉軸 (30 minutes)

二次轉軸基本是以 10Hz 轉軸，經過推導及驗證後，可以 datalogger 中輸出的 30 分鐘平均和共變異數直接做二次轉軸，結果與 10 Hz 經程式計算後的結果相合。旋轉角度θ (X-Y 平面繞 Z 軸旋轉)及α (X-Z 平面繞 Y 軸旋轉)與以 10Hz 數據轉軸一樣:

$$\theta = \tan^{-1}\left(\frac{\overline{V_0}}{\overline{U_0}}\right) \tag{C.12}$$

$$\alpha = \tan^{-1}\left(\frac{\overline{W_0}}{\sqrt{\overline{U_0}^2 + \overline{V_0}^2}}\right) \tag{C.13}$$

轉軸公式如下:

$$\overline{U_2} = (\overline{U_0}\cos\alpha + \overline{V_0}\sin\alpha)\cos\theta + \overline{W_0}\sin\theta \tag{C.14}$$

$$\overline{V_2} = \overline{V_0}\cos\alpha - \overline{U_0}\sin\alpha \tag{C.15}$$

$$\overline{W_2} = \overline{W_0}\cos\theta - (\overline{U_0}\cos\alpha + \overline{V_0}\sin\alpha)\sin\theta \tag{C.16}$$

$$\overline{w'c'}_2 = \overline{w'c'}_0\cos\theta - (\overline{u'c'}_0\cos\alpha + \overline{v'c'}_0\sin\alpha)\sin\theta \tag{C.17}$$

$$\begin{aligned}\overline{w'^2}_2 = {} & \overline{w'^2}_0\cos^2\theta - 2\overline{w'u'}_0\cos\theta\sin\theta\cos\alpha \\ & - 2\overline{w'v'}_0\cos\theta\sin\theta\sin\alpha + \overline{u'^2}_0\cos^2\alpha\sin^2\theta \\ & + \overline{v'^2}_0\sin^2\alpha\sin^2\theta + 2\overline{u'v'}_0\sin\alpha\cos\alpha\sin^2\theta\end{aligned} \tag{C.18}$$

$$\overline{v'^2}_2 = \overline{v'^2}_0\cos^2\alpha - 2\overline{v'u'}_0\cos\alpha\sin\alpha + \overline{u'^2}_0\sin^2\alpha \tag{C.19}$$

$$\overline{u'^2}_2 = \overline{w'^2}_0 \sin^2\theta + 2\overline{u'v'}_0 \cos\alpha \sin\alpha \cos^2\theta + 2\overline{w'}_0 \sin\theta(\overline{u}_0 \cos\alpha \cos\theta + \overline{v}_0 \sin\alpha \cos\theta) + \overline{v'^2}_0 \sin^2\alpha \cos^2\theta + \overline{u'^2}_0 \cos^2\alpha \cos^2\theta \tag{C.20}$$

$$\overline{w'u'}_2 = \overline{w'u'}_0 \cos^2\theta \cos\alpha + \overline{w'v'}_0 \sin\alpha \cos^2\theta + \overline{w'^2}_0 \cos\theta \sin\theta - \overline{u'^2}_0 \sin\theta \cos^2\alpha \cos\theta - 2\overline{u'v'}_0 \sin\theta \sin\alpha \cos\alpha \cos\theta - \overline{w'u'}_0 \cos\alpha \sin^2\theta - \overline{v'^2}_0 \sin^2\alpha \cos\theta \sin\theta - \overline{w'v'}_0 \sin^2\theta \sin\alpha \tag{C.21}$$

$$\overline{w'v'}_2 = \overline{w'v'}_0 \cos\alpha \cos\theta - \overline{w'u'}_0 \sin\alpha \cos\theta + \overline{u'^2}_0 \sin\alpha \sin\theta \cos\alpha - \overline{v'^2}_0 \sin\alpha \sin\theta \cos\alpha + \overline{u'v'}_0 \sin^2\alpha \sin\theta - \overline{u'v'}_0 \sin\theta \cos^2\alpha \tag{C.22}$$

$$\overline{u'v'}_2 = \overline{u'v'}_0 \cos^2\alpha \cos\theta - \overline{u'^2}_0 \sin\alpha \cos\alpha \cos\theta - \overline{u'v'}_0 \sin^2\alpha \cos\theta + \overline{w'v'}_0 \sin\theta \cos\alpha - \overline{u'w'}_0 \sin\alpha \sin\theta + \overline{v'^2}_0 \sin\alpha \cos\alpha \cos\theta \tag{C.23}$$

上式中u'、v'、w'為沿 X、Y 及 Z 方向的風速變動量，c'為純量變動量。下標為 0 表示為原始資料，下標為 2 表示資料已經過二次轉軸。

(a)

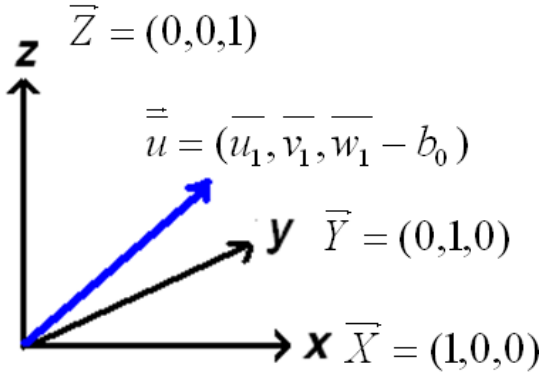
$\overrightarrow{Z} = (0,0,1)$
z
$\overrightarrow{u} = (\overline{u_1}, \overline{v_1}, \overline{w_1} - b_0)$
y
$\overrightarrow{Y} = (0,1,0)$
x
$\overrightarrow{X} = (1,0,0)$

(b)

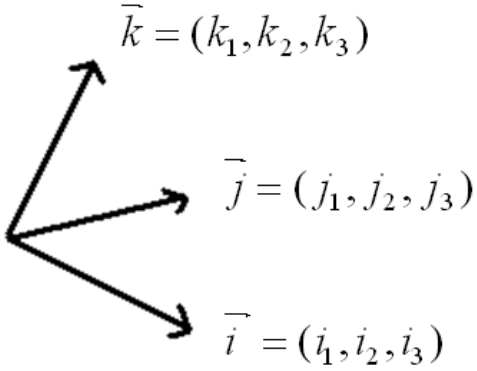
$\overrightarrow{k} = (k_1, k_2, k_3)$
$\overrightarrow{j} = (j_1, j_2, j_3)$
$\overrightarrow{i} = (i_1, i_2, i_3)$

圖 C.1

附錄 D 所有儀器

本實驗地的樹冠層平均高度為 27 m，觀測塔 A 高 35 m，觀測塔 B 高 40 m。為檢驗 constant flux layer 的假設及發展渦流相關系統應用於坡度地形之技術研究，塔 A 及塔 B 分別各架設兩套系統:塔 A 架設 open-path eddy-covariance 系統於 28 m 及 closed-path eddy-covariance 系統於 33 m，而塔 B 架設兩套 open-path eddy-covariance 系統於 32 m 及 40 m，用於量測二氧化碳、水氣、動量(momentum)及可感熱(sensible heat)通量，其中塔 A 之風速計 CSAT3 朝向北方，而風速計 81000 的黑盒子朝向南方；在冠層以上也有量測氣壓、降雨量及淨輻射。另外也於冠層以上及以下量測二氧化碳濃度、氣溫、溼度、風速及光合作用輻射(PAR)等剖面，同時也量測土壤熱通量及溫溼度剖面。並且為計算植被的光合作用效率，在地表及地表下放置土壤溫度計與土壤水分量測計，且於地表下放置土壤熱流計，量測土壤熱通量。

本研究 eddy-covariance 系統的量測頻率為 10Hz，時間平均為 30 分鐘。其餘儀器之量測頻率為 1 次/ 30s，時間平均為 30 分鐘，表 D.1 為塔 A 所使用的儀器及其設置高度，而塔 B 資料列於表 D.2，儀器的配置則如圖 D.1(a)(b)所示。

表 D.1　All instrument locations and brief instructions (Tower A).

儀器名稱	型號	數量	說明	架設高度	反應時間	紀錄速率	需要紀錄原始資料
渦流相關系統 一	YOUNG 81000	1	eddy-covariance system 設置於冠層以上兩個不同的高度，用來量測可感熱、水氣及二氧化碳通量，同時檢驗 constant flux 的假設	33 (m)	10 Hz	10 Hz 資料並每30分鐘平均值	U(m/s) V(m/s) W(m/s) Tv(℃)
	LI7000	1		33 (m)	10 Hz	10 Hz 資料並每30分鐘平均值	CO_2(μmol/mol) H_2O(mmol/mol) Pressure (kPa)
渦流相關系統 二	CSAT3	1		28 (m)	10 Hz	10 Hz 資料並每30分鐘平均值	Ux(m/s) Uy(m/s) Uz(m/s) T(℃)
	LI7500	1		28 (m)	10 Hz	10 Hz 資料並每30分鐘平均值	CO_2(mmol/m^3) H_2O (mmol/m^3) Pressure (kPa)
二氧化碳/水分分析儀	LI840	1	共6個抽氣點，分布在冠層以上及以下	2,10, 18,25, 30,35 (m)	Maximum Gas Flow Rate: 1 liter/min (應可1s有一筆)	每層各抽氣5分鐘，一循環共 30 分鐘，作為每30分鐘的各層平均值	CO_2(μmol/mol) H_2O(mmol/mol) T(℃)儀器檢查用

淨輻射計	NR-Lite	1	得樹冠層頂之淨輻射值	27.5 (m)	60 Hz	每30秒一筆 得每30分鐘 平均值	Rn(W/m^2)
紅外線表面溫度計	IRTS	1	得樹冠層頂之溫度	27.5 (m)	> 1 s (target) 2minutes (body)	每30秒一筆 得每30分鐘 平均值	T(℃)
光量子計 Photosynthetically Active Radiation PAR	LI-190	2	electromagnetic Spectrum from 400 -700 nm	27.5 (m)	10 μs	每30秒一筆 得每30分鐘 平均值	Micromoles of quanta per second per square meter ($\mu mol\ s^{-1}\ m^{-2}$)
	E90			13 (m)			
溫濕度計	HMP45C	2	氣溫、溼度剖面	28(m) 13 (m)	T: 0.15 seconds RH:15seconds with membrane filter	每30秒一筆 得每30分鐘 平均值	T(℃) RH(%)
雨量計	TE525 MM	1	為確定天候，因 eddy-covariance system 極易受下雨影響	27.5 (m)	Rainfall per Tip (least count): 0.1 mm	連續記錄	降雨量(mm)
土壤熱流計	HTP01	2	得土壤熱通量	皆 5 (cm)		每30秒一筆 得每30分鐘 平均值	Soil heat flux(W/m^2)
表面溫度計	107	1	與土壤溫度剖面算得 Storage term	0 cm	Time Constant In Air: Between 30 and 60 seconds in a	每30秒一筆 得每30分鐘 平均值	T(℃)

土壤溫度計	107	2	得土壤溫度剖面	-5 (cm) -10(cm)		每30秒一筆得每30分鐘平均值	T(℃)
土壤濕度計	257	2	得土壤溼度剖面	-5 (cm) -10(cm)	0-200 kPa **	每30秒一筆得每30分鐘平均值	soil water potential (kPa)
土壤濕度計	CS616	2	得土壤溼度剖面	-5 (cm) -10(cm)		每30秒一筆得每30分鐘平均值	Volumetric soil water content (%)

表 D.2　All instrument locations and brief instructions (Tower B).

儀器名稱	型號	數量	說明	架設高度
三維度超音波風速風向計	CSAT3 (Campbell)	2	1. Eddy-covariance system 設置於冠層以上兩個不同的高度，用來量測可感熱、水氣及二氧化碳通量，同時檢驗 constant flux 的假設 2. CSAT3 及 LI7500 需離塔水平距離 1.5m 以上	32 m 及 40m
開放式二氧化碳/水分分析儀	LI-7500 (LI-COR)	2		32 m 及 40m
二氧化碳分析儀	LI-820 (LI-COR)	5	1. 四套，每套三個抽氣點，共十二個抽氣點，分布在冠層以上及以下 2. （40m 處皆設有 Li7500 及 Li820，可比較兩個系統所量 CO2 濃度的差異 3. 第五套為土壤二氧化碳之用	0.5, 2.5, 6, 10, 14, 18, 22, 25, 28, 32, 36, 40 m
溫溼度計(含通風罩)	HMP45C	12	高度與二氧化碳抽氣點同	0.5, 2.5, 6, 10, 14, 18, 22, 25, 28, 32, 36, 40 m
風速風向計	034B	6		2.5, 6, 14, 22, 28, 32 m
超音波風速風向計	WindSonic4-L-2-D	6	32m 處皆設有 034B、CSAT3 及 WS4-L，可比較三個系統所量風速的差異	0.5, 10, 18, 25, 32, 36 m

光量子計	PAR sensor, LI-190	5		30 m 及 12 m
淨輻射計	NR-Lite	2		2.5, 6 18, 25, 30 m
土壤熱流計	HFP01SC	2	皆設於地表以下 8 cm，一在塔東，一在塔西，相距 5m，以求空間平均的土壤熱流	8 cm
土壤溫度計	TCAV	2		2, 6, 10, 20cm
土壤水分計	CS616	8	兩兩一組，分別設於四個深度	5, 15, 20, 50 cm
紅外線溫度計	IRR-P (COMPBELL)	2	量測冠層表面溫度及地面溫度，1.5m 高的紅外線溫度計需架設在土壤溫度計的上方	30 m 及 1.5 m
雨量計	TE525MM	1		30m
氣壓計	CS106	1		30m
資料蒐集器	CR3000 (CAMPBELL)	2		

(a)

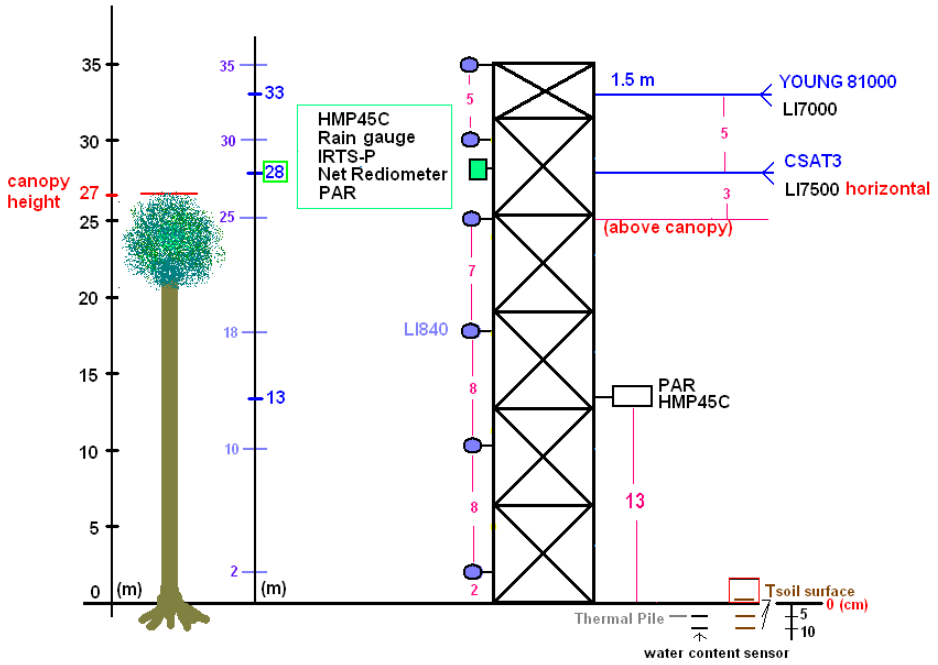
canopy height
HMP45C
Rain gauge
IRTS-P
Net Rediometer
PAR
1.5 m
YOUNG 81000
LI7000
CSAT3
LI7500 horizontal
(above canopy)
LI840
PAR
HMP45C
Tsoil surface
Thermal Pile
water content sensor
(m)

(b)

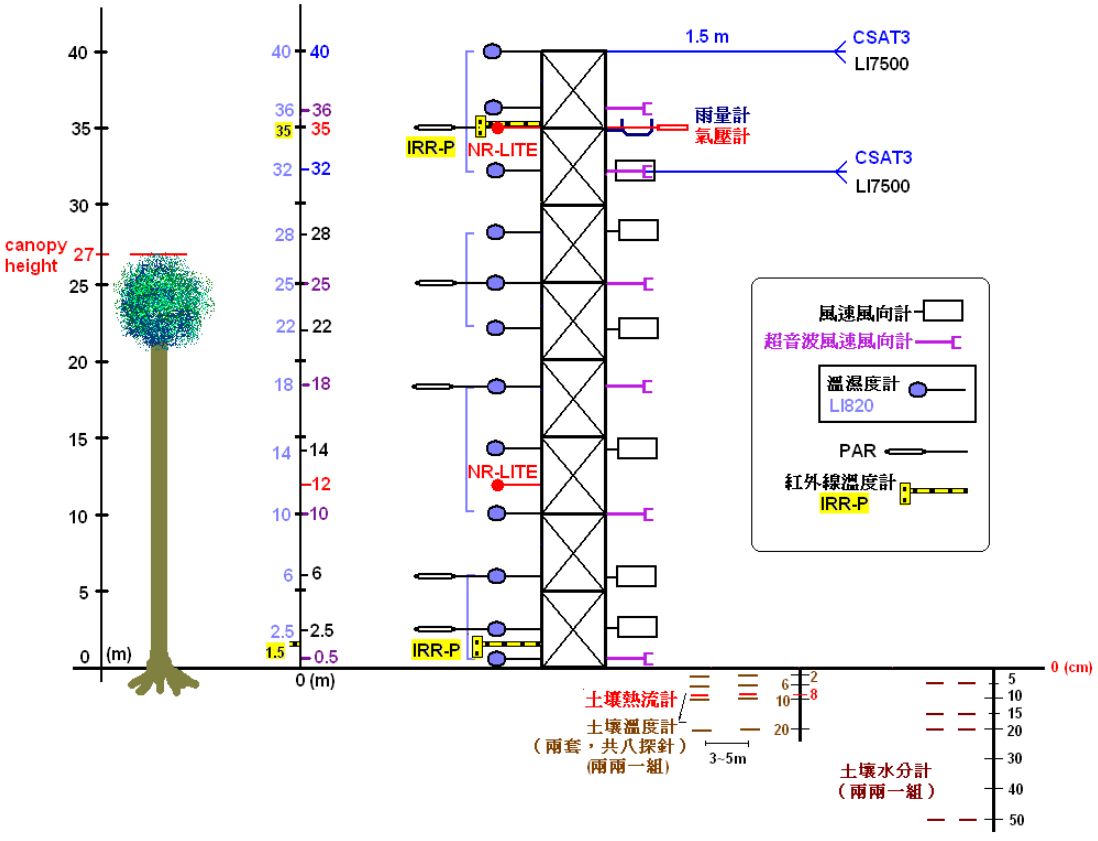
canopy height
1.5 m
CSAT3
LI7500
雨量計
氣壓計
IRR-P
NR-LITE
CSAT3
LI7500
NR-LITE
IRR-P
風速風向計
超音波風速風向計
溫濕度計
LI820
PAR
紅外線溫度計
IRR-P
土壤熱流計
土壤溫度計
（兩套，共八探針）
(兩兩一組)
3~5m
土壤水分計
（兩兩一組）
(m)
0 (m)
0 (cm)

圖 D.1

附錄 E 遠端傳輸(GSM)

全球行動通訊系統(Global System for Mobile Communications,簡稱 GSM)，其較以前的標準最大的不同是他的信號和語音通道都是數位式的，此優勢可應用於遠距離數據之傳輸，在中華電信的申請服務中，歸類於行動數據/傳真，功能是透過數位式行動數據，可隨時隨地利用個人電腦設備發送或接收數據。

GSM 的設備包含：一個主機(MOD)，一 SIM 卡(附有兩個門號，一個為虛擬異號數據 0911-582643，另一為行動電話號碼 0910-794575)，MOD 轉接 RS232 頭，天線及電源線。其他設備包含：RS232 線，電腦(含電話插孔)，電話線及 LoggerNet 軟體程式。設備圖請見圖 E.1。

連接於 DataLogger 的 GSM 主機(MOD)內需插入一 SIM 卡，外附接有一天線以及 MOD 轉接 RS232 頭，將電源線接上，可見 GSM 主機上會閃綠燈號，再將連於 DataLogger 的 RS232 接上 MOD 轉接 RS232 頭，就可由遠端電腦如撥打手機般的連上操作(圖 E.2)。電腦須接上電話線(太新的電腦無此插孔)，電腦中的操作使用 LoggerNet，其中的設定詳見附錄圖 E.3 和圖 E.4，若連接上，主機綠燈號會持續亮著，特別注意到：學校的電話因需按 0 接總機再撥打出去，並不能使用，目前 CR800S、CR3000 可成功接收，但 CR23x 的 rs232 插槽接不上。

確認設備都裝置好並設定好後，按下 CONNECT，會聽到撥號生，就如數據機撥接的擦擦聲，當電腦聯結上 DataLogger 時，GSM 主機上綠燈號會維持亮著，之後就可用電腦進行控制。

(a) MOD轉接RS232(橘色)

天線

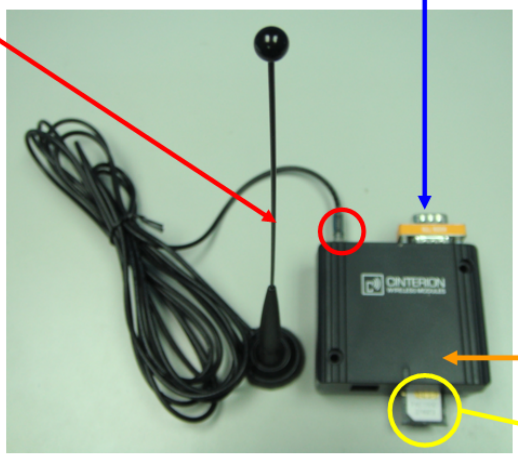

主機

(SIM卡插槽)

(b) 電源線[12V, 1.2A](接主機,頭像電話線頭)

RS232線

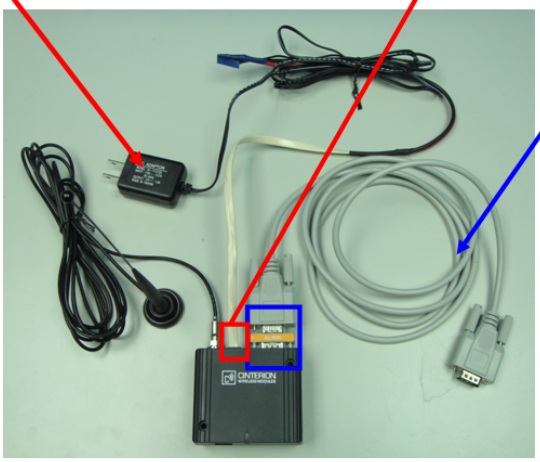

圖 E.1

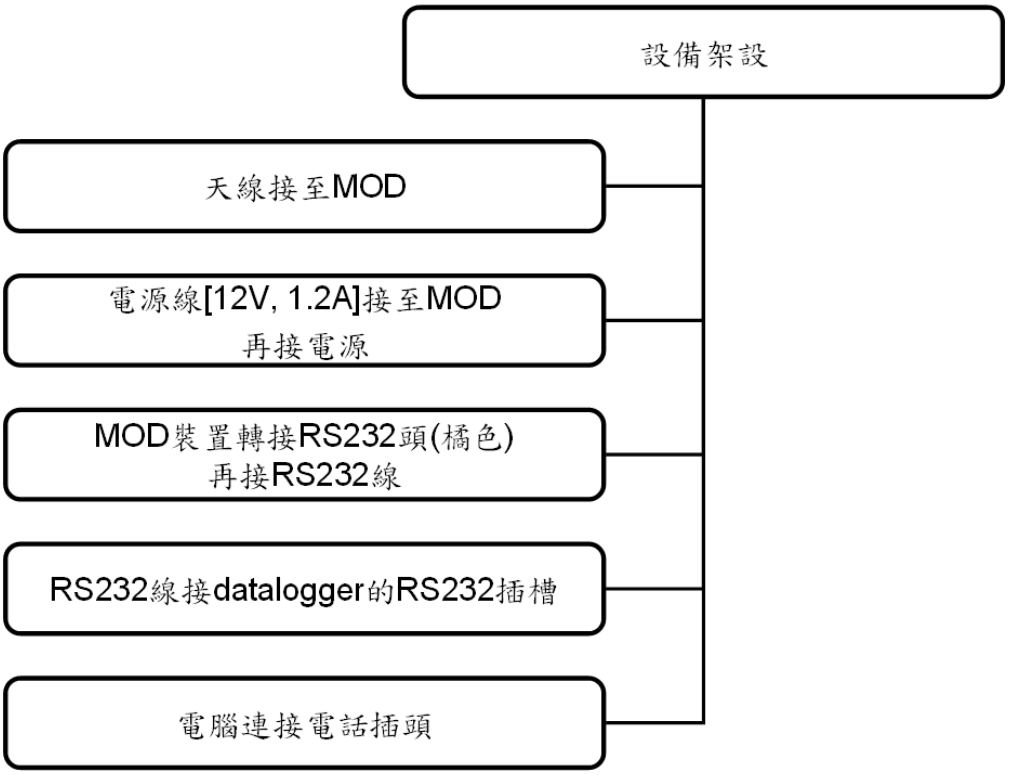
設備架設
天線接至MOD
電源線[12V, 1.2A]接至MOD
再接電源
MOD裝置轉接RS232頭(橘色)
再接RS232線
RS232線接datalogger的RS232插槽
電腦連接電話插頭

圖 E.2

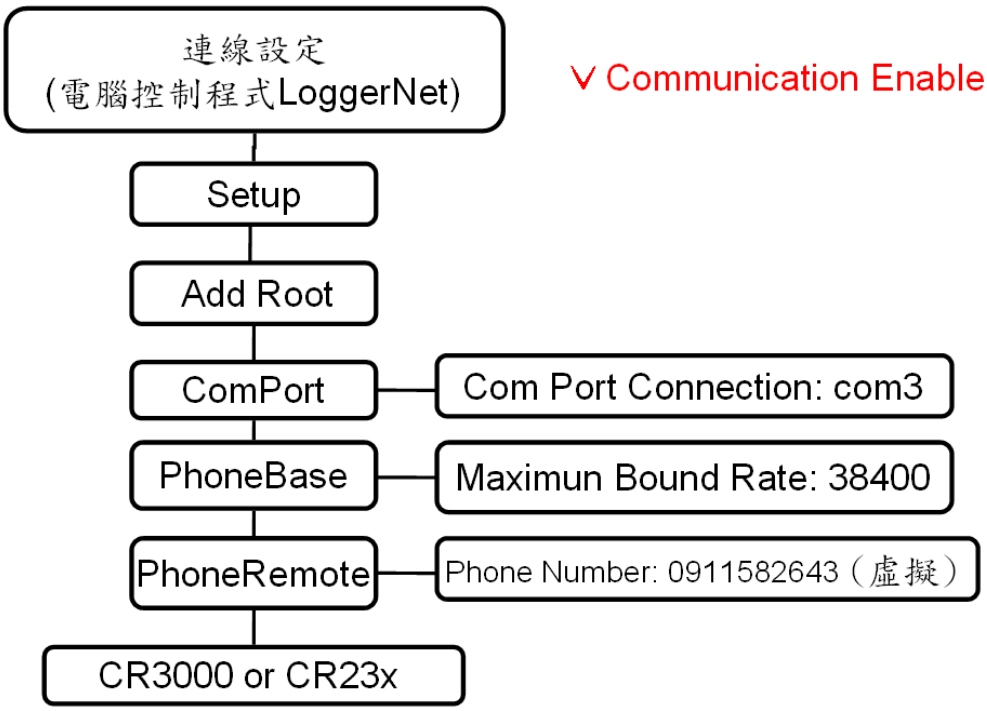
連線設定
(電腦控制程式LoggerNet)
V Communication Enabled
Setup
Add Root
ComPort
Com Port Connection: com3
PhoneBase
Maximun Bound Rate: 38400
PhoneRemote
Phone Number: 0911582643（虛擬）
CR3000 or CR23x

圖 E.3

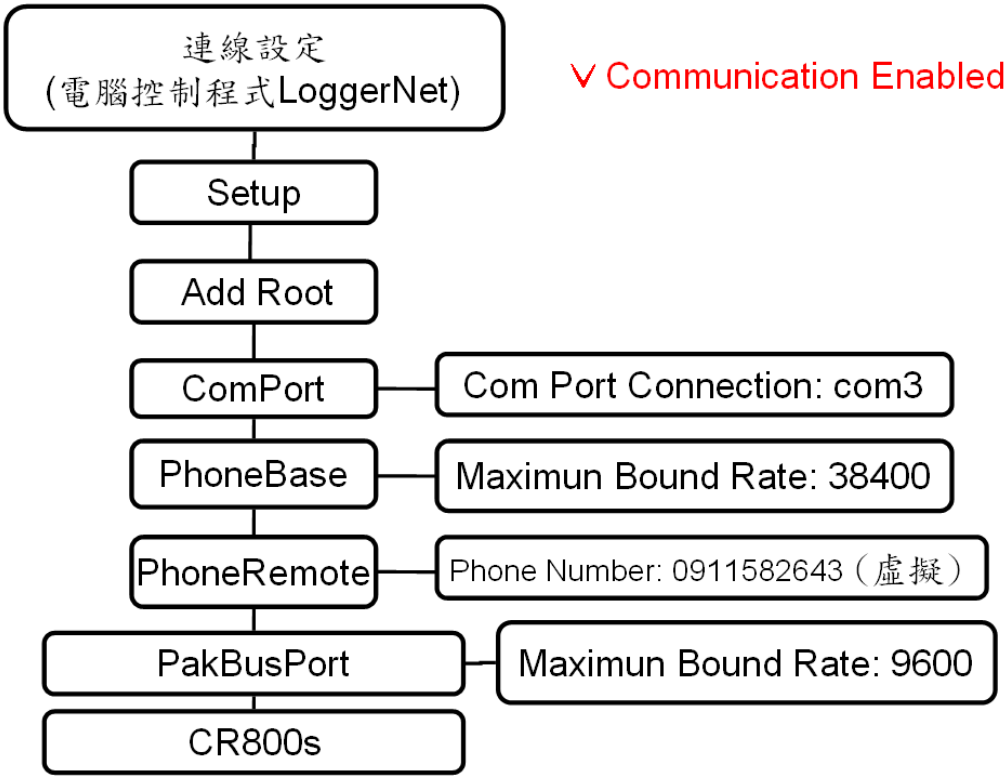
連線設定
(電腦控制程式LoggerNet)
V Communication Enabled
Setup
Add Root
ComPort
Com Port Connection: com3
PhoneBase
Maximun Bound Rate: 38400
PhoneRemote
Phone Number: 0911582643（虛擬）
PakBusPort
Maximun Bound Rate: 9600
CR800s

圖 E.4

附錄 F 通量來源區域(Footprint)

利用Hsieh等(2000)的通量來源模式(該模式廣被AmeriFlux採用，且已被引用超過60次，為一可靠之模式)，進行通量來源區域分析。此通量系統的監測涵蓋範圍(即通量來源區域)與高度及氣候狀況有關，監測的方向與風的來向相同。兩塔附近的平均樹高為27公尺，塔B上40和32公尺處的渦流相關系統，於unstable 狀態下(日間陽光充足時)，40公尺處的監測範圍為距離量測塔250公尺以內，32公尺處的監測範圍為距離量測塔175公尺以內。在stable 狀態下(夜間)，40公尺處的監測範圍達3000公尺，32公尺處的監測範圍達2500公尺。而在near neutral狀態下(多雲、傍晚或清晨時)，40公尺處的監測範圍為1250公尺，32公尺處的監測範圍為900公尺。塔A上28公尺處的渦流相關系統，於unstable狀態下監測範圍為距離量測塔125公尺以內，在stable 狀態下監測範圍達2000公尺，而在near neutral狀態下監測範圍為600公尺(表F.1)。各塔上不同高度處在不同大氣穩定度的通量來源區域比例如圖F.1~3所示，這三組渦流相關系統日間的觀測區域落在柳杉更新林範圍內，夜間的觀測區域則較廣。

參考文獻:

Hsieh, C. I., G. G. Katul, and T. W. Chi, 2000: An approximate analytical model for footprint estimation of scalar fluxes in thermally stratified atmospheric flows, *Advances in Water Resources*, Vol. 23-7, pp. 765-772.

表 F.1 The footprints under different conditions.

Condition(Stability)	Tower	Zm(m)	Footprint range
Stable(ζ=100 m)	B	40	20000m x 3000m
		32	10000m x 2500m
	A	28	5800m x 2000m
Neutral(ζ=0.01 m)	B	40	1800m x 1250m
		32	900m x 900m
	A	28	500m x 600m
Unstable(ζ=-100 m)	B	40	80m x 250m
		32	40m x 175m
	A	28	25m x 125m

(a)

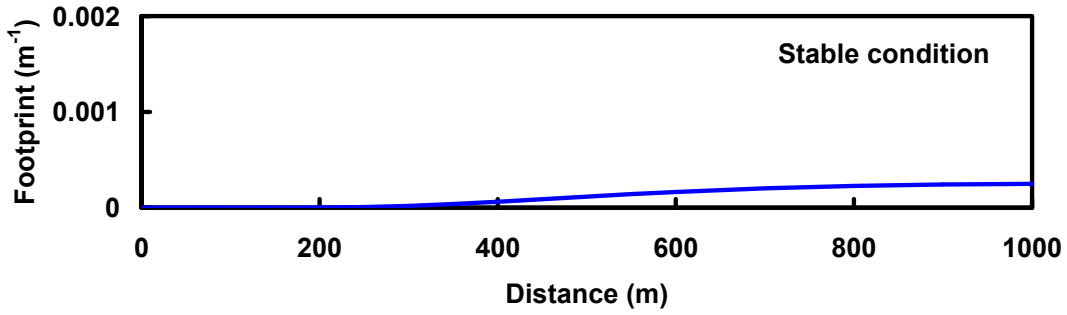
Footprint (m-1)
0.002
0.001
0
Stable condition
0
200
400
600
800
1000
Distance (m)

(b)

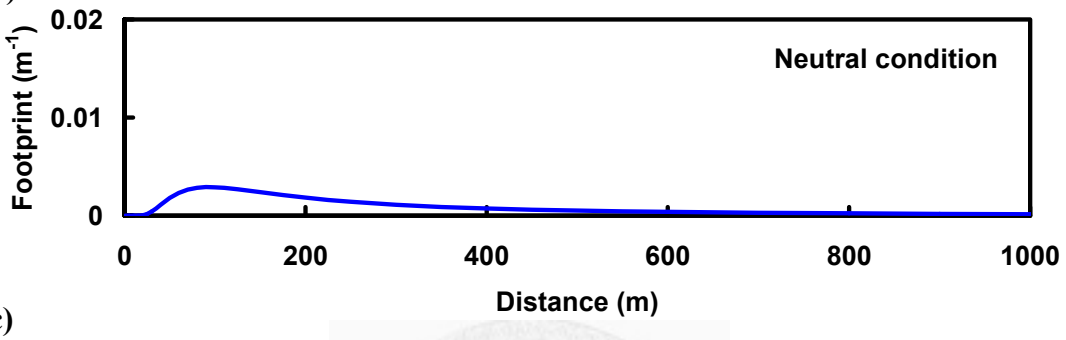
Footprint (m-1)
0.02
0.01
0
Neutral condition
0
200
400
600
800
1000
Distance (m)

(c)

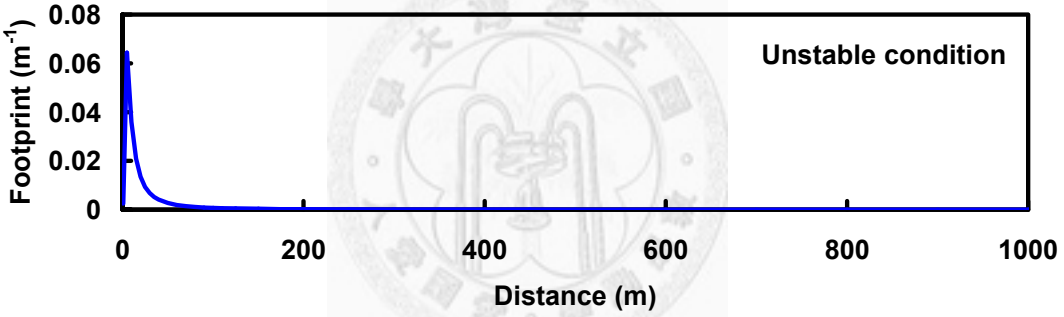
Footprint (m-1)
0.08
0.06
0.04
0.02
0
Unstable condition
0
200
400
600
800
1000
Distance (m)

圖 F.1

(a)

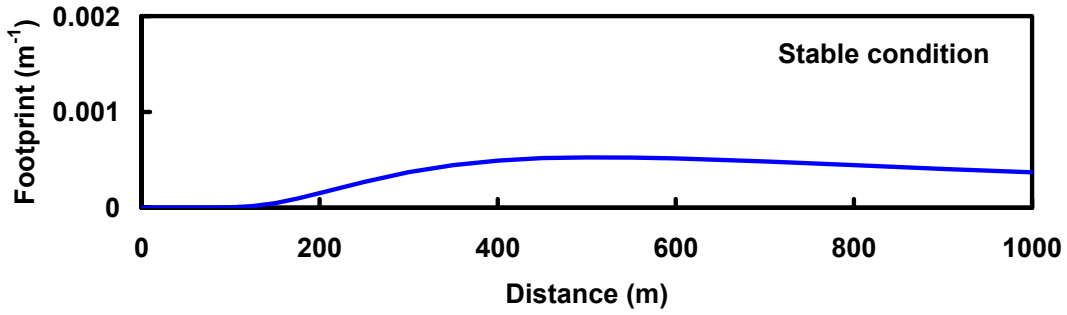
Footprint (m-1)
0.002
0.001
0
Stable condition
0
200
400
600
800
1000
Distance (m)

(b)

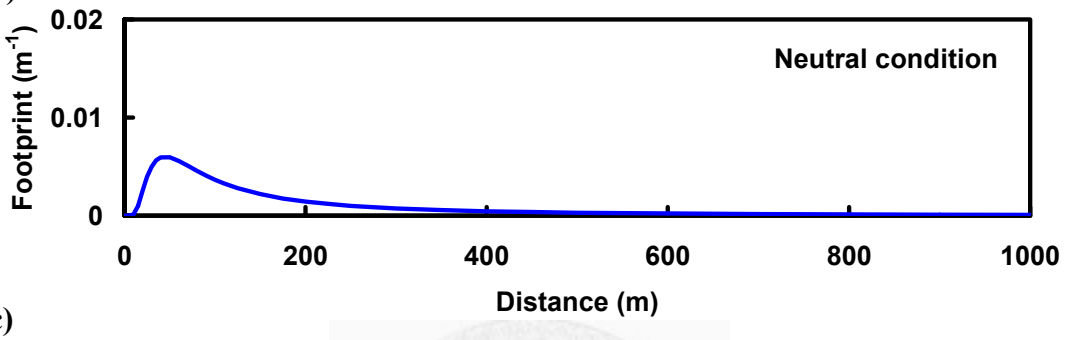
Footprint (m-1)
0.02
0.01
0
Neutral condition
0
200
400
600
800
1000
Distance (m)

(c)

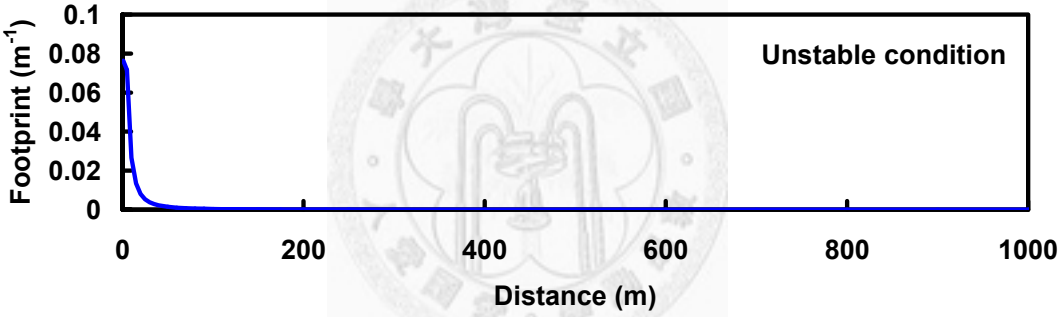
Footprint (m-1)
0.1
0.08
0.06
0.04
0.02
0
Unstable condition
0
200
400
600
800
1000
Distance (m)

圖 F.2

(a)

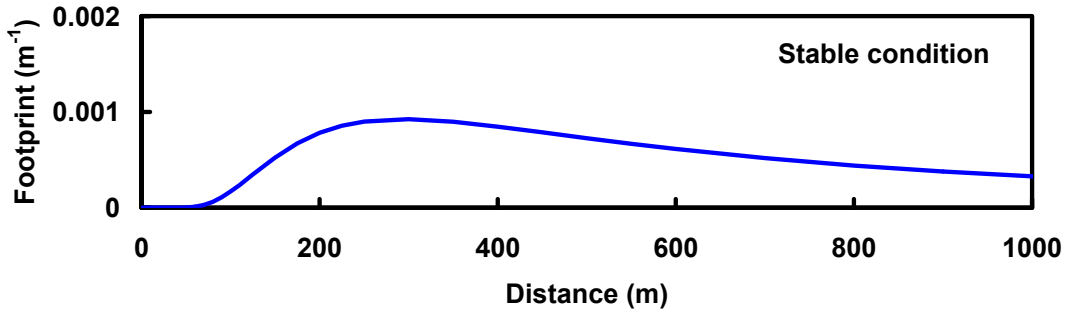
Footprint (m-1)
0.002
0.001
0
Stable condition
0
200
400
600
800
1000
Distance (m)

(b)

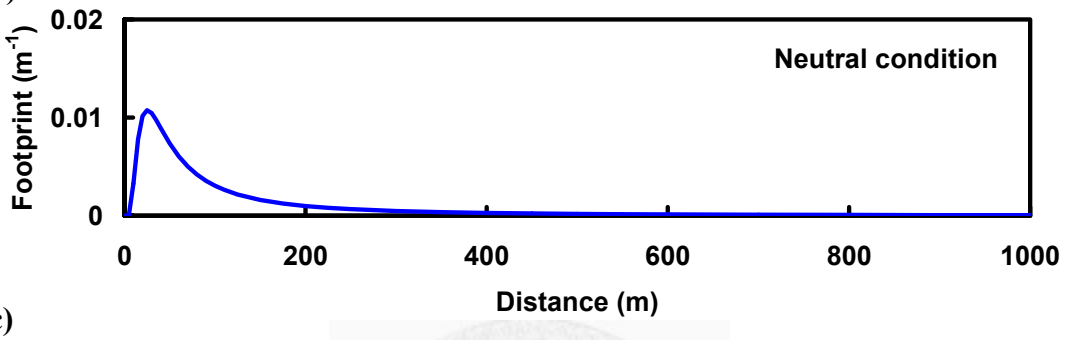
Footprint (m-1)
0.02
0.01
0
Neutral condition
0
200
400
600
800
1000
Distance (m)

(c)

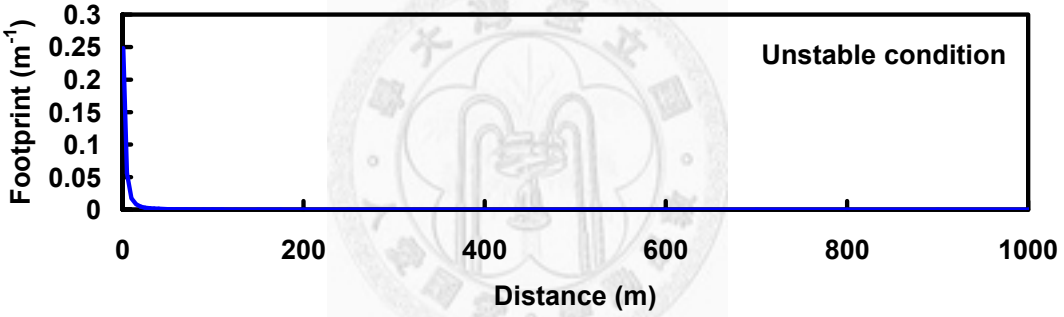
Footprint (m-1)
0.3
0.25
0.2
0.15
0.1
0.05
0
Unstable condition
0
200
400
600
800
1000
Distance (m)

圖 F.3

附錄 G 全天 CV 值及 RV 值隨平均時間長短之變化

圖 G.1 及圖 G.2 是檢測全天的空間變異性隨所取的平均時間間距長短的變化，取 2010 年 78 至 81 天，共 4 天計算，從圖 G.1(a)中可見可感熱、潛熱及二氧化碳通量之 CV 值在平均時間小於 6 小時變動很大，而到平均時間大於 12 小時時，變動會趨於平穩，數值約在 0.1~0.3 之間；標準差的部份，圖 G.1(b)也顯示平均時間大於 12 小時，變動會趨於一定值，且都小於 0.15；但圖 G.1(c)中的標準化標準差並沒有隨平均時間的增加而趨於平穩的特性。在 RV 值的變化中，從圖 G.2(a)和(b)中可見，在平均時間小於 6 小時，通量和標準差的部份變動較 CV 值來得小，也約是當平均時間大於 12 小時後較為穩定，而圖 G.2(c)中的標準化標準差仍是無此特性。

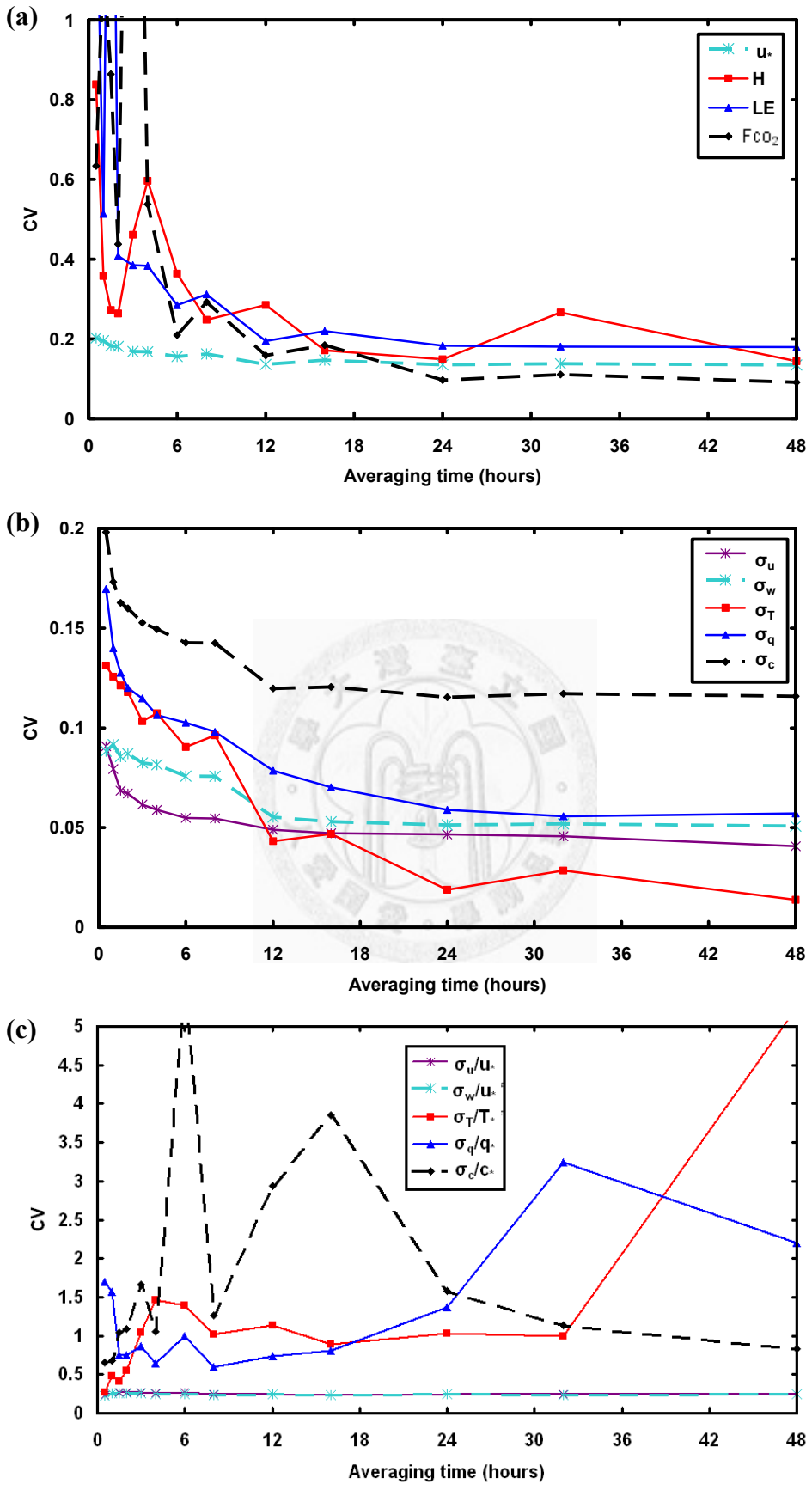
(a)
CV
Averaging time (hours)
u*
H
LE
Fco2
(b)
CV
Averaging time (hours)
σu
σw
σT
σq
σc
(c)
CV
Averaging time (hours)
σu/u*
σw/u*
σT/T*
σq/q*
σc/c*

圖 G.1

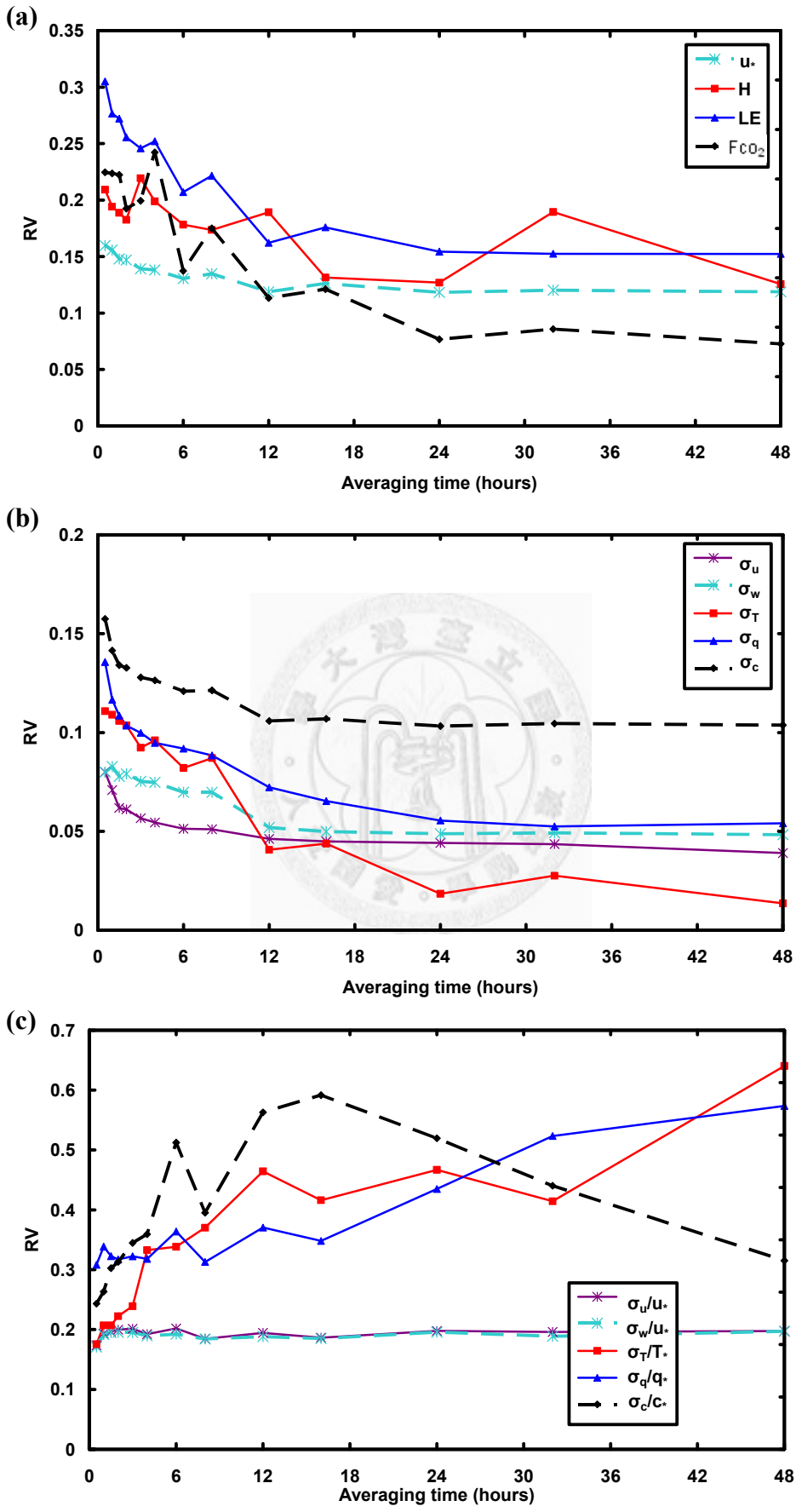
(a)
RV
Averaging time (hours)
u*
H
LE
Fco2
(b)
RV
Averaging time (hours)
σu
σw
σT
σq
σc
(c)
RV
Averaging time (hours)
σu/u*
σw/u*
σT/T*
σq/q*
σc/c*

圖 G.2

附錄 H 風速與潛熱、二氧化碳通量之關係

為研究風速與潛熱、二氧化碳通量之關係，將風速對潛熱通量(LE)以及風速對二氧化碳通量(Fco_2)作圖，以平均風速為x軸，以潛熱或二氧化碳通量為y軸，且因白天、晚上影響通量之機制不同，故將白天和晚上分開作圖討論，白天分界為早上九點至下午五點，而晚上是取晚上八點至隔日凌晨五點。

白天時，由圖H.1 及圖H.2 中可分別看見LE與風速、Fco_2與風速之關係，雖然趨勢不明顯，但隱約可看出：當風速增加時，LE和Fco_2都會微微地隨著增加；而晚上的部份，從圖H.3 中可見，相較於白天，LE隨風速增加而增加的趨勢較為顯著，特別是風速最強的部份，可看出LE明顯增加，由此可知：當風速增加時，會帶動蒸發散量增加，但在圖H.4 中，Fco_2並未有隨風速增加而增加的情形，根據以上所顯示的現象，推論當蒸發散量隨風速增加時，在白天時也會連帶影響植物光合作用的增強，但是植物晚上的呼吸作用並不會受到風速強弱的影響而有改變。

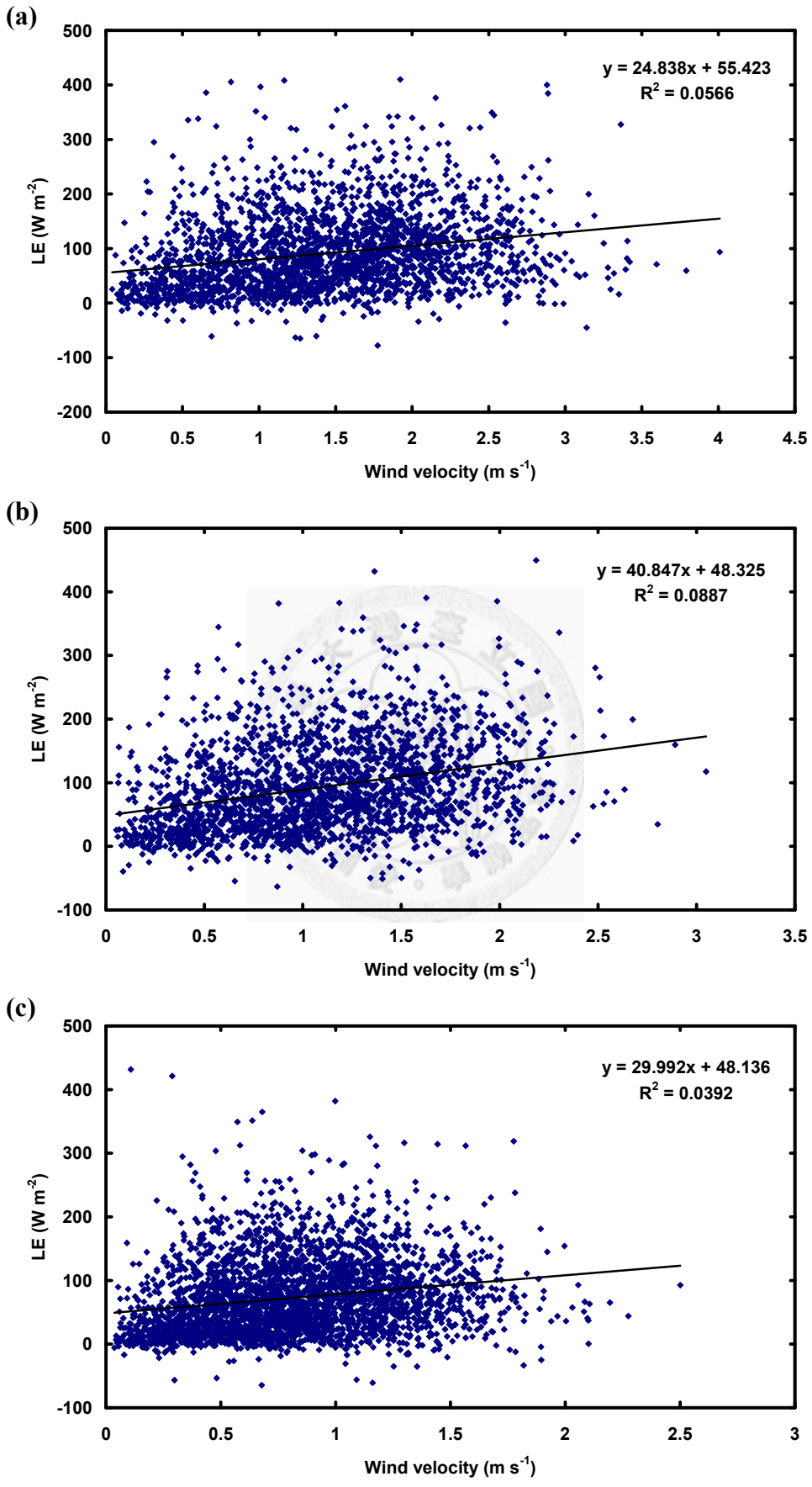
(a)
y = 24.838x + 55.423
R2 = 0.0566
LE (W m-2)
Wind velocity (m s-1)
(b)
y = 40.847x + 48.325
R2 = 0.0887
LE (W m-2)
Wind velocity (m s-1)
(c)
y = 29.992x + 48.136
R2 = 0.0392
LE (W m-2)
Wind velocity (m s-1)

圖 H.1

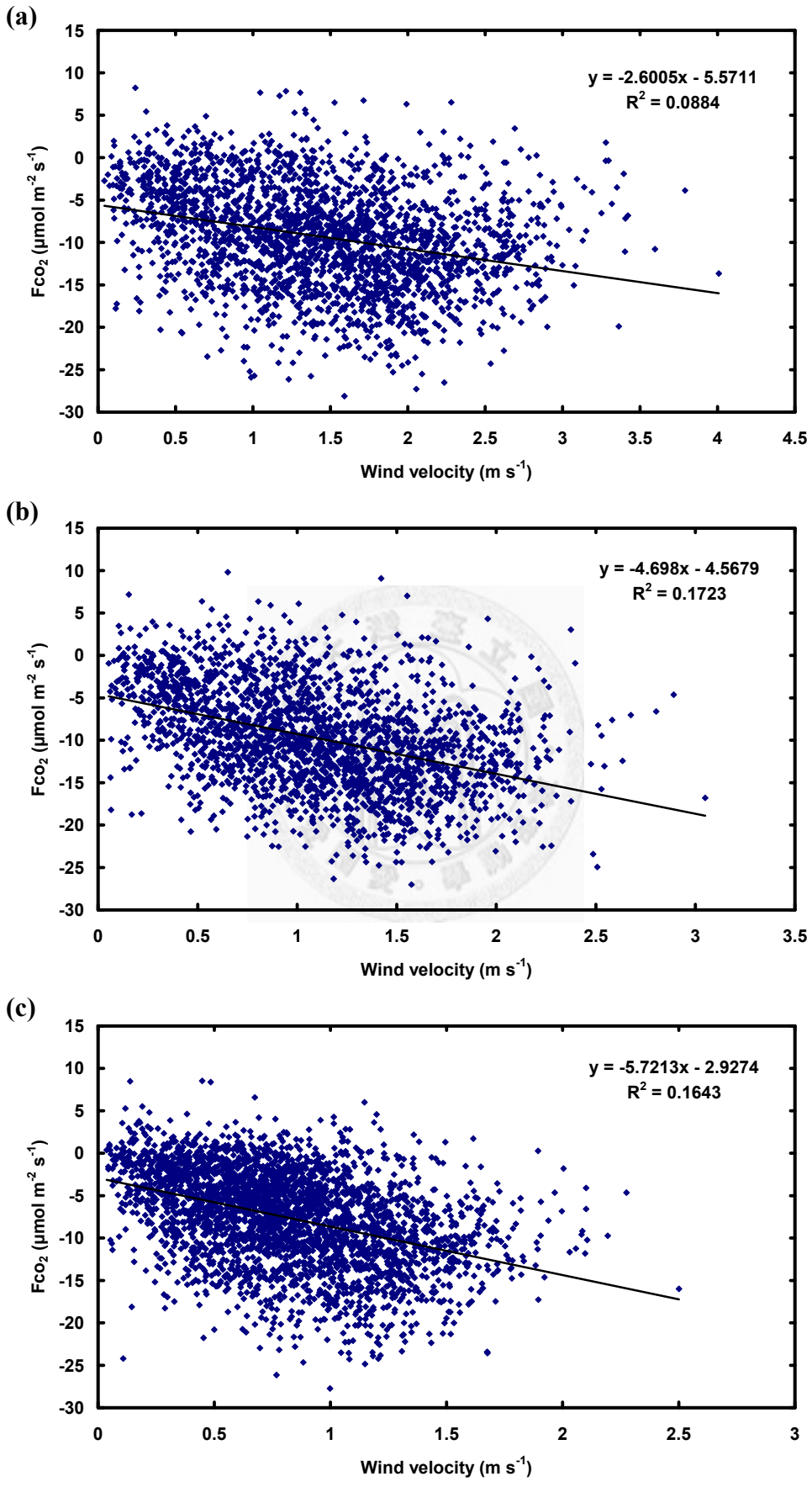
(a)
y = -2.6005x - 5.5711
R2 = 0.0884
Fco2 (μmol m-2 s-1)
Wind velocity (m s-1)
(b)
y = -4.698x - 4.5679
R2 = 0.1723
Fco2 (μmol m-2 s-1)
Wind velocity (m s-1)
(c)
y = -5.7213x - 2.9274
R2 = 0.1643
Fco2 (μmol m-2 s-1)
Wind velocity (m s-1)

圖 H.2

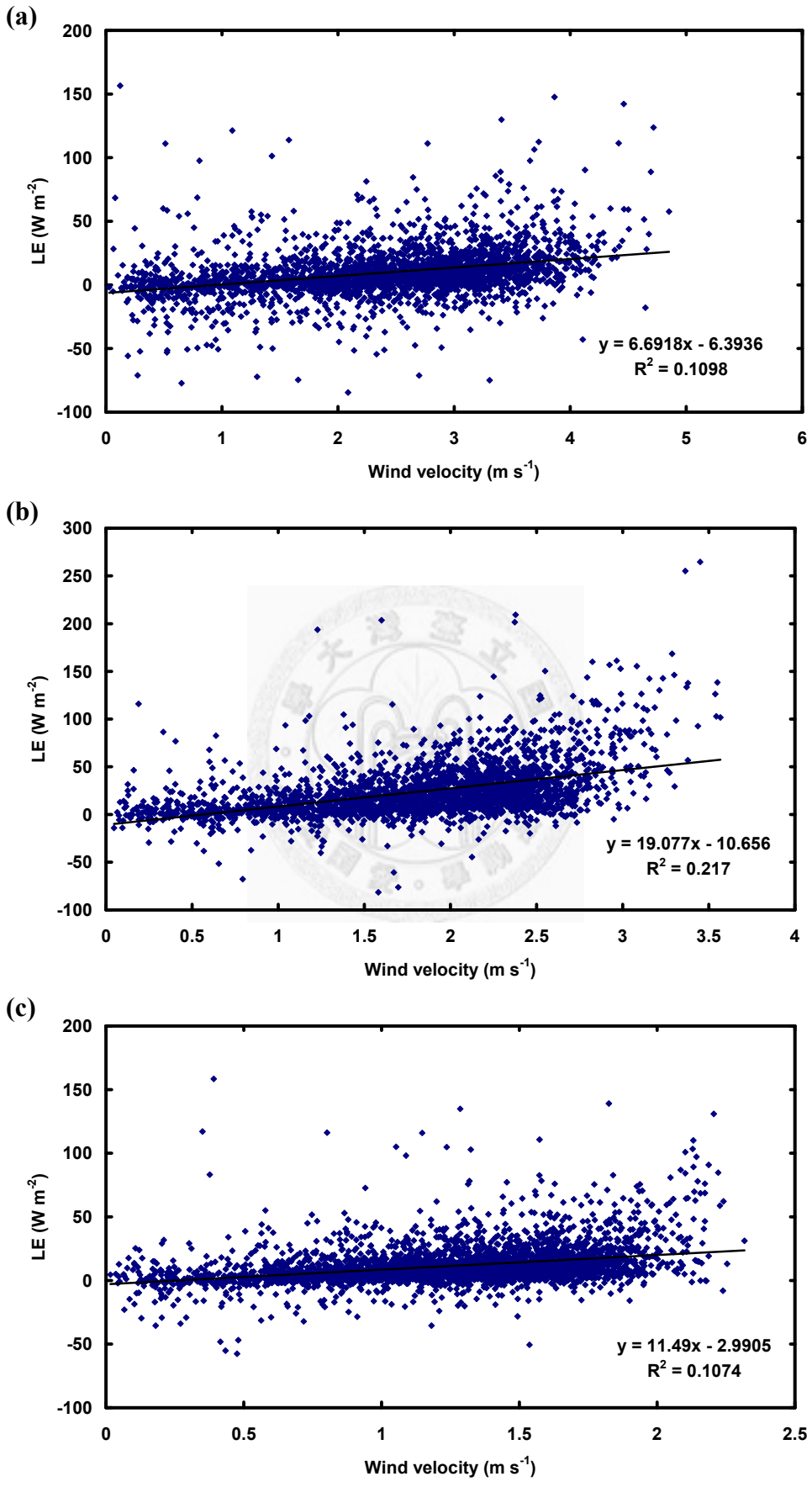
(a)
LE (W m-2)
Wind velocity (m s-1)
y = 6.6918x - 6.3936
R2 = 0.1098
(b)
LE (W m-2)
Wind velocity (m s-1)
y = 19.077x - 10.656
R2 = 0.217
(c)
LE (W m-2)
Wind velocity (m s-1)
y = 11.49x - 2.9905
R2 = 0.1074

圖 H.3

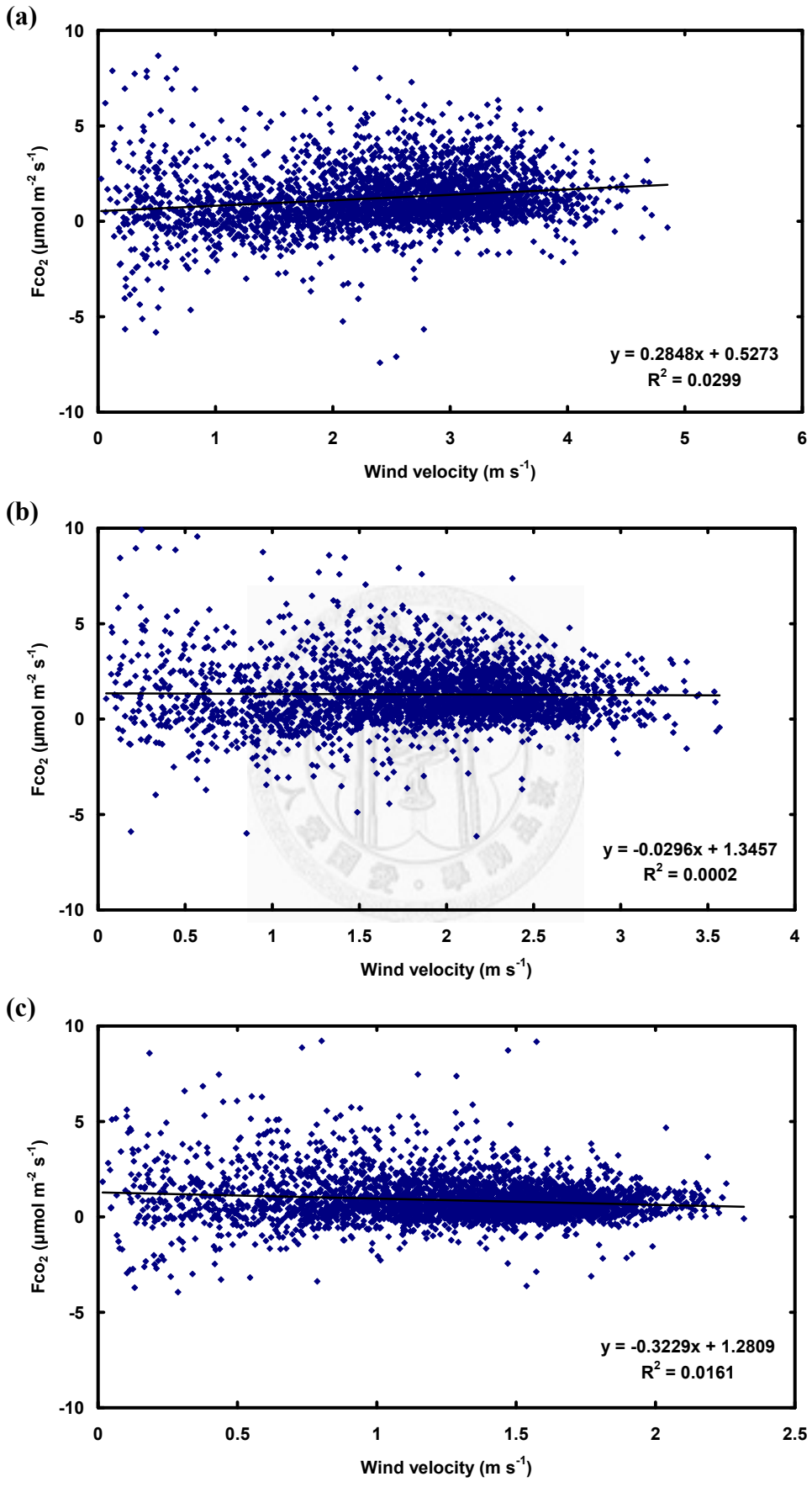
(a)
Fco2 (μmol m-2 s-1)
Wind velocity (m s-1)
y = 0.2848x + 0.5273
R2 = 0.0299
(b)
Fco2 (μmol m-2 s-1)
Wind velocity (m s-1)
y = -0.0296x + 1.3457
R2 = 0.0002
(c)
Fco2 (μmol m-2 s-1)
Wind velocity (m s-1)
y = -0.3229x + 1.2809
R2 = 0.0161

圖 H.4